FLUID-FLUID INTERFACES AND THE EFFECT OF INTERFACIAL PHENOMENA ON CHEMICAL TRANSPORT IN POROUS MEDIA WITH MULTIPLE FLUIDS

By

HEONKI KIM

A DISSERTATION PRESENTED TO THE GRADUATE SCHOOL
OF THE UNIVERSITY OF FLORIDA IN PARTIAL FULFILLMENT
OF THE REQUIREMENTS FOR THE DEGREE OF
DOCTOR OF PHILOSOPHY

UNIVERSITY OF FLORIDA

DECEMBER 1998

ACKNOWLEDGMENTS

I would like to express my deep gratitude to my advisors, Drs Michael D. Annable and P. Suresh C. Rao, for their encouragement, support and direction throughout this research.

I would like to thank Drs William R. Wise, Paul A. Chadik, Kirk Hatfield and Kurt D. Pennell for their helpful comments and valuable suggestions during past three years.

I would also like to extend my deep appreciation to my colleagues, Jim Jawitz, Randy and Gloria Sillan, Claire Shukla, Clayton Clark, and Dr. Chen who have watched the progress of this research and were always willing to take part in discussions for better understanding of contaminant hydrology.

I would especially thank Ms. Irene Poyer for her great support in the lab. Without her help, this work would not have been achieved.

The support from Dr. Chang Whan Kim at Yonsei University in Korea since as early as 1987 in every aspect, is greatly appreciated.

My very special thanks go to my wife, Hea-young, Ryu, and my daughter, Jeong-Yon, whose love, encouragement and perseverance have given me strength during my graduate studies. Finally, consistent support from both of my parents and parents-in-law, mentally as well as financially, is greatly appreciated.

TABLE OF CONTENTS

ACKNOWLEDGMENTS ii

LIST OF FIGURES vi

ABSTRACT x

CHAPTERS

1. INTRODUCTION 1

   Research Objectives and Organization 3
   Surface Excess of Organic Chemicals 5
   Models for Interfacial Area Estimation 8
      Thermodynamic Models 8
      Semi-Empirical Models 10
      Ideal Porous System-Pendular Ring Model 14
      Mass Transfer Model 16

2. INFLUENCE OF AIR-WATER INTERFACIAL ADSORPTION AND GAS-PHASE PARTITIONING ON THE TRANSPORT OF ORGANIC CHEMICALS IN UNSATURATED POROUS MEDIA 19

   Introduction 19
   Theoretical Background 21
   Materials and Methods 25
      Materials 25
      Miscible Displacement Experiments 26
      Surface Tension Measurements 28
   Results and Discussion 29
      Retardation of Chemicals 29
      Estimation of Air-Water Interfacial Area 33
   Summary 34

3. GASEOUS TRACER APPLICATION FOR THE ESTIMATION OF AIR-WATER INTERFACIAL AREAS, INTERFACIAL MOBILITY, AND WATER CONTENTS IN PARTIALLY SATURATED POROUS MEDIA 44

Introduction 44
Materials and Methods 47
Data Analysis 49
Results and Discussion 50
    Water-Partitioning Tracer 50
    Interfacial Tracer 51
Summary 56

4. EFFECTS OF WATER-PARTITIONING AND AIR-WATER INTERFACIAL ADSORPTION ON THE GASEOUS TRANSPORT OF ORGANIC CONTAMINANTS IN UNSATURATED POROUS MEDIA 65

Introduction 65
Theoretical Background 67
Materials and Methods 68
    Materials 68
    Miscible Displacement Experiments 69
Results and Discussion 71
Summary 76

5. EXPERIMENTAL EVALUATION OF THE QUANTITATIVE VALIDITY OF INTERFACIAL TRACERS 85

Introduction 85
Theoretical Background 87
    Surfactant Adsorption at the NAPL-Water Interface 87
    Interfacial Tracer Displacement Experiment - Interfacial Area Calculation 89
    Comparison of Isotherms 90
Materials and Methods 91
    Materials 91
    Column Displacement Experiments 92
    Interfacial Tension Measurement 93
Results and Discussion 94
    NAPL-Water Interfacial Area 94
    Interfacial Adsorption Isotherm 97
Summary 99

6. TRANSPORT OF INTERFACIAL AND WATER-PARTITIONING TRACERS : IMPACT OF NON-EQUILIBRIUM SORPTION AND NONLINEAR ADSORPTION ISOTHERM 107

Introduction 107
Theoretical Background 109
    Two-Region Model 109
    Two-Site Model 112
    Nonlinear Isotherm 113
Temporal Moment Analysis 114
Experimental 116
Results and Discussion 116
    Gaseous Transport 116
    Aqueous Transport 122
    Effect of Pulse Size on the Retardation Factor 125
Summary 127

7. CONCLUSIONS AND RECOMMENDATIONS 144

Conclusions 144
Recommendations 147

APPENDIX 149

REFERENCES 152

BIOGRAPHICAL SKETCH 159

LIST OF FIGURES

Figure

1-1 The log K_{iw} – log K_{ow} relationship for organic compounds; K_{iw} - surface adsorption coefficient (water to air-water interface), centimeter; K_{ow} - octanol water partitioning coefficient (dimensionless); data from Hoff et al.(1993b), Valsaraj (1994) 18

2-1 Detailed column configuration for the unsaturated column experiments 37

2-2 Experimental set-up for unsaturated column experiments 38

2-3 Breakthrough curves for bromide and four alcohols at three different water contents 39

2-4 Breakthrough curves for the transport of aromatic compounds and bromide; Cl-chloro: bnz-benzene: eth-ethyl: pnl-phenol 40

2-5 Effect of water saturation on the total retardation factors (R_t) of alcohols (a), and aromatic compounds (b). All the retardation sources (soil sorption, gaseous partitioning, and air-water interfacial adsorption) were taken into account for the predicted curves (solid lines); nonanol, m - alcohol mixture solutions: s - single component solution; notation for aromatic compounds is the same as in Fig. 2-4 41

2-6 Measured surface tensions of *n*-octanol and *n*-nonanol; C^o represents the influent alcohol concentration used during the column experiments 42

2-7 Correlation of the specific air-water interfacial areas (a_i) calculated from the retardation of *n*-octanol (in mixture) and *n*-nonanol (in mixture (m) and single-component solution(s)) with the degree of water saturation (S_w); an empirical curve from SDBS displacement experiments by Kim et al.(1997) were overlaid for comparison; vertical lines represent data from one experiment with a suite of alcohols 43

3-1 Experimental set up for gaseous interfacial and water-partitioning tracer experiments 59

3-2 Breakthrough curves of the water-partitioning tracers at different water saturations; tracer concentration was normalized so that the total mass of applied tracers for all the experiments at different water saturations was reduced to 0.1 pore volume 60

3-3 The measured volumetric water content with respect to the actual water content estimated by column weight : solid line - ideal 1:1 line 61

3-4 Breakthrough curves of the gaseous interfacial tracer (*n*-decane) at different water saturations; tracer concentration was normalized so that the total mass of *n*-decane for all the experiments at different water saturations was reduced to 0.1 pore volume; inset graph for the methane BTCs at two different water saturations 62

3-5 Measured specific air-water interfacial areas (a_i) using gaseous and aqueous interfacial tracers; SDBS (Kim, et al., 1997): alcohols (from Chap. 2): regression curve (*n*-decane): $a_i = -196.0\ ln\ S_w - 58.9$ ($r^2 = 0.978$) 63

3-6 The ratio of interfacial velocity to the bulk pore-water velocity (α) with the observed sodium dodecylbenzene sulfonate (SDBS) retardation factors (Kim et al., 1997) and the hypothetical retardation factors of SDBS estimated based on the specific air-water interfacial areas (a_i) measured by gaseous interfacial tracer (*n*-decane) experiments 64

4-1 The breakthrough curves of *n*-nonane and chlorobenzene at different water saturations (medium : Dover AFB soil) 78

4-2 Estimated specific air-water interfacial areas of the columns packed with Dover AFB soil and a clean sand in water saturation range of 5 - 55 % 79

4-3 Observed and predicted total retardation factors of VOCs for Dover AFB soil. The components (β') of predicted total retardation factor of chlorobenzene were shown with the observed total retardation factor 80

4-4 The fractions of predicted total retardation factors of *p*-xylene for the Dover AFB soil and clean sand. The fractional retardation factors (f) were normalized with respect to the predicted total retardation factors, which were reduced to unity 81

4-5 The fraction (f_i) of predicted total retardation factors of interfacial (air-water) adsorption for VOCs used in this study 82

4-6 Comparison of VOC breakthrough curves at water saturation of 0.117: dual - mixture injection; solo - single component injection 83

4-7 Breakthrough curves of *n*-heptane at water saturation of 0.146 with different injection volumes; the volume of *n*-heptane and air mixture taken from the head space in the sample preparation vial, used as the input pulse 84

5-1 Schematic diagram of the experimental set-up 101

5-2 Interfacial tensions between NAPL-surfactant aqueous solutions 102

5-3 Breakthrough curves of interfacial tracers : (a) SDBS (CMC=2.2 mM), *n*-decane column; (b) CPC (CMC = 0.9 mM), *n*-decane column; (c) SDBS, PCE column 103

5-4 Retardation factors of SDBS and CPC as a function of tracer influent concentrations from *n*-decane glass bead column experiments 105

5-5 Interfacial adsorption isotherms of SDBS and CPC calculated from interfacial tension data and the Gibbs equation (solid line), and column (*n*-decane) experiment data 106

6-1 Breakthrough curves of the interfacial tracers; Dover AFB soil, water saturation 0.15 132

6-2 Breakthrough curves of methane at different pore-gas velocities, sand column, water saturation 0.31 133

6-3 The normalized, temporal, central moments of volatile organic chemicals with respect to the retardation factor 134

6-4 Normalized breakthrough curves of methylene chloride (gaseous water-partitioning tracer) at different water contents, sand 135

6-5 The change of the normalized, temporal, central moments of methylene chloride (water-partitioning tracer) with volumetric water content change 136

6-6 Fitted BTCs of methylene chloride using 2-site model; squares-observed data, solid line-fitting; (a) water content 0.070, (b) water content 0.141, (c) water content 0.184 137

6-7 The breakthrough curves of tracers: (a) bromide, (b) CPC 0.0596 mM, (c) CPC 0.199 mM; pore water velocity 0.9 cm/min.; rectangle - front side of BTC, closed triangle - back side of BTC, open triangle - inverted back side of BTC. 138

6-8 Normalized breakthrough curves of CPC with different input concentrations, glass bead column, coated with n-decane; data from Chap. 5 139

6-9 The adsorption isotherm of CPC at the *n*-decane-water interface at 22°C (a); and regression result using Freundlich isotherm model (Eq. 6-27) for the CPC concentration up to the saturation point (CPC conc.=5×10^{-7} mol/cm^3)(b): squares - observed data; solid line - regression 140

6-10 Breakthrough curves of CPC: (a) observed, C_o=0.056 mM, (b) simulated BTC using equilibrium, nonlinear isotherm, 2-site model, N=0.353 (Freundlich isotherm model), (c) simulated BTC using equilibrium, linear isotherm model, (d) fitted BTC using non-equilibrium, nonlinear isotherm (N=0.353), 2-site model, $\beta = 0.52$, $\omega = 1.33$: all BTCs have the same retardation factor of 3.21 141

6-11 Breakthrough curves of CPC; the fitting parameters (β and ω) for the frontal side of the BTC were used to predict the back side of BTC 142

6-12 Breakthrough curves of CPC; the size of input pulse is not corrected; influent concentrations are shown in Table 6-3 143

Abstract of Dissertation Presented to the Graduate School
of the University of Florida in Partial Fulfillment of the
Requirements for the Degree of Doctor of Philosophy

FLUID-FLUID INTERFACES AND THE EFFECT OF INTERFACIAL PHENOMENA ON CHEMICAL TRANSPORT IN POROUS MEDIA WITH MULTIPLE FLUIDS

By

HEONKI KIM

December 1998

Chairman: Michael D. Annable
Cochairman: P. Suresh C. Rao
Major Department: Environmental Engineering Sciences

The physical morphology and quantity of the interfaces between immiscible fluids in porous media is of great interest in subsurface contaminant hydrology. Although the quantity of fluid-fluid interfacial areas in porous media contaminated with water-immiscible fluids has been recognized as a controlling factor of many physico-chemical processes, experimental techniques to measure this quantity have not been available until an interfacial tracer method was developed in 1995. The objectives of this study are (1) to validate the interfacial tracer technique in both aqueous and gaseous applications, (2) to characterize the effect of interfacial adsorption of organic contaminants at the fluid-fluid interfaces on their aqueous and gaseous transport, (3) and to investigate the non-ideal behavior of chemical transport that is subject to the interfacial adsorption and partitioning in water (gaseous transport).

The measured non-aqueous phase liquid (NAPL)-water interfacial areas using different interfacial tracers (anionic and cationic surfactants) were consistent. The interfacial tracer technique applied to different NAPL-water systems with the same NAPL-water interfacial areas returned reasonably close measured values of NAPL-water interfacial areas. Most of the measured values are in good agreement with the calculated NAPL-water interfacial area of the system. These results verify that the aqueous phase interfacial tracer technique for NAPL-water system is robust. For a porous system containing air and water without NAPL, two different chemical species (alcohols and anionic surfactant) were tested. The measured air-water interfacial areas were consistent.

The adsorption at the air-water interface significantly affected the gaseous transport of most of the volatile organic chemicals (VOCs) used in this study (e.g., xylene, ethylbenzene, PCE, TCA, aliphatic hydrocarbons). The fractions of the retardation of each chemical based on the retardation sources (water and air-water interface) during gaseous transport with respect to the total retardation was calculated with different types of soils (sand and a soil collected at Dover Air Force Base, DE) and the chemical properties of the VOCs. The observed retardation of the VOCs during gaseous transport was in excellent agreement with the predicted based on the air-water interfacial areas measured using interfacial tracers. However, the transport of VOCs in the aqueous phase was not significantly affected by the interfacial adsorption because of a small specific air-water interfacial area in the medium (sand).

No significant non-equilibrium effect due to rate-limited adsorption processes was found for gaseous interfacial tracers over the range of water saturations achieved in this study. Thus, gaseous adsorption at the air-water interface is not considered to be rate-limited with respect to the pore-gas velocities used. However, a noticeable shift of the breakthrough curves (BTCs) of aqueous interfacial tracers (NAPL-water system) was observed. This effect was interpreted using a non-equilibrium, nonlinear transport model. The BTCs of gaseous water-partitioning tracers were also found to deviate from the predicted based on the local equilibrium assumption. The functional relationships between water saturation, air-water interfacial area, and the degree of non-equilibrium for the water-partitioning gaseous tracers were discussed.

The findings from this study support the validity and applicability of the interfacial tracer technique for both NAPL-water and air-water systems. Considering that a number of important physical, chemical, and biological processes are influenced by the existence of fluid-fluid interfaces in the subsurface environment, a substantial expansion of research capabilities is provided by this simple, however robust technique.

CHAPTER 1
INTRODUCTION

Understanding the physical and chemical characteristics of the interfaces between immiscible fluids is of great importance in the field of contaminant hydrology because of the influence of the interfaces on the fate of organic contaminants in the subsurface environment. Along with the solid-liquid interface, that has been studied extensively during past several decades, the fluid-fluid interface affects the spatial distribution, transport, and transformation of organic contaminants when immiscible fluids co-exist in a porous system. Since water is the common fluid in a natural subsurface environment, interfaces between immiscible fluids are formed by one or more water-immiscible fluids such as air, or non-aqueous phase liquids (NAPLs).

Interfaces between immiscible fluids affect several different processes occurring in porous media: (1) Mass balance. In some occasions, the interface may have a substantial capacity of adsorbing chemicals increasing the total mass of the chemical in the system. The fraction of adsorbed chemical at the interface is dependent on the surface activity of a chemical as well as the quantity of the interface. (2) Transport. With significant specific fluid-fluid interfacial area and surface (or interfacial) activity of a chemical, the adsorption of a chemical at the interface results in slower transport of the chemical than the velocity of flowing domain, which, in general, can be either air or water. At the same time, the chemical concentration profile during the transport as well as the mean travel velocity of a chemical can also be affected by the interfacial adsorption, particularly since the sorption isotherm of a chemical at the interface deviates from a simple linear relationship. The more non-linear the sorption isotherm is, the more deviation of the chemical breakthrough curves (BTCs) from the ideal case is expected. Since the adsorption and desorption processes of a chemical on the fluid-fluid interface are not always instantaneous, an additional effect of sorption kinetics on the transport behavior is also expected. (3) Transformation. The rate of chemical reactions can be altered due to the interface. The oxidative degradation of organic chemicals due to microbial activity in a subsurface environment depends on the dissolved oxygen level in the aqueous phase. Since the air-water interface is one of the governing factors that controls the overall mass transfer rate of oxygen, the quantity of the air-water interfacial area may affect the degradation rate of a chemical. The fluid-fluid interface can also behave as a catalyst that enhances the reaction of surface active chemicals, when the reaction requires a specific molecular arrangement. (4) Mass transfer. In a porous medium containing NAPL and water, the overall mass transfer rate of the NAPL components to the aqueous phase is controlled by the NAPL-water interfacial area. The specific gas exchange rate in an air-water porous system can be a function of the air-water interfacial area.

Although the importance of the fluid-fluid interface in many aspects of subsurface contaminant hydrology has been well recognized by a number of previous studies (e.g., Miller et al., 1990; Powers et al.,1992), a comprehensive, quantitative study to correlate the interfacial phenomena occurring in porous media to the transport behavior of organic contaminants has not been attempted. This is mainly because of the lack of an appropriate experimental method to measure the interfacial area between immiscible fluids in porous media. Although there are several optical/imaging techniques developed recently such as nuclear magnetic resonance imaging, scanning probe microscopy, optical microscopy, and photoluminescent imaging for the characterization of interfaces between immiscible fluids in porous media (Ronen et al., 1986, Herman and Lemasters, 1993, Wiesendanger, 1994, Montemagno and Gray, 1995), a reliable, ready-to-use technique with standard lab equipment for the quantitative measurement of the interfacial areas at Darcy scale has not been available. A tracer technique has been developed recently for the interfacial area measurement (Saripalli et al., 1997). Now that the method is available, it is possible to correlate the physical and chemical processes affected by the existence of fluid-fluid interfaces to the quantity of interfacial area.

Research Objectives and Organization

The overall objectives of this research are three fold: (1) validation of the interfacial tracer technique for both air-water and NAPL-water systems, (2) investigation of the quantitative relationship between the measured fluid-fluid interfacial areas and retardation during transport due to adsorption at the interface, and (3) estimation of the effect of non-ideal adsorption behavior of chemicals at the fluid-fluid interface on the shapes of breakthrough curves.

In Chapter 2, air-water interfacial areas as a function of water saturation were measured using *n*-alcohols, applied as the aqueous interfacial tracers. Since the air-water interfacial areas of the medium (sand) had been measured in a previous study using an anionic surfactant, a comparison of measured interfacial areas was made. The effect of adsorption at the air-water interface on the aqueous transport of surface active chemicals (*n*-alcohols) and volatile organic chemicals (VOCs) was also investigated. Since the sorption in soil (sand) and gas-phase partitioning of VOCs also contribute the overall retardation of the chemicals, the relative composition of the retardation based on the sorption mechanisms was also estimated.

In Chapter 3, a gaseous interfacial tracer technique was introduced for air-water interfacial area measurements with the same soil used in Chapter 2. The difference in the measured air-water interfacial areas using the aqueous and gaseous interfacial tracers was identified and quantified. The difference in the observed retardation factors of gaseous and aqueous tracers was further interpreted in light of the mobility of the air-water interface during aqueous tracer application.

In Chapter 4, the effect of interfacial adsorption at the air-water interface on the gaseous transport of VOCs was investigated. A gaseous interfacial tracer technique was employed to determine the specific air-water interfacial areas as a function of water saturation. The composition of the retardation factors during the gaseous transport were investigated based on the retention sources such as interfacial adsorption, water-partitioning, and soil sorption. The change of the fraction of the retardation due to interfacial adsorption was estimated with respect to different soil types, water saturations, and chemicals.

In Chapter 5, the validity of the aqueous phase interfacial tracer technique was tested using a controlled porous system with a known NAPL-water interfacial area. First, the consistency in the measured NAPL-water interfacial areas using different tracer concentrations was evaluated. Second, two different interfacial tracers (cationic, and anionic surfactants) were tested to verify if different tracers return the same result. And finally, different NAPL types were used to check the consistency in the measured NAPL-water interfacial areas.

In Chapter 6, the effect of rate-limited sorption kinetics, and the non-linear sorption isotherm on the breakthrough curves of chemicals during both aqueous and gaseous transport was investigated. The spread and distortion of BTCs, quantified as central second and third moments, of water-partitioning gaseous tracers was correlated to the degree of water saturation and the corresponding air-water interfacial areas. The skewness of the BTCs of gaseous and aqueous interfacial tracers was also examined. For aqueous interfacial tracers, the effect of the input pulse type on the retardation factor and the shape of BTCs was investigated.

Surface Excess of Organic Chemicals

By definition, the surface excess concentration is the excess, per unit area of interface, of the amount of any component actually present in the system over that present in a reference system of the same volume in which the bulk concentrations in two phases remain uniform up to a hypothetical dividing surface (Rosen, 1989). When a chemical adsorbs at the interface resulting in locally higher concentration at the dividing surface than the bulk concentration, this chemical is called "surface active." Surface active agents, or surfactants, are liquid-soluble organic chemicals which have exceptionally high surface excess concentrations, resulting in a significant change in the surface property (i.e., surface free energy) of the liquid. Most organic chemicals of environmental interest do have the characteristic of accumulating at the interface of two immiscible fluids, although the extent of surface excess is far lower than those of common surfactants. Since the air-water interface is ubiquitous in the unsaturated subsurface (vadose zone), the role of surface adsorption of the chemicals must be carefully assessed for a better understanding the nature of the contaminant distribution and fate.

The relationship between surface excess and bulk concentration of a chemical is expressed with the equilibrium distribution coefficients, K_{ia} and K_{iw}, where K_{ia} represents the ratio of surface excess to the bulk gaseous concentration, and K_{iw} represents that with respect to the bulk aqueous concentration. Since the unit of the bulk concentrations in the aqueous and gaseous phases is mass (or mol) per volume (L^3) and the unit of surface excess is mass per unit area (L^2), the distribution coefficients for surface adsorption have a unit of length (L). This length unit of the surface distribution coefficient implies the depth of bulk phase that contains the same mass of the chemical as that adsorbed at the interface. For those chemicals of environmental concern, the K_{ia} and K_{iw} values are available in literature (Hoff et al., 1993a, b; Valsaraj, 1994). With other important chemical properties, such as saturated gaseous and aqueous concentrations, the K_{ia} and K_{iw} values for commonly found chemicals are listed in Table 1-1. Hoff et al. (1993b) attempted to correlate the saturated aqueous concentrations of organic compounds to their K_{iw} values to obtain an empirical expression;

$$\log K_{iw} = -8.58 - 0.769 \log C_{sw} \qquad 1\text{-}1$$

where K_{tw} has a unit of centimeter, and C_{sw} is the saturated concentration in the aqueous phase (mol/cm^3). Note that the surface distribution coefficient, K_{tw} is inversely proportional to the aqueous saturated concentration, C_{sw}, implying that more hydrophobic compounds, which have less solubility in water, tend to adsorb more at the air-water interface. Alcohols and normal carboxylic acids are not included for the regression (Eq. 1-1), because the molecular structures of alcohols and carboxylic acids are distinctive, such that exceptionally large mass is accumulated at the air-water interface while maintaining high bulk aqueous concentration. The Gibbs free energy, enthalpy, and entropy changes during surface adsorption from either the aqueous or gaseous phase were discussed by Valsaraj (1994) for common organic contaminants. The octanol-water partitioning coefficient (K_{ow}), which is often used as a indicative measure of the relative hydrophobicity of organic chemicals, can also be used to correlate the hydrophobicity and K_{iw} (Fig. 1-1). The relationship between log K_{ow} and log K_{tw} is especially useful when the hydrophobicity of a chemical species is compared within the homolog series.

The surface distribution coefficients (K_{tw} and K_{ta}) of most of the organic chemicals, except alcohols and carboxylic acids, listed in Table 1-1 are fairly constant over relatively wide range of bulk phase concentrations. However, beyond a certain bulk concentration, the distribution coefficients are not constant anymore, changing as the function of the bulk concentrations. This tendency is due to the status of the adsorbed layer of the chemicals at the interface. When a chemical has relatively small surface activity, the layer of the adsorbed molecule is considered as a pseudo-gas state, where there is little intermolecular interaction between adsorbed molecules. As the number of adsorbed molecules at the interface increases, the film is condensed. Therefore, the interaction between the adsorbed molecules in unavoidable. This lateral interaction, which is usually enhances the surface pressure change, causes a non-linear relationship for the bulk and surface excess concentrations. Some chemicals reach this condensed film state at very low bulk aqueous concentration. Surfactant, alcohols are examples of these chemicals. Thus, there is no constant K_{iw} for a surfactant. At the same time, the surface pressure change in air-water systems with ionic surfactants are heavily dependent on the background ionic strength in the aqueous solution. Therefore, the K_{iw} values for surfactants must be measured for each particular system condition.

Models for Interfacial Area Estimation

Before experimental methods were developed, several different models were utilized for estimation of fluid-fluid interfacial areas in porous media. These models are classified into four categories: (1) thermodynamic interpretation of the porous systems, (2) semi-empirical models that depend partially on measurable parameters such as a soil-moisture release curve, (3) ideal porous systems-pendular ring models, (4) mass transfer models.

Thermodynamic Models

Models which use a thermodynamic approach have been reported by Leverett (1941), Morrow (1970), and Bradford and Leij (1997). Based on the fundamental relationship between the capillary pressure across the fluid boundary, surface curvature, and the free energy change, or the work necessary to change the interfacial area, expressions for the fluid-fluid interfacial area were developed. Leverett described that the change of surface free energy (ΔF) is equal to the integral of capillary pressure with respect to the water saturation (S_w) change:

$$\Delta F = - \int_{S_{w1}}^{S_{w2}} P_c \, dS_w \qquad 1\text{-}2$$

where P_c is the capillary pressure (dyn/cm^2). A general form of Helmholtz free energy change of a system with two immiscible fluids (here denoted as *n* and *w*) (Morrow, 1970) is:

$$dF = - EdT + \sum_{i=1}^{j} \mu_i dn_i - P_n dV_n - P_w dV_w + \gamma dA_{nw} \qquad 1\text{-}3$$

where E is entropy (erg/°K mol), T is temperature (°K), μ_i is the chemical potential (erg/mol) of chemical i, n_i is the number of moles of chemical i, P and V represent the pressure and volume of the fluids, γ is the surface tension (dyn/cm), and A_{nw} is the total area (cm^2) in the system. Assuming there are no chemicals present in the system ($dn_i = 0$), any changes (e.g., drainage or imbibition) occur under isothermal condition ($dT = 0$), and the fluids are incompressible ($dV = 0$, e.g., water), the surface free energy per unit surface area, of surface tension is:

$$\gamma = \left(\frac{\partial F_s}{\partial A_{nw}} \right)_{T,V,n} \qquad 1\text{-}4$$

where F_s is the surface free energy. Substitution of Eq. 1-4 into Eq. 1-2 yields:

$$a_2 - a_1 = \frac{F_2 - F_1}{\gamma} = \frac{1}{\gamma} \int_{S_{w2}}^{S_{w1}} P_c \, dS_w \qquad 1\text{-}5$$

where a_2, and a_1 are the interfacial area between the immiscible fluids per unit volume of pore space, at water saturations of S_{w1} and S_{w2}, respectively, and F is the surface free energy.

For the special case that $S_{wl} = 1$, obviously, $a_1 = 0$, thus a_2 becomes the total interfacial area at the fluid saturation of S_{w2}. Although 1-5 is simple and useful, it is valid only when a fluid in the system wets the solid surface completely or the solid-liquid contact area is constant, so that the change in solid-liquid surface area does not share the external work (i.e., the integral part of Eq. 1-5).

Bradford and Leij (1997) expanded Eq. 1-5 for more general cases including the effects of solid-liquid interface, non-zero contact angle, and porous systems with more than two fluids. For a system with two fluids, the expression suggested by Bradford and Leij is:

$$\Phi_{nw}(S^{w}_{nw}) + C_{nw} = \gamma_{nw} \cos(\phi_{snw}) \, a_{sn}(S^{w}_{nw}) + \gamma_{nw} \, a_{nw}(S^{w}_{nw}) \qquad 1\text{-}6$$

$$\Phi_{nw}(S^{w}_{nw}) = \int_{S_{wl}}^{S_{W2}} P_{nw} \, dS^{w}_{nw} \qquad 1\text{-}7$$

where C_{nw} is a constant of integration equal to $\gamma_{nw}a_{nw}$ when $P_{nw} = 0$, γ_{nw} is the interfacial tension between wetting and non-wetting fluids, ϕ_{snw} is the contact angle formed by the solid surface and the two fluids, $S^{w}{}_{nw}$ is the saturation of the wetting fluid, and a_{sn} and a_{nw} are the areas per unit pore volume at the soil-nonwetting fluid and at the wetting-nonwetting fluids, respectively. When $\phi_{snw} = 0$, and for the primary drainage that $C_{nw} = 0$, Eq. 1-6 reduces to Eq. 1-5.

Semi-Empirical Models

Semi-empirical models are those that utilize the capillary pressure-saturation relationship with some kind of geometric simplifications of the fluid-fluid interface or/and the pore spaces in porous media. Examples are those proposed by Rose and Bruce (1949), Skopp (1985) and Cary (1994).

Rose and Bruce (1949) used the basic concept of capillary rise in circular tubes:

$$P_c = Dgh = \frac{2\gamma}{r} \qquad 1\text{-}8$$

where D is the density difference between fluid phases (gram/cm^3), g is the gravitational constant (cm/sec^2), h is the height of the fluid above level of zero curvature (cm), and r is the pore radius (cm). Using an assumption that for soil systems, twice the "hydraulic radius, f", that is defined as the ratio of porosity to surface area per unit bulk fluid volume, can be used for r in Eq. 1-8 (Carman, 1941). Then, the interfacial area in an air-water system can be estimated as:

$$A_b = \frac{f\,P_c}{\gamma} = \frac{P_c n S_n}{\gamma} \qquad 1\text{-}9$$

where A_b is the specific interfacial area (cm^2/cm^3) between immiscible fluids per unit volume of the bulk soil, n is the porosity and S_n is the saturation of solid-wetting fluid.

Cary (1994) used a so called "capillary bundle model" that replaces the soil pores with a bundle of capillary tubes, in such a way that the pressure-saturation relationship of the hypothetical capillary tubes is the same as the soil of interest. In the capillary bundle model, the air-water interfacial area formed on the surface of capillary tubes with a radius r (cm) is:

$$\Delta s = 2\pi L r \qquad 1\text{-}10$$

where Δs represents the air-water interfacial area per unit volume of the medium (cm^2/cm^3), and L is the hypothetical length of the tubes (cm). And the specific volume of these tubes, $\Delta\theta$ (cm^3/cm^3) is:

$$\Delta\theta = \pi L r^2 \qquad 1\text{-}11$$

Eliminating πL by combining Eqs 1-10 and 1-11 gives:

$$\Delta s = \frac{2\Delta\theta}{r} \qquad 1\text{-}12$$

The specific air-water interfacial area at a water saturation is the sum of Δs over a water saturation range from the water saturation of interest to the porosity of the medium:

$$a_i = \sum \Delta s = 2 \sum_{\theta(r)}^{\theta(r_o)} \frac{\Delta\theta}{r} \qquad 1\text{-}13$$

where a_i is the specific air-water interfacial area (cm^2/cm^3). The functional relationship between $\Delta\theta$ and r was proposed by Cary (1994):

$$\frac{1}{r} = \frac{1}{r_o}\left(\frac{\theta_o}{\theta}\right)^b \left[\frac{\lambda\theta_m}{\theta} + 1\right] \qquad 1\text{-}14$$

where r_o (cm) is the radius of pores at the air-entry pressure of the medium, θ_o is the porosity, and θ_m is the specific volumetric water content when only a monolayer of water film is present on the surface of the solid particles, and λ is a fitting factor related to the surface area of solid particles. Combining Eqs 1-13 and1-14 gives an integral form of the expression that relates a_i to θ:

$$a_i = \frac{2\theta_o}{r_o} \int_{\theta}^{\theta_o} \left[\frac{\lambda\theta_m}{\theta^{(b+1)}} + \frac{1}{\theta^b}\right] d\theta \qquad 1\text{-}15$$

Although Eq. 1-15 is simple and easy to use with a Brooks-Corey constant b(Corey, 1994), estimated from the soil-moisture release curve, the estimated a_i values may be significantly underestimated due to the simplification of pore geometry especially at high water saturations. It was also found that the estimation of a_i using Eq. 1-15 varied widely depending upon the air-entry pressure determined by the Brooks-Corey model (Kim, 1996).

Skopp (1985) derived an expression that correlates the volumetric water content θ to the specific air-water interfacial area a_i, which was used for the calculation of mass transfer rate of gas (oxygen) in soils. Assumptions associated with this model are: (1) the soil water exists in tubular-shape soil pores, (2) only the meniscus at the water tube contributes to the air-water interfacial area, (3) the radius of the water tube is a function of the soil matric potential ψ_m, (4) the soil surface that is not in contact with the water tube does not contribute the air-water interface, and (5) the length of each water tube has a functional relationship with the radius r. One of the preliminary solutions for a_i of this model is:

$$a_i = \frac{12\theta}{5r} \qquad 1\text{-}16$$

where r is the radius of water tube at the water saturation θ. Using one of the ψ_m-θ relationships (Campbell, 1974):

$$\psi_m = -d\left(\frac{n}{\theta}\right)^m \qquad 1\text{-}17$$

and the capillary rise model:

$$\psi_m = \frac{2\gamma\cos(\alpha)}{r\rho_w} \qquad 1\text{-}18$$

where d and m are fitting constants, α is the contact angle between air, water, and the soil surface, and ρ_w is the density of water (g/cm^3), the final equation assuming $\alpha = 0$ is:

$$a_i = \left(\frac{6d\rho_w n}{5\gamma}\right)\left(\frac{\theta}{n}\right)^{1-m} \qquad 1\text{-}19$$

Equation 1-19 was used to evaluate the a_I for several different values of the constant m by Skopp (1985), and the a_I values are at least two orders magnitude smaller than the reported, measured values (Conklin et al., 1995; Saripalli et al., 1997; Brusseau et al., 1997; Kim et al., 1997). This resultant underestimation of a_I values is obviously due to the assumptions associated with the model development. Nonetheless, Eq. 1-19 may be appropriate for the air-water interface that contributes to the overall gas transfer rate between the bulk gaseous and aqueous phases neglecting the existence of water film that is not taken into account for the derivation of Eq. 1-19.

Pore-scale network models were used by Reeves and Celia (1996) to study the functional relationship between capillary pressure, fluid saturation, and the interfacial area between immiscible fluids. This model consists of spherical pore bodies and pore throats which connect the pore bodies. Pore bodies are placed such that a cubic lattice with constant node spacing is achieved, thus the nodes have six orthogonal connections to their neighbors. Since all the geometric parameters are known, it is possible to calculate the fluid-fluid interfacial area as a function of water saturation and/or the capillary pressure. One of the advantages of this model is that the system parameters, including the interfacial area and fluid volumes, can be accurately calculated during any stage of drainage-imbibition cycles.

Ideal Porous System-Pendular Ring Model

Gvirtzman and Roberts (1991) developed a conceptual model which describes the spatial distribution of two immiscible fluids in the pore space of media packed with spherical particles. This model is an expanded version from that of Rose (1958), who suggested a pendular ring concept to describe the shape of wetting fluid in porous media of spherical particles. Gvirtzman and Roberts (1991) generalized this model for more complicated systems which consist of spherical particles with different sizes, and are packed randomly, but homogeneously. The volume of the wetting fluid, the interfacial area between wetting and non-wetting fluids, and the solid surface area in contact with the wetting fluid for a single pendular ring with zero contact angle are (Rose, 1958):

$$V_r = 2\pi R^3\left\{2-2\cos\varphi-\tan\varphi\left[2\sin\varphi-\tan\varphi+\left(\frac{\pi}{2}-\varphi\right)\left(\frac{\cos\varphi-1}{\cos\varphi}\right)\right]\right\} \qquad \text{1-20}$$

$$A_{nw} = 4\pi R^2\left(\frac{1-\cos\varphi}{\cos\varphi}\right)\left[\left(\frac{\pi}{2}-\varphi\right)\tan\varphi-(1-\cos\varphi)\right] \qquad \text{1-21}$$

$$A_{sw} = 4\pi R^2(1-\cos\varphi) \qquad \text{1-22}$$

where V_r is the volume of a pendular ring, A_{nw} is the interfacial area between wetting and nonwetting fluids, A_{sw} is the solid surface area covered with the wetting fluid, R is the radius of a sphere, φ is the angle formed by the center of the sphere, the contact point between two spheres, and the lines that connect the center of the sphere and the points on the sphere where the fluid-fluid interface meets. There is another form of expression available in the literature (Gvirtzman and Roberts, 1991) for cases in which the contact angle is a finite value rather than zero. Since Eqs 1-20 ~ 1-22 represent the volume and interfacial areas of an individual pendular ring, proper multiplication factors are necessary for the specific values of those quantities (i.e., per unit volume of the bulk medium basis). For cubic packing, the factor is $3/8R^3$ and $6/(R^3\,4\surd 2)$ for rhombohedral packing. Note that this model is not applicable when the water content becomes large enough to connect the pendular rings.

Mass Transfer Model

Estimation of the fluid-fluid contact area (especially NAPL-water interfacial area) using the dissolution rate of the NAPL components to the aqueous phase was attempted (Hoffman, 1971; Zilliox and Muntzer, 1975; Fried et al., 1979). This method was tested for the experiments where the aqueous phase flows underneath a body of lighter-than-water-NAPL. The interfacial area was defined as (Fried et al., 1979; Miller et al, 1990):

$$a_i = f[L(t_b + t_d)] \tag{1-23}$$

where L is the length of the NAPL-containing zone, t_b is the thickness of zone with residual NAPL, and t_d is another zone where the dispersion of dissolved NAPL occurs. Although the simplicity of Eq. 1-23 is appealing, the difficulties for determining those thickness parameters limits the use of this approach (Miller et al., 1990).

Table 1-1. Surface distribution coefficients of selected organic compounds; C_{sa} -saturated concentration in gaseous phase; C_{sw} - saturated concentration in water; K_H -Henry's law constants, at 25 °C.

compounds	log K_{ia} (cm)	log K_{iw} (cm)	log C_{sa} (mol/cm^3)	log C_{sw} (mol/cm^3)	log K_{ow}	K_H (kPa m^3/mol)
n-alkanes						
pentane	−5.273	−3.574	−4.560	−6.273	3.62	125 ± 10
hexane	−3.574	−3.100	−5.089	−6.958	4.11	170 ± 25
heptane	−4.633	−2.667	−5.607	−7.534	4.66	230 ± 50
octane	−4.267	−2.185	−6.159	−8.238	5.18	300 ± 50
nonane	−3.971	−1.670	−6.730	−8.766	5.80	500 ± 200
decane	−3.615	−1.147	−7.303	−9.437	6.7	700 ± 250
aromatics						
benzene	−4.304	−4.952	−5.291	−4.642	2.13	0.550 ± 0.025
toluene	−3.930	−4.492	−5.813	−5.253	2.69	0.670 ± 0.035
ethylbenzene	−3.600	−4.047	−6.292	−5.844	3.13	0.80 ± 0.07
isopropylbenzene	−3.385	−3.613	−6.607	−6.381	–	0.130 ± 0.025
flurobenzene	−4.259	−4.733	−5.386	−4.798	–	0.63 ± 0.06
chlorobenzene	−3.908	−4.737	−6.190	−5.367	–	0.35 ± 0.05
m-dichlorobenzene	−3.566	−4.385	−7.009	−6.088	–	0.36 ± 0.02
chlorinated compounds						
dichloromethane	−4.643	−5.622	−4.631	−3.808	1.25	0.26 ± 0.02
trichloromethane	−4.411	−5.226	−4.975	−4.163	1.96	0.38 ± 0.03
tetrachloromethane	−4.772	−4.465	−5.213	−5.292	2.83	2.0 ± 0.4
1,1,1-trichloroethane	−4.535	−4.482	−5.185	−5.262	–	2.8 ± 0.04
perchloroethene	−4.485	−4.519	−6.000	−6.074	–	2.3 ± 0.4
trichloroethane	−4.578	−4.980	−5.398	−5.077	–	0.12 ± 0.02
1-chlorobutane	−4.347	−4.487	−5.261	−4.925	2.39	1.71
1-bromobutane	−4.071	−4.132	−5.654	−5.353	2.53	1.22
1,2-dichloroethane	−4.096	−5.410	−5.349	−4.056	1.45	0.11 ± 0.01
n-alcohols						
butanol	–	−5.284	–	–	0.88	–
pentanol	–	−4.775	–	–	1.16	0.00124
hexanol	–	−4.272	–	–	2.03	0.00190
heptanol	–	−3.770	–	–	2.41	0.00118
octanol	–	−3.268	–	–	3.15	0.00158
aliphatic acids						
valeric acid	–	−4.620	–	–	1.45	–
caproic acid	–	−4.180	–	–	1.90	–
heptanoic acid	–	−3.585	–	–	2.72	–
octanoic acid	–	−2.921	–	–	3.22	–

* Data from Hoff et al.(1993b), Valsaraj (1994), and Yaws et al.(1991), – data not available; Units for parameters are before log-conversion.

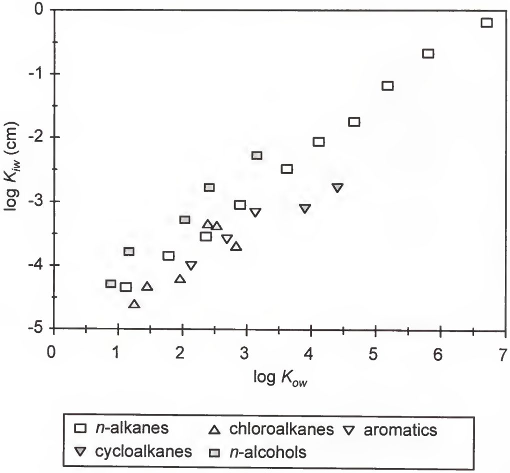

Figure 1-1. The log K_{iw} – log K_{ow} relationship for organic compounds; K_{iw} - surface adsorption coefficient (water to air-water interface), centimeter; K_{ow} - octanol water partitioning coefficient (dimensionless); data from Hoff et al.(1993b), Valsaraj (1994).

CHAPTER 2

INFLUENCE OF AIR-WATER INTERFACIAL ADSORPTION AND GAS-PHASE PARTITIONING ON THE TRANSPORT OF ORGANIC CHEMICALS IN UNSATURATED POROUS MEDIA

Introduction

Because air coexists with water and the solid matrix in the vadose zone, chemical distribution between the aqueous and gaseous phases, and adsorption at the air-water interface become potential sources of chemical retention in addition to the uptake by the solid phase (adsorption or partitioning). In water-unsaturated soils, the significance of air-water interfacial adsorption of organic contaminants with respect to other solute sorption sources were discussed in recent reports (Pennell et al., 1992; Brusseau et al., 1997). In an unsaturated soil with a fine texture and at a very low water saturation, more than half of the applied mass of some volatile aromatic compounds (e.g., *p*-xylene) was found at the air-water interface (Pennell et al., 1992). The effect of air-water interfacial adsorption on the gas-phase transport of several volatile organic chemicals has been reported using a gas chromatographic technique (Karger et al., 1971a, b; Okamura and Sawyer, 1973; Dorris and Gray, 1981; Brusseau et al., 1997). Straight-chain alcohols dissolved in pure water have been found to decrease the surface tension significantly (Posner et al., 1952; Clint et al., 1968), indicating their accumulation at the air-water interface. Aromatic compounds, without surfactant-like chemical structures (e.g., hydrophobic tail and charged functional group), were also observed to accumulate at the air-water interface to a certain degree depending on their hydrophobicities (Blank and Ottewill, 1964; Hauxwell and Ottewill, 1968, 1970; Hoff et al., 1993a,b).

Experimental determination of the air-water interfacial areas in water-unsaturated porous media has been reported independently by Saripalli et al. (1997), Kim et al. (1997), Brusseau et al.(1997), and Karkare and Fort (1996). Two types of measurement techniques have been reported. One method is to induce water migration using a water-insoluble surfactant under static conditions (Karkare and Fort, 1996), and the other method is to measure chemical adsorption at the air-water interface either from gaseous phase (Brusseau, 1997) or aqueous phase (Saripalli et al., 1997; Kim et al., 1997) under dynamic flow conditions. In this study, the retardation of *n*-octanol and *n*-nonanol was analyzed to estimate the effective air-water interfacial area of the system using the same experimental and calculation procedure reported recently by Kim et al.(1996, 1997).

In the present chapter, the effect of an air-water interface on the retardation of organic chemicals during aqueous-phase miscible displacements in a partially water-saturated column packed with a clean sand was examined. Contribution of various solute sorption mechanisms to observed retardation was estimated and compared with experimental results. The effective air-water interfacial areas estimated from *n*-octanol and *n*-nonanol retardation were compared with those obtained by displacement experiments with an anionic surfactant as an interfacial tracer (Kim et al., 1997).

Theoretical Background

Aqueous transport of organic compounds in a water-unsaturated medium is subject to retardation due to sorption by the solids, partitioning into the gas phase, and accumulation at the air-water interface. The effect of partitioning of a chemical to any potential domains in a water-unsaturated porous medium on the average travel velocity of the chemical is often expressed using a partial differential equation derived based on mass conservation and continuity. Assuming no convective or diffusive gaseous transport, and steady water flow in a homogeneous porous medium, the one-dimensional advective-dispersive model equation is (van Genuchten and Wierenga, 1986):

$$R_t \frac{\partial C_w}{\partial t} = -v_x \frac{\partial C_w}{\partial x} + D_w \frac{\partial C_w^2}{\partial^2 x} \qquad \text{2-1}$$

where R_t is the total retardation factor (dimensionless), C_w is the aqueous concentration (mol/L), v_x is the pore water velocity (cm/min), D_w is the hydrodynamic dispersion coefficient (cm^2/sec), x is distance (cm) and t is time. In applying Eq.2-1 for unsaturated steady water flow, a homogeneous volumetric water content (θ_w) is required. This condition was satisfied in our experiments by appropriate manipulation of the inlet and outlet boundary conditions for the column experiments. The total retardation factor, R_t, contains all terms which account for the retention of a chemical in the porous medium:

$$R_t = 1 + \beta_T \qquad \text{2-2}$$

where

$$\beta_T = \beta_d + \beta_a + \beta_i \qquad \text{2-3}$$

with

$$\beta_d = \frac{\rho\, K_d}{\theta_w};\quad \beta_a = \frac{\theta_a\, K_H}{\theta_w};\quad \beta_i = \frac{a_i\, K_{iw}}{\theta_w} \qquad 2\text{-}4$$

In the above equations, ρ is the bulk density of the medium (g/cm^3); K_d is the sorption coefficient of a chemical to the solid matrix (ml/g); θ_a and θ_w are volumetric gas and water contents (dimensionless), respectively; K_H is the Henry's constant (dimensionless); K_{iw} is the adsorption coefficient for the chemical accumulation at the air-water interface (cm); and a_i is the specific air-water interfacial area (cm^2/cm^3).

According to Eqs 2-3 and 2-4, the relative contribution of each term to the overall retardation factor, R_t, can be evaluated as follows:

$$f_d = \frac{\beta_d}{\beta_T};\quad f_a = \frac{\beta_a}{\beta_T};\quad f_i = \frac{\beta_i}{\beta_T} \qquad 2\text{-}5$$

Note that f_d, f_a, and f_i represent, respectively, the fractional contributions to the measured total retardation as a result of soil sorption, gas-phase partitioning, and interfacial adsorption.

The phase distribution constants (K_d, K_H, and K_{iw}) needed in Eq. 2-4 can be estimated using data from independent batch or column experiments. The soil sorption coefficient, K_d, can be estimated from a sorption isotherm measured in a series of batch experiments or from miscible displacement experiments in a saturated column ($\beta_i = 0$, $\beta_a = 0$). If the sorbed concentration of a chemical (S, g/g) is a simple linear function of the equilibrium aqueous concentration (C_w, mol/L), then:

$$S = K_d\, C_w \qquad 2\text{-}6$$

In Henry's region, the gaseous concentration of an organic compound (C_g, mol/L) is also proportional to the aqueous concentration of the compound:

$$C_g = K_H C_w \tag{2-7}$$

The gas-phase partitioning coefficients, or Henry's constants (K_H), in the dilute aqueous solutions of volatile organic compounds are also available in the literature (Mackay and Shiu, 1981; Yaws et al., 1991).

Unlike the Henry's constant (K_H) and the sorption coefficient (K_d), direct measurement of surface (or interfacial) excess of a compound at the air-water interface in unsaturated porous media is usually not feasible. However, using the Gibbs adsorption equation, an adsorption isotherm for the surface excess of a compound at the air-water interface can be determined using surface tension (or interfacial tension) data (Rosen, 1989; Saripalli et al., 1997; Kim et al., 1997):

$$\Gamma = -\frac{1}{RT}\left(\frac{\partial \gamma}{\partial C_w}\right)_T C_w \tag{2-8}$$

where Γ is the surface excess of a chemical (mol/cm^2), R is the ideal gas constant (erg/mol·°K), T is the absolute temperature (°K), and γ is the surface tension (dynes/cm). The assumptions associated with Eq. 2-8 are that the aqueous molar concentration of the compound of interest is close to its actual activity (e.g., C_w<10mM), and the compound is nonionic (Rosen, 1989). Since γ is a nonlinear function of C_w, the interfacial adsorption isotherm is nonlinear (Adamson, 1989). When the change of γ is a linear function of C_w over a limited concentration range (as will be shown to be the case for our experiments), Eq. 2-8. simplifies to a linear model:

$$\Gamma = K_{iw} C_w \tag{2-9}$$

with K_{iw} being the concentration-independent adsorption coefficient. The thermodynamic parameters for air-water interfacial adsorption of organic compounds of environmental importance are available in the literature (Valsaraj, 1994).

As seen in Eq. 2-4, when the interfacial adsorption coefficient (K_{iw}) and the air-water interfacial area per unit volume of bulk matrix (a_I) are sufficiently large, the product of these terms must be taken into account for estimating the total retardation factor of an organic compound. At the same time, if the interfacial adsorption is within a detectable range (e.g., β_I >0.01), and if the contribution of the other two terms (soil sorption, β_d, and gas-phase partitioning, β_a) are known, it will be possible to estimate the specific air-water interfacial area (a_I) in a water-unsaturated medium.

The total retardation factor (R_t) for an organic compound can be estimated from a mass balance analysis for a step input (Nkedi-Kizza et al., 1987), and temporal moment analysis for a pulse input (Valocchi, 1985). For a step input of a chemical solution, the total retardation factor is:

$$R_t = \frac{\int[1 - C_t(t)/C_t^o]dt}{\int[1 - C_{nt}(t)/C_{nt}^o]dt} = \frac{\bar{t}_t}{\bar{t}_{nt}} \qquad 2\text{-}10$$

where C is the effluent concentration of a chemical (mol/L); C^o is the influent concentration (mol/L) with subscripts, t and nt,denoting the adsorbing chemical and non-reactive tracer, respectively; and $\bar{t}$ is the mean travel time of a chemical for transport through the system. The total retardation factor from a breakthrough curve generated by applying a pulse input is calculated by the ratio of the normalized first temporal moment of the chemical to that of a non-reactive tracer:

$$R_t = \frac{\mu_t}{\mu_{nt}} \qquad 2\text{-}11$$

where μ is the pulse-corrected, normalized, first temporal moment of a chemical (subscript t), and a non-reactive tracer (subscript nt).

Materials and Methods

Materials

Three classes of organic compounds were investigated: (1) four straight-chain alcohols (*n*-hexanol, *n*-heptanol, *n*-octanol, and *n*-nonanol); and (2) three chlorinated aromatic hydrocarbons (chlorobenzene, *o*-dichlorobenzene, and *o*-chlorophenol); and (3) two alkylbenzenes (ethylbenzene and *p*-xylene). Reagent-grade (purity >99%) alcohols were supplied by Aldrich Chemical Co., while reagent-grade (purity >99%) aromatic compounds were purchased from Fisher Scientific Co.; all of the chemicals were used as received. Bromide as sodium bromide (purity >99%) was supplied by Mallinckrodt Chemical Works Co., and used as a non-reactive tracer. HPLC-grade water (Fisher Scientific Co.) was used in all batch and column experiments.

Two different stock solutions were prepared for the alcohol displacement experiments. The first stock solution contained all of the alcohols and bromide at the following concentrations: *n*-hexanol, 4.9 mmol/L; *n*-heptanol 1.1 mmol/L; *n*-octanol, 0.44 mmol/L; *n*-nonanol, 0.35 mmol/L; and 0.35 mmol/L of bromide. The second stock solution contained only 0.35 mmol/L of *n*-nonanol and the same concentration of bromide. An aqueous stock solution of the aromatic compounds was prepared at the following concentrations: chlorobenzene, 0.73 mmol/L; ethylbenzene, 0.21 mmol/L; *p*-xylene, 0.24 mmol/L; *o*-chlorophenol, 1.5 mmol/L; *o*-dichlorobenzene, 0.22 mmol/L; and 0.35 mmol/L of bromide. These stock solutions were used as the displacing solutions for the miscible displacement experiments in both saturated and unsaturated sand columns.

The sand sample used for the column experiments was cleaned using the following procedure. A bulk sample of blast sand was first sieved to different sizes, washed with tap water several times, and then dried in an oven at 105 °C for 24 hours. In order to remove any organic carbon residue, the sand samples were baked in a muffle furnace at 500 °C for more than 24 hours. Baked sand samples were then remixed with a known size distribution : 1 mm~500 μm (diameter, based on sieve size), 20 %; 500~300 μm, 40 %; 300~180 μm, 30 %; 180~105 μm, 10 %. The source and treatment procedure of the sand sample used in this study are the same as in the previous study (Kim et al., 1997).

Miscible Displacement Experiments

The experimental procedures used were essentially identical to those used in an earlier study (Kim et al., 1997). A glass column (10.4 cm length, 5.45 cm diameter), which has the same design described by Annable et al. (1993), was packed with the sand mixture. Small increments of the sand were added successively into the column which was initially filled with water. This packing procedure eliminated air entrapment in the water-saturated sand column. Considerable care was taken not to generate any layer formation during the packing process. The saturated hydraulic conductivity of the packed column was 10.7 cm/hour. The air-entry pressure was about 25 mbar and the porosity was 0.35. A stainless steel capillary barrier (air-entry pressure of 250 mbar) was sealed at the bottom of the column. A glass fiber filter paper was placed at the top of the packed sand. The top of the sand column was sealed with a stainless steel plate to prevent volatilization losses. A small orifice at the top plate allowed atmospheric pressure at the upper region of the column during the unsaturated flow experiments. The packed sand column was used for both saturated and unsaturated flow experiments without repacking. Detailed configuration of the column was shown in Fig. 2-1.

Prior to unsaturated flow experiments, water-saturated displacement experiments were conducted for both the alcohol mixture solution and the aqueous solution of aromatic compounds to obtain the values for the soil sorption coefficients (K_d). Aqueous solutions were displaced through the saturated columns in an upward mode. For the unsaturated column experiments, the required degree of unsaturation was achieved by maintaining a steady flux boundary condition at the inlet and a constant negative pressure at the bottom of the column. The inlet of the solution was changed to the top of the column, and a stainless steel tubing (35~100 cm) was installed at the outlet end to maintain a constant negative pressure at the bottom of the column equal to the length of the tubing. The target level of water saturation was achieved by controlling primarily the influent flow rate of the solution for each experiment. Short stainless steel tubings (35, 38 cm) were used only for high water saturation conditions. Volumetric water contents were measured gravimetrically after establishing steady state water flow conditions (i.e., outlet flow rate is equal to inlet flow rate), both before and after the displacement experiments. These were compared with the estimates based on the mean residence time of bromide. A step input of aqueous solution was used for the alcohols. For the aromatic compounds, a 0.2~0.4 pore volume solution pulse was applied to the column.

Effluent samples from the column were collected using a fraction collector (ISCO, Retriever 500) and analyzed using a gas chromatograph (Perkin Elmer, AutoSystem) equipped with flame ionization detector. Non-reactive tracer (bromide) was analyzed using a high performance liquid chromatograph with an ion exchange column (Dionex, AS4A) and a UV detector (LDC Analytical, spectroMonitor® 3100) set at 205 nm. Schematic diagram of the unsaturated column experiments is shown in Fig. 2-2. Based on the measured breakthrough curves, the total retardation factors (R_t) were determined using Eq. 2-10 (alcohols) and Eq. 2-11 (aromatic compounds)

Surface Tension Measurements

Surface tensions of *n*-octanol and *n*-nonanol aqueous solutions were measured by the drop-weight method (Harkins and Brown, 1919). A series of *n*-octanol and *n*-nonanol aqueous solutions were prepared from stock solutions. At least ten droplets of the alcohol solution from a glass tubing (radius 0.2445 cm) were collected and weighed using a chemical balance (Mettler AE260). Drop forming rate was 30 ± 2 sec/drop. The loss of solution weight during droplet collection was less than 0.4% of the total weight. An aliquot of each sample from the glass tubing was taken for the gas chromatography (GC) analysis to estimate the exact alcohol concentrations in the solution.

Results and Discussion

Retardation of Chemicals

A consistent trend of increasing total retardation with decreasing water content was observed for the *n*-alcohols and the two classes of aromatic compounds (Figures 2-3 and 2-4). Also, with decreasing water content the solute breakthrough curves are quite skewed and show considerable tailing (Figures 2-3 and 2-4), which might be the result of a rate-limiting mass transfer processes during miscible displacement (Brusseau et al.,1997; Kim et al., 1997). Note that according to Eqs 2-2~4, the total retardation factor (R_t) increases with decreasing water content no matter which domain is the major contributor to the total retardation factor provided that a_t term in Eq. 2-4 is either constant or increases as water content decreases.

The relative contribution of different modes of solute retention can be calculated since the values of all of the parameters in Eq. 2-4 can be estimated from independent sources. From the retardation factors measured under saturated water flow conditions, the K_d values were estimated, and used to predict the contribution of soil sorption (β_d) at all other water contents. This requires the assumption that K_d is independent of θ_w, at least over the range of θ_w we investigated. Contribution of the gas-phase partitioning (β_a) can be estimated given the published values for the Henry's constants (see Table 2-1). The use of Henry's constants requires that the experiments are conducted at low solute concentrations (Schwarzenbach et al., 1993). The interfacial adsorption coefficient, K_{iw}, can be estimated based on published data (Posner et al., 1952; Hoff et al., 1993b; Valsaraj, 1994) or from the air-water interfacial tensions measured in the presence of the organic compound under investigation (Saripalli et al., 1997; Kim et al., 1997) (see Table 2-1). The specific air-water interfacial area (a_i) at different water saturations was estimated using the following empirical regression equation reported earlier (Kim et al., 1997), based on measured data for surfactant adsorption:

$$a_i = -64.7\ S_w + 64.7 \quad ; \quad r^2 = 0.99 \qquad \text{2-12}$$

where $S_w = \theta_w / (\theta_a + \theta_w)$ is the degree of water saturation. In Figure 2-5, the measured and predicted retardation factors are compared. In all cases, the predicted decrease in the total retardation factor (R_t) with increasing water saturation (S_w) was in good agreement with the experimental observations.

. Since the Henry's constant (K_H) values for the *n*-alcohols are quite small, the partial contribution to the retardation factor due to gaseous partitioning, $\beta_a = K_H\ \theta_a/\theta_w$, is essentially negligible. However, large K_{iw} values of for the alcohols result in a significant contribution, $\beta_i = a_i K_{iw} / \theta_w$, due to adsorption at the air-water interface (Table 2-1). For example, for the predicted $\beta_T = 0.99$ for *n*-nonanol at $\theta_w = 0.12$, the fractional contributions (f) of gaseous partitioning, soil sorption, and interfacial adsorption were 0.001, 0.12, and 0.88, respectively. Note that the K_{iw} values for the *n*-alcohols decrease as the carbon chain length decreases. Accordingly, at a given water content and under the same experimental conditions, the retardation factors of the *n*-alcohols with longer carbon chains are larger than those of the alcohols with relatively short carbon chains.

The major factor contributing to the retardation of aromatic compounds investigated in this study is different from that for the *n*-alcohols described above. Due to relatively small air-water interfacial adsorption coefficients (K_{iw}), and large gaseous partitioning coefficients

(K_H), the retardation of chlorobenzene, ethylbenzene, and *p*-xylene is dominantly due to gaseous partitioning during the miscible displacement. For *o*-dichlorobenzene, with a relatively small K_H compared to other aromatic compounds used in this study, the soil sorption is responsible for 70 % of the observed retardation (Table 2-1). Even though the contribution of air-water interfacial adsorption of the aromatic compounds to the total retardation factors was not significant in this study, the effect of interfacial adsorption could have an important role in systems with a much larger specific air-water interfacial area. Similarly, for soils having a larger organic carbon content and larger K_d values, the contribution of soil sorption to retardation can be substantial.

Although the individual fractions (β) of predicted retardation factors were not listed in Table 2-1 for experiments conducted at higher water contents (θ_w>0.12), the results were consistent with those listed in the table for both aromatic compounds and alcohols.

The retardation factor of *n*-nonanol in a solution without any other organic compounds except sodium bromide is slightly larger than that of *n*-nonanol in a mixture of alcohols (Fig. 2-5a). This effect of other alcohols in the solution on the surface excess of *n*-nonanol is caused by a combination of reasons. An alcohol in a mixture solution may have a different chemical activity from that in a pure aqueous solution, and more importantly, there may be a significant surface activity difference between an alcohol in a mixture and that in an aqueous solution with only the alcohol of interest. The predicted R_t values of aromatic compounds were based on K_{iw} and K_H estimated from data for single-component solutions. However, the R_t values measured for multi-component experiments do not deviate significantly from the predicted values (Fig. 2-5b). This may not always be the case for other experimental systems. It is not clear whether the K_{iw} value of an aromatic compound will change significantly due to other dissolved chemical species. In a water unsaturated system with a relatively small quantity of air-water interfacial area (e.g., the sand used in this study), the fraction of the retardation factor due to interfacial adsorption will be still negligible unless a dramatic increase of surface excess is induced by other compounds (e.g., anionic surfactant with dissolved electrolytes). Henry's constant of an aromatic compound is known to be affected by other organic/inorganic compounds depending on their concentrations. When the retardation factor of an organic compound is substantially different from that predicted by the Henry's constant, a correction (for the aqueous activity coefficient change) will be necessary to obtain an accurate Henry's constant of the compound.

Mass recovery of aromatic compounds during unsaturated flow experiments varied from 60 % to 100 % depending on the sampling duration and the magnitude of Henry's constants. However, no mass loss was observed for alcohols under the same experimental conditions. Since alcohols (e.g., *n*-hexanol) are typically less resistant to microbial degradation than aromatic compounds, the mass loss of aromatic compounds is considered to be caused by volatilization. Under slow flow rate conditions, a longer sampling duration (collecting column effluent samples in open GC vials) was necessary to obtain a minimum quantity of sample (2 ml) for GC analysis. Assuming volatilization is the only source of mass loss and that the mass loss is directly proportional to the aqueous concentrations of aromatic compounds in samples, no correction for the R_t calculation is required. Note that while the mass recovery (zeroth moment) may not be 100 % due to volatilization, the nomalized first moment is not impacted. However, if most mass loss is due to microbial activity during the column experiments, a correction must be incorporated (Annable et al., 1998), which will increase the uncorrected R_t about 15~20 % with about 40 % mass loss.

Estimation of Air-Water Interfacial Area

Equation 2-4 can also be used to estimate the specific air-water interfacial area (a_i) accessible to an aqueous interfacial tracer during an unsaturated displacement. The surface tension of *n*-octanol and *n*-nonanol aqueous solutions were measured over a range of alcohol concentrations (Fig. 2-6) and the K_{iw} values were calculated based on the Gibbs adsorption equation (Eq. 2-8). The surface tension-concentration curves for both alcohols are essentially linear ($r^2 > 0.99$) at the column input concentrations (C^o) used in the miscible displacement experiments. In the previous study (Kim et al., 1997), sodium dodecylbenzenesulfonate (SDBS) was used as the tracer to estimate the effective specific air-water interfacial areas as a function of water content for the same sand sample. An empirical equation (Eq. 2-12) derived based on the SDBS retardation data, was used as a reference for the interfacial area calculation in this study. Only *n*-octanol and *n*-nonanol results were used to estimate the interfacial areas. The other alcohols did not provide retardation factors large enough to be statistically reliable for interfacial area estimation. However, a comparison between estimated and predicted retardation factors (using Eq. 2-12) at a volumetric water content of 0.12 was attempted for all the alcohols (Table 2-1).

The calculated specific air-water interfacial areas are consistent with the result from the SDBS experiments (Fig. 2-7). Greater scattering in data points were observed for the interfacial areas estimated from *n*-octanol compare to *n*-nonanol. This is due to the small total retardations that generated more relative errors in the interfacial areas. The air-water interfacial areas estimated from the experiments with the solutions containing only *n*-nonanol was slightly larger than those of aqueous solutions with alcohol mixture. Based on the assumption that a mixture of surface active compounds (e.g., *n*-alcohols) with different K_i values does not significantly change the adsorption characteristics of each compound, application of the mixture will provide a better opportunity to obtain adequate retardation factor(s) for at least one or more compounds when the air-water interfacial area is unknown. If more than one compound can be applicable for the air-water interfacial area determination, confirmation of the acquired air-water interfacial area by multiple compounds will be possible. A similar strategy of using multiple partitioning tracers to estimate residual NAPL saturation in porous media has been used by Jin et al.(1995).

Summary

In laboratory column experiments, the aqueous-phase transport of four *n*-alcohols (*n*-hexanol ~ *n*-nonanol), three chlorinated aromatic compounds (chlorobenzene, *o*-dichlorobenzene, and *o*-chlorophenol), and two alkylbenzenes (ethylbenzene, and *p*-xylene) in a water-unsaturated porous medium (sand) was investigated. The influence of gas-phase partitioning and interfacial adsorption on solute retardation during steady unsaturated water flow was evaluated over a range of water contents. Air-water interfacial adsorption was a significant factor for the retardation of *n*-alcohols. For example, nearly 90% of the measured retardation of *n*-nonanol could be attributed to interfacial adsorption at a water saturation of 34%. Aromatic compounds used in this study were not significantly affected by adsorption at the air-water interface because of both low air-water interfacial area (0~50 cm^2/cm^3)

generated in the unsaturated porous medium, and the small interfacial-adsorption coefficients. Instead, gas-phase partitioning was the primary mechanism responsible for the measured retardation of most of the aromatic compounds evaluated in this study. Using the batch-measured interfacial adsorption coefficients for *n*-octanol and *n*-nonanol and the column-measured retardation factors, the effective air-water interfacial areas were estimated. These values agreed closely with those reported earlier, based on displacement experiments with an anionic surfactant as an interfacial tracer.

Table 2-1. The sorption coefficients and the contribution of different modes of solute retention to the total retardation factor at a water content of 0.12.

chemical	K_d ml/g	K_H (a) dimensionless	K_{iw} (b) cm	β_d	β_a	β_i (c)	R_t predicted	R_t experiment
			alcohols					
n-hexanol	ND[d]	7.64×10^{-4}	9.36×10^{-5}	ND	1.5×10^{-3}	0.033	1.03	1.15
n-heptanol	ND	4.74×10^{-4}	4.39×10^{-4}	ND	9.1×10^{-4}	0.155	1.16	1.24
n-octanol	0.0021	6.48×10^{-4}	9.73×10^{-4}	0.029	1.2×10^{-3}	0.345	1.38	1.46
n-nonanol	0.0084	6.75×10^{-4}	2.45×10^{-3}	0.12	1.3×10^{-3}	0.868	1.99	2.11
			aromatic compounds					
chlorobenzene	0.00843	0.127	2.09×10^{-5}	0.117	0.243	0.007	1.37	1.39
o-dichlorobenzene	0.0274	0.0766	-	0.379	0.147	-	1.53	1.49
o-chlorophenol	0.00633	2.3×10^{-5}	-	0.088	4.4×10^{-5}	-	1.09	1.06
p-xylene	0.0127	0.286	6.98×10^{-5}	0.176	0.548	0.025	1.75	1.74
ethylbenzene	0.0105	0.344	7.07×10^{-5}	0.145	0.659	0.025	1.83	1.91

(a) data from Yaws et al., (1991) (all alcohols), Lide (1993) (*o*-chlorophenol), Mackay and Shiu (1981) (chlorobenzene, *o*-dichlorobenzene, *p*-xylene, ethylbenzene)

(b) data from Posner et al., (1952) (*n*-hexanol, *n*-heptanol), Valsaraj (1994) (ethylbenzene, chlorobenzene), Pennell et al., (1992) (*p*-xylene), data not available for *o*-dichlorobenzene and *o*-chlorophenol

(c) an air-water interfacial area of 42.5 cm^2/cm^3 estimated using Eq. 2-12 was used to predict β_i

(d) ND : not detectable at 10^{-4} cm^3/g level (K_d)

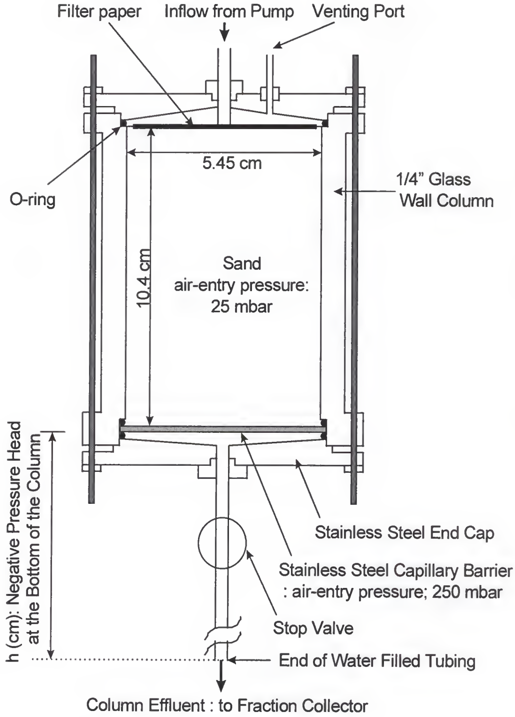
Filter paper
Inflow from Pump
Venting Port
5.45 cm
O-ring
1/4" Glass Wall Column
10.4 cm
Sand
air-entry pressure:
25 mbar
h (cm): Negative Pressure Head at the Bottom of the Column
Stainless Steel End Cap
Stainless Steel Capillary Barrier
: air-entry pressure; 250 mbar
Stop Valve
End of Water Filled Tubing
Column Effluent : to Fraction Collector

Figure 2-1. Detailed column configuration for the unsaturated column experiments.

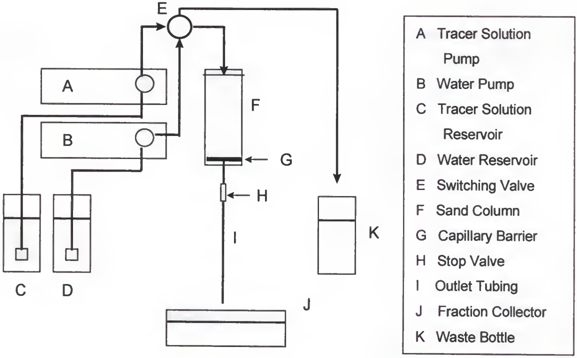

Figure 2-2. Experimental set-up for unsaturated column experiments.

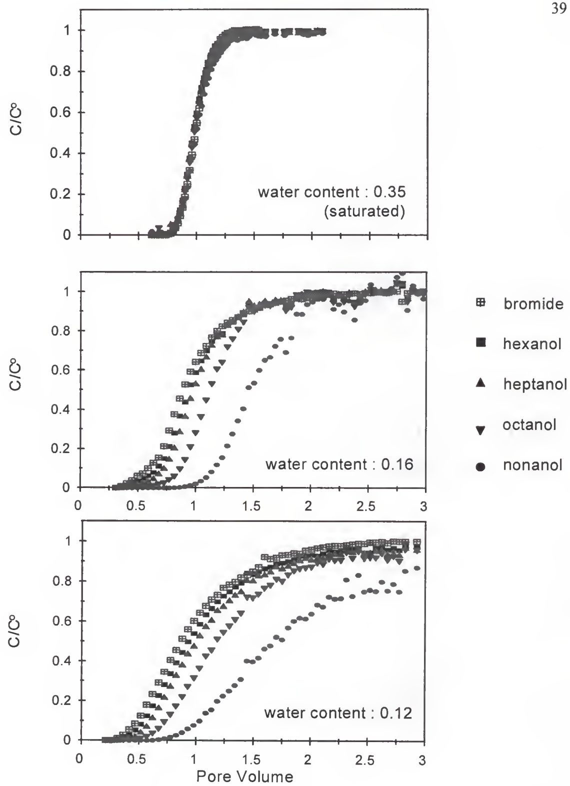

Figure 2-3. Breakthrough curves for bromide and four alcohols at three different water contents.

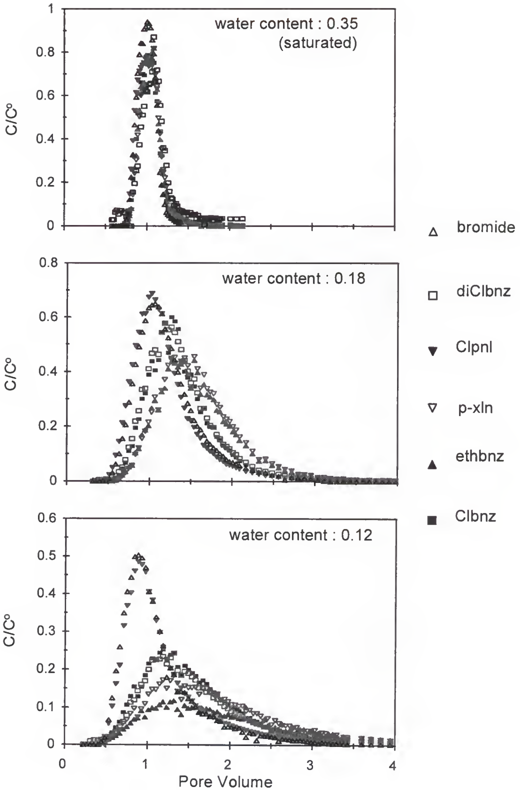

Figure 2-4. Breakthrough curves for the transport of aromatic compounds and bromide; Cl-chloro: bnz-benzene: eth-ethyl: pnl-phenol.

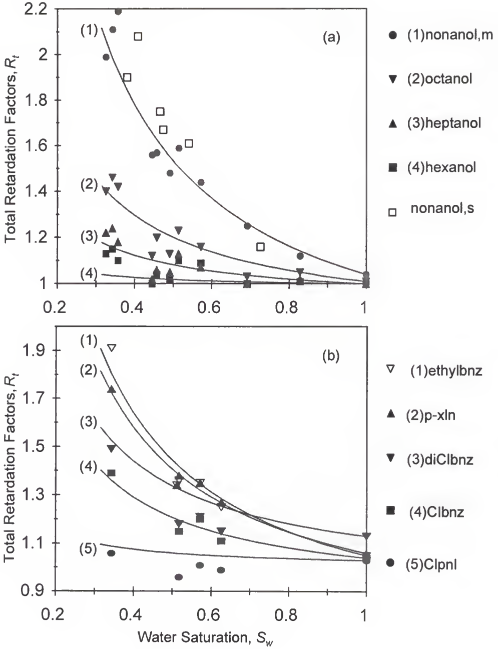

Figure2-5. Effect of water saturation on the total retardation factors (R_t) of alcohols (a), and aromatic compounds (b). All the retardation sources (soil sorption, gaseous partitioning, and air-water interfacial adsorption) were taken into account for the predicted curves (solid lines); nonanol, m - alcohol mixture solution: s - single component solution; notation for aromatic compounds is the same as in Fig. 2-4.

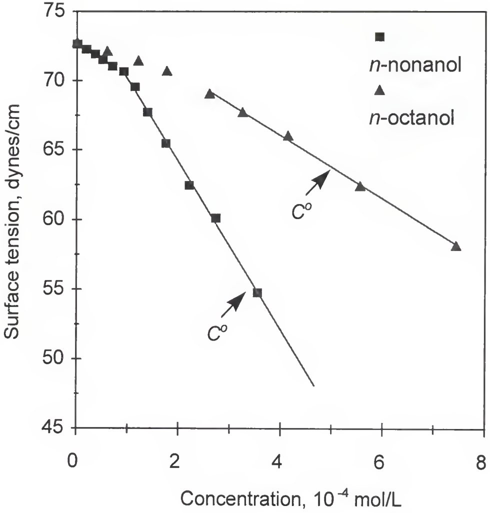

Figure 2-6. Measured surface tensions of *n*-octanol and *n*-nonanol; C^o represents the influent alcohol concentration used during the column experiments.

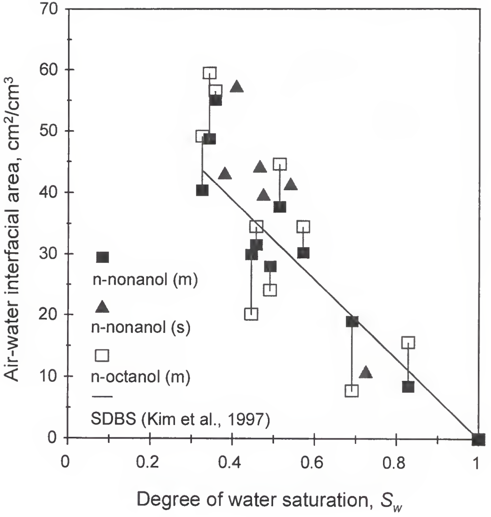

Figure 2-7. Correlation of the specific air-water interfacial areas (a_i) calculated from the retardation of *n*-octanol (in mixture) and *n*-nonanol [in mixture (m) and single-component solution(s)] with the degree of water saturation (S_w); an empirical curve from SDBS displacement experiments by Kim et al. (1997) were overlaid for comparison; vertical lines represent data from one experiment with a suite of alcohols.

CHAPTER 3
GASEOUS TRACER APPLICATION FOR THE ESTIMATION OF AIR-WATER INTERFACIAL AREAS, INTERFACIAL MOBILITY, AND WATER CONTENTS IN PARTIALLY SATURATED POROUS MEDIA

Introduction

It has been recognized that many environmentally important physical/chemical processes occurring in unsaturated soils (e.g., in vadose zone) are strongly influenced by the quantity and morphology of the air-water interface. The air-water interface is one of the major controlling factors of mass and energy transfer processes, such as evaporation, volatilization, gas exchange, heat flow in water-unsaturated soils (e.g., Skopp, 1985). The air-water interface often affects the distributions of organic contaminants under conditions where the interface itself acts as a significant pool of organic compounds (e.g., Posner et al., 1952; Dorris and Gray, 1981; Hauxwell et al., 1992; Pennell et al., 1992; Valsaraj, 1994), which may alter the transport of surface-active organic contaminants. Water retention and flow in soils has been studied extensively over the past three decades (Bear, 1972; Freeze and Cherry, 1979; Hillel, 1982; Iwata et al., 1988), but a thorough understanding of the behavior of air-water interfaces has not been achieved because methods for experimental measurement of air-water interfaces had been lacking.

Significant advances were made in developing models for prediction of the fluid-fluid interfacial areas (including the air-water interface) and pore-scale distributions of immiscible fluids in porous media. These models were based on either physical simplification of complex pore-scale geometry (e.g., Skopp, 1985; Miller et al.,1990; Gvirtzman and Roberts, 1991; Cary, 1994; Reeves and Celia, 1996) or thermodynamic interpretation of multi-fluid porous media (Leverett, 1941; Gray and Hassanizaheh, 1991; Bradford and Leij, 1997). Lack of direct experimental proof of the model predictions has inevitably led to questions regarding their validity to predict the interfacial areas between immiscible fluids. Experimental approaches to measure fluid-fluid interfacial areas in porous media started to appear only recently (Kakare and Fort, 1996; Saripalli et al; 1997, 1998a,b; Kim et al., 1997; Brusseau et al., 1997).

Saripalli et al. (1997, 1998a, b) and Kim et al (1997) reported on the use of a water-soluble anionic surfactant, sodium dodecylbenzene sulfonate (SDBS), to measure oil-water and air-water interfacial areas in porous media. A field-scale application of this technique to measure oil-water interfacial areas in an aquifer contaminated with fuel hydrocarbons was described by Annable et al. (1998a). Kakare and Fort (1996) proposed the use of a water-insoluble surfactant to measure air-water interfacial areas. Their method involves quantifying the water movement induced from the addition of a water-insoluble surfactant, and relating it to changes in interfacial tension resulting from surfactant adsorption. Brusseau et al (1997) reported an experimental technique, based on the use of *n*-heptane as the gaseous interfacial tracer, to determine the air-water interfacial areas in water unsaturated soil columns.

The air-water interfacial areas determined by different experimental methods (i.e., aqueous and gaseous tracers, and induced water migration) may not necessarily represent an identical physical interfacial domain. For example, the aqueous interfacial tracer may not be able to detect all of the air-water interface present in the system. Aqueous tracers are likely to underestimate the interfacial areas due to the mobility of the interface even when the tracer does detect all of the interface (Kim et al., 1997). However, air-water interfacial areas obtained from aqueous tracer experiments can be useful for the prediction of transport behavior of surface-active organic contaminants which are subject to adsorption at the same air-water interface as that detected by the aqueous tracer (see Chapter 2). On the other hand, the air-water interfacial areas measured by gaseous interfacial tracers may be close to the absolute values for the media, though the interfaces that are not hydrodynamically connected to mobile gaseous phase are excluded from the measured areas. The air-water interfacial areas measured by gaseous tracers, by the same reason as aqueous tracers, can provide important information for the prediction of the gaseous transport of surface-active volatile organic compounds (VOCs) in the vadose zone. Finally, the method proposed by Kakare and Fort (1996) measures all the air-water interfaces by using pre-adsorbed surfactant at the all the interface to induce water migration toward zone with no adsorbed surfactant at the interface.

A number of methods, for either field- or lab-scale applications, were developed for the estimation of water contents in water-unsaturated porous media. Conventional methods include using tensiometers (measures soil matric potential), neutron thermalization, gamma ray attenuation, time-domain reflectometry, and electric resistence blocks (Gardner, 1986). In unsaturated soils with continuous gaseous phase, water-partitioning gaseous tracers were successfully used for water content measurements at a single water content (Brusseau et al., 1997). Water-partitioning gaseous tracers for water content measurement can be any organic or inorganic compounds with appropriate vapor pressure at the temperature of the porous medium of interest and minimal adsorption at the solid matrix. It is required that the background concentrations of the chemicals used as water partitioning tracers should low enough not to interfere with quantitative monitoring of the tracer.

In this chapter, the results of a series of column experiments for measuring the specific air-water interfacial areas as a function of the water saturation using a gaseous interfacial tracer (*n*-decane) were presented. Water contents were estimated using water-partitioning tracers (chloroform and methylene chloride) or directly measured gravimetrically. Based on the difference in air-water interfacial areas measured using gaseous and aqueous tracers, the interfacial velocity relative to that of the bulk pore-water was estimated.

Materials and Methods

Reagent grade *n*-decane, used as gaseous interfacial tracer, and chloroform and methylene chloride, used as gaseous water-partitioning tracers, were purchased from Fisher Scientific Co., with purity of >99 %. Methane gas, from Aldrich Chemical Co., with 99 % of purity was used as the non-reactive gaseous tracer. Ultra-pure nitrogen (>99.999 %) was used as the carrier gas for gas chromatograph (GC) experiments.The chemical properties of the tracers used are shown in Table 3-1.

A stainless steel column (30.0 cm × 1.0 cm) was packed with a clean sand; the pretreatment of this sand and results from previous studies were described by Kim et al.(1997). The porosity of the packed column was 0.36, estimated gravimetrically. A small increment of water (100~200 μL) was injected into both ends of the column, which was completely dry initially, to achieve the desired water content. After water injection, the column was sealed with stainless steel plugs, and heated at 150 °C for more than 24 hours to distribute the water evenly throughout the column. The column was then cooled down to the room temperature (22°C), and installed in a modified GC (Shimadzu, GC-14A) for gaseous miscible displacement experiments. The carrier gas (nitrogen) was saturated with water by passing through a 1-L flask filled with water to preclude moisture loss from the soil column during the gaseous tracer experiments. The temperature of all the GC components, except flame ionization detector (FID), was maintained at room temperature (22°C), while the temperature of FID was set at 230°C. Water saturation of the sand-packed column was measured gravimetrically before and after each experiment. A schematic diagram of the experimental set up is shown in Figure 3-1.

About 3~10 μL of head space of the tracer containing vials (40-mL vial with 5~10 mL of neat tracer) was withdrawn with a gas-tight syringe, and injected into the GC injection port as a Dirac pulse. The net weights of injected chloroform and methylene chloride were approximately 2~5 μg, and 0.1 μg level for *n*-decane. Methane gas was depressurized to ambient atmospheric pressure before injection. About 1~ 5 μL methane gas was injected with the same manner as other tracers. Pore carrier gas velocity during a gaseous tracer displacement experiment was maintained constant at about 10~17 cm/min. The tracer concentrations in the column effluent was continuously monitored by a FID detector during each tracer displacement experiment and a strip chart recorder (Fisher Co., Recordall, Series 5000) was used for a real-time data collection.

Data Analysis

The specific air-water interfacial areas (a_i) were calculated based on the total retardation factors (R_t) for *n*-decane pulse displacement experiment :

$$R_t = 1 + \frac{\theta_w}{\theta_a K_H} + \frac{\rho K_d}{\theta_a K_H} + \frac{a_i K_{ia}}{\theta_a} \qquad 3\text{-}1$$

The total retardation factors (R_t) for *n*-decane were estimated from the normalized first temporal moments (Eq. 2-10, 11) of methane and *n*-decane breakthrough curves (BTCs). The water partitioning term [$\theta_w/(\theta_a K_H)$] and the soil sorption term [$\rho K_d/(\theta_a K_H)$] were not included in estimating a_i because of the extremely low water solubility of *n*-decane (Table 3-1). A published value for *n*-decane vapor-phase adsorption coefficient (K_{ia} = 0.226 μm) at the air-water interface (Hoff et al., 1993b) was used for the a_i calculation.

Volumetric water contents (θ_w) were estimated using the retardation factors (R_t) of the water partitioning tracers (methylene chloride and chloroform) and Eq. 3-1. The soil sorption term, [$\rho K_d/(\theta_a K_H)$], and interfacial adsorption term [$a_i K_{ia}/\theta_a$] were not used for the θ_w estimation due to negligible soil sorption and interfacial adsorption for the water partitioning tracers.

Results and Discussion

Water-Partitioning Tracer

Application of water-partitioning gaseous tracers allows measurement of water saturation ($S_w = \theta_w / \varepsilon$, ε; porosity) in the gas-flow domain that the air-water interfacial area is to be measured by the gaseous interfacial tracer. When the spatial extent that the gaseous interfacial tracer is to be applied is not confined with a physical boundary (as the stainless steel column used in this study), it is necessary to measure the water saturation of the swept volume in the flow domain. Since identical flow configuration can be used for water-partitioning and interfacial tracer, the physical domain that both of the tracers are to be applied is the same, assuming that the gaseous diffusion does not determine the swept volume for the tracers.

Even though the idea that gaseous chemicals can be used as water-partitioning tracers for water content measurement has been demonstrated previously (e.g., Brusseau et al.,1997), a thorough investigation of the validity of water-partitioning tracers over a wide range of water contents has not been performed. In this study, two chlorinated methanes (methylene chloride and chloroform) were used as water-partitioning tracers. These chemicals were selected as the gaseous tracers because they have optimum Henry's law constants, minimal air-water interfacial adsorption coefficients (Table 3-1), are not likely to be present as background concentrations, and can be detected using either FID or, preferably, electron capture detector (ECD) with a low detection limit. Water-partitioning tracer experiments were conducted up to 56 % water saturation, and the lowest water saturation achieved was about 1.5 %.

The BTCs for methylene chloride and chloroform at different water saturations are shown with the non-reactive tracer (methane) in Figure 3-2. It is evident that the retardation of the water partitioning tracers increases as S_w increases, due to tracer partitioning into the bulk water phase. The water contents estimated using water-partitioning tracers were in excellent agreement with those measured directly by gravimetric techniques (Fig. 3-3). The relative error of the measured water contents with respect to the gravimetrically determined water contents was less than 5 % throughout the experiments. No significant difference was found in measured water contents using methylene chloride and chloroform.

Interfacial Tracer

The breakthrough curves (BTCs) of *n*-decane (Fig. 3-4) demonstrate that the gas-phase retardation of *n*-decane decreases with increasing water saturation. At the same water saturation, BTC for methane was more dispersed than that of *n*-decane; this is attributed to faster gaseous diffusion for methane. The BTC of *n*-decane also spreads as the air content increases due to longer residence time in the column. Based on the symmetrical BTCs, significant rate-limited mass transfer processes were absent during gaseous transport of *n*-decane and methane.

Specific air-water interfacial areas (a_I) estimated using *n*-decane as a gaseous interfacial tracer are shown in Figure 3-5, and are overlaid with the data from aqueous tracer experiments reported earlier (Chapter 2; Kim et al., 1997). The porous medium (sand) used in this study is the same as that used in the aqueous tracer experiments. The a_I measured using *n*-decane vapor as a gaseous interfacial tracer increases exponentially as the water saturation decreases, while the a_I measured using the aqueous tracers increases linearly with decreasing water saturation. This nonlinear relationship between a_i and θ_w, in general, agrees with those predicted by model simulation results (e.g., Cary, 1994). At a very low water content ($\theta_w = 0.005$; water saturation, $S_w = 1.5$ %), the measured a_i (1,500 $cm^2\ cm^{-3}$), which is not included in the regression function, is much larger than that predicted (780 cm^2/cm^3) from the fitting function. The sharp increase of a_i in the low water content region is, as described by Cary (1994), the result of microscopic surface roughness of the geosorbents (sand, in this study) that is reflected at the air-water interface as the thickness of the water film becomes very thin.

A significant difference was found in the a_i values measured using the gaseous and aqueous tracers (Fig. 3-5), and the difference increases as the water saturation decreases. Two possible causes for this difference are: (1) mobility of the adsorbed tracers at the air-water interface during the aqueous transport experiments; (2) and accessibility of the air-water interface to the tracers introduced either through the gaseous or liquid mobile phase. The adsorbed aqueous interfacial tracers at the air-water interface may move in the same direction as the bulk water flow with a velocity that is somewhere between zero (stagnant) and slightly higher than the pore water velocity as in film flow down an inclined plane. Gaseous flow, however, does not induce nearly as significant water flow at the air-water interface. At low water saturation, some fraction of water (thus, air-water interface) may not be accessible to the aqueous phase tracer. This hydrodynamically isolated water in the porous medium may still be accessible to the gaseous tracer because the gaseous phase is dominantly continuous. The opposite is true at high water saturations; the aqueous tracer may detect most of the air-water interface, while the gaseous tracer may see only a fraction of the interface.

Assuming that all of the air-water interface is accessible to both aqueous and gaseous tracers at the middle range of water content where both tracer techniques are applicable, the interface mobility term should be incorporated for the aqueous transport of surface-active chemicals. The modified one-dimensional advective (equilibrium, steady state water flow) model with the interfacial mobility terms for the aqueous transport is:

$$\frac{\partial}{\partial t}[\theta_w C_w + a_i \Gamma] = -\frac{\partial}{\partial x}[q_w C_w + q_i C_i] \qquad 3\text{-}2$$

Based on the relationship between the surface excess (Γ) and the hypothetical concentration in the interfacial phase:

$$\theta_i C_i = a_i \Gamma = a_i K_{iw} C_w \qquad 3\text{-}3$$

the concentration at the air-water interface, C_i, is the function of C_w:

$$C_i = \frac{a_i K_{iw} C_w}{\theta_i} \qquad 3\text{-}4$$

Defining the pore water velocities, v_b in bulk aqueous phase, and v_i at the air-water interface:

$$v_b = \frac{q_w}{\theta_w}, \qquad v_i = \frac{q_i}{\theta_i} \qquad 3\text{-}5$$

Substitution of Eqs 3-3~5 to Eq. 3-2 results in:

$$\theta_w \frac{\partial C_w}{\partial t} + a_i K_{iw} \frac{\partial C_w}{\partial t} = -v_b \theta_w \frac{\partial C_w}{\partial x} - v_i a_i K_{iw} \frac{\partial C_w}{\partial x} \qquad 3\text{-}6$$

Rearrangement of Eq. 3-6 yields:

$$\left[1 + \frac{a_i K_{iw}}{\theta_w}\right]\frac{\partial C_w}{\partial t} = -\left[v_b + \frac{v_i a_i K_{iw}}{\theta_w}\right]\frac{\partial C_w}{\partial x} \qquad 3\text{-}7$$

Using newely defined parameters, R_c and α, Eq. 3-7 becomes simplified as:

$$R_c \frac{\partial C_w}{\partial t} = -v_b \left[1 + \frac{\alpha a_i K_{iw}}{\theta_w}\right] \frac{\partial C_w}{\partial x} \qquad 3\text{-}8$$

where

$$R_c = 1 + \frac{a_i K_{iw}}{\theta_w} \qquad 3\text{-}9$$

and

$$\alpha = \frac{v_i}{v_b} \qquad 3\text{-}10$$

through Eqs 3-2~10, R_c is the corrected retardation factor (dimensionless) of an aqueous interfacial tracer excluding other sorption terms (e.g., soil sorption, gas-phase partitioning) for a hypothetical system with non-moving interface, C_w (mol/cm^3) is the tracer concentration in the bulk water phase, α is the ratio of water velocities between the bulk water and the interface (dimensionless), K_{iw} (cm) is the adsorption coefficient of the aqueous interfacial tracer based on the aqueous equilibrium tracer concentration, a_i (cm^2/cm^3) is the specific air-water interfacial area measured by the gaseous interfacial tracer, v_i and v_b are the pore water and interfacial velocities (cm/min^3), respectively, t is time (min), and x is distance (cm).

Based on the difference in the air-water interfacial areas measured using gaseous and aqueous tracers, it is possible to estimate the velocity ratio, α, defined in Eq. 3-10. Since we assumed that there is no detectable mobility at the air-water interface during gaseous flow and all the air-water in the porous medium is accessible to both aqueous and gaseous tracers, the a_i measured using gaseous tracer is assumed to represent all the air-water interface formed in the medium. Therefore, a hypothetical retardation factor (R_c) of the aqueous tracer can be calculated based on the a_i value from the gaseous tracer experiments with no mobility at the air-water interface. The difference between the experimentally observed retardation factor, R^*, of the aqueous tracer and R_c is the result of mobility of the air-water interface. Based on Eq. 3-8, the observed velocity (v^*, cm/min) of an interfacial tracer is:

$$v^* = \left[\frac{\theta_w + \alpha a_i K_{iw}}{\theta_w + a_i K_{iw}}\right] \cdot v_b \qquad 3\text{-}11$$

The observed advective velocity of an interfacial tracer (v^*) is the same as that of the bulk water when the mean velocities at the interface (v_i) and in the bulk water (v_b) are the same ; that is, $\alpha = 1$. When the interface is immobile ($v_i = 0$, $\alpha = 0$), the observed velocity of the interfacial tracer is:

$$v^* = \frac{1}{R_c} v_b \qquad 3\text{-}12$$

Using Eqs 3-9~11, the velocity ratio between interface and bulk water (α) is:

$$\alpha = \left[\frac{R_c}{R^*} - 1\right]\left[\frac{\theta_w}{a_i K_{iw}}\right] \qquad 3\text{-}13$$

In order to calculate α, the observed retardation factors, R^*, were estimated from an empirical equation based on the experiment using sodium dodecylbenzene sulfonate (SDBS) as an aqueous interfacial tracer and a K_{iw} value of 5.06×10^{-3} cm (Kim et al., 1997; Eq. 2-12):

The corrected retardation factors, R_c, with non-moving interface were estimated based on the air-water interfacial areas measured by the gaseous tracer (*n*-decane). The relationship between α and the degree of water saturation, S_w, is shown in Figure 3-6 with the observed (R^*) and hypothetical (R_c) retardation factors. Within the S_w range where both of the aqueous and gaseous tracer experiments data are available, the velocity of the air-water interface was estimated to be about 23 to 36 % of the bulk pore water velocity (Fig. 3-6). Note that α decreases in a linear fashion ($r^2 = 0.983$) as S_w decreases even though the difference between observed and hypothetical retardation factors increases with decreasing S_w. This result implies that less water is in direct contact with the mobile water domain at lower S_w. Since molecular diffusion is the only process for the interfacial tracer to reach the air-water interface in this region, more non-equilibrium effects, manifested as early breakthrough and tailing of BTCs are expected. This excessive broadening effect of the aqueous tracer BTCs was observed for the column displacement experiments with SDBS as the aqueous interfacial tracer (Kim et al., 1997).

Summary

A series of gaseous tracer experiments were conducted to estimate specific air-water interfacial areas and water contents in a partially water-saturated sand column. A straight chain hydrocarbon (*n*-decane) was used as the gaseous interfacial tracer. Methylene chloride and chloroform were used as the water-partitioning gaseous tracers. A gas chromatographic technique was employed for both of the tracer experiments at room temperature using nitrogen as the mobile phase, with water acting as the immobile liquid. Tracer experiments covered water saturations (S_w) up to 56 %. Air-water interfacial area (a_I) measured using *n*-decane decreases exponentially as water content increases. At $S_w < 2$ %, the a_I changed more rapidly than predicted from the fitting function. The largest a_I of about 1,500 cm^2/cm^3 was measured at the lowest S_w (1.4 %), and the smallest a_I was about 80 cm^2/cm^3 at $S_w \approx 56$ %. The air-water interfacial areas measured using a gaseous tracer were found to be 2~3 times larger than those measured using an aqueous interfacial tracer within the S_w range where the aqueous tracer data are available. In the S_w range where both aqueous and gaseous interfacial tracer data were available, the velocity of the air-water interface was estimated to be between 23~36 % of the pore-water velocity. The water contents measured using water-partitioning tracers were mostly within ± 5 % of those based on gravimetric measurements.

Table 3-1. Chemical properties of the tracers used in this study (at 25 °C unless otherwise stated)

Tracer	Molecular weight	Vapor pressure[a] (kPa)	Solubility in water[a] (g/m^3)	Henry's law constant[b] H, (dimensionless)	Air-water interfacial adsorption coefficient[c] K_{ia}, (μm)
methane	16.0	27,260	24.1	28.4	–
n-decane	142.3	0.175	0.052	210	2.26
methylene chloride	84.9	46.53 (20 °C)	13,200 (20 °C)	0.110	0.186
chloroform	119.4	32.80 (20 °C)	8,000 (20 °C)	0.181	0.347

[a] Data from Mackay and Shiu (1981); [b] Yaws et al. (1991); [c] Hoff et al. (1993b)

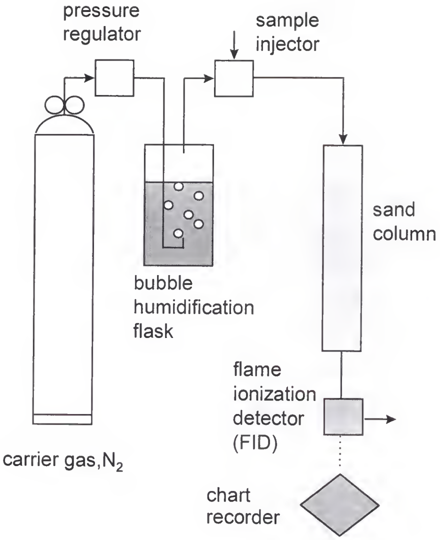

Figure 3-1. Experimental set up for gaseous interfacial and water-partitioning tracer experiments.

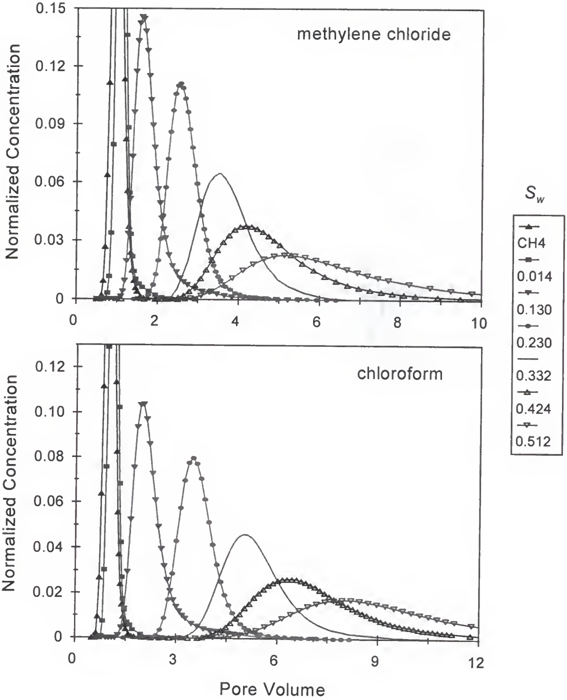

Figure 3-2. Breakthrough curves of the water-partitioning tracers at different water saturations; tracer concentration was normalized so that the total mass of applied tracers for all the experiments at different water saturations was reduced to 0.1 pore volume.

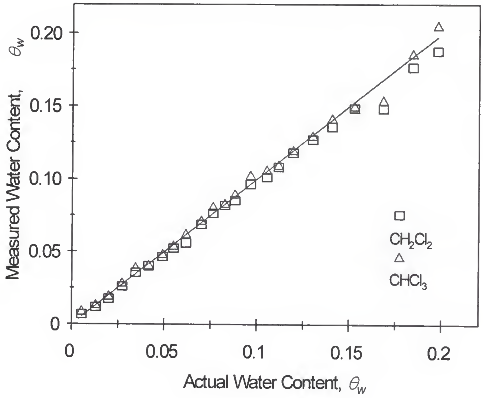

Figure 3-3. The measured volumetric water contents with respect to the actual water contents estimated by column weight : solid line - ideal 1:1 line.

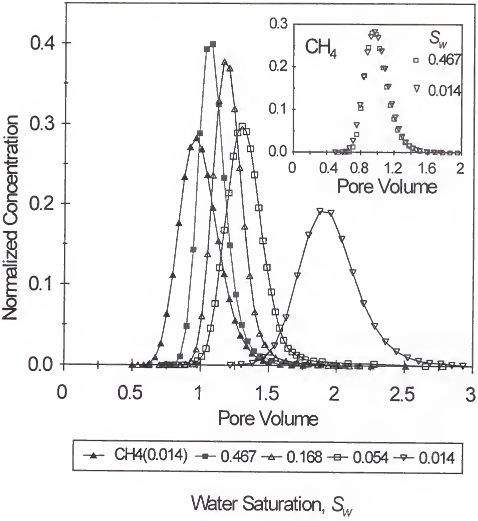

Figure 3-4. Breakthrough curves of the gaseous interfacial tracer (*n*-decane) at different water saturations; tracer concentration was normalized so that the total mass of *n*-decane for all the experiments at different water saturations was reduced to 0.1 pore volume; inset graph for the methane BTCs at two different water saturations.

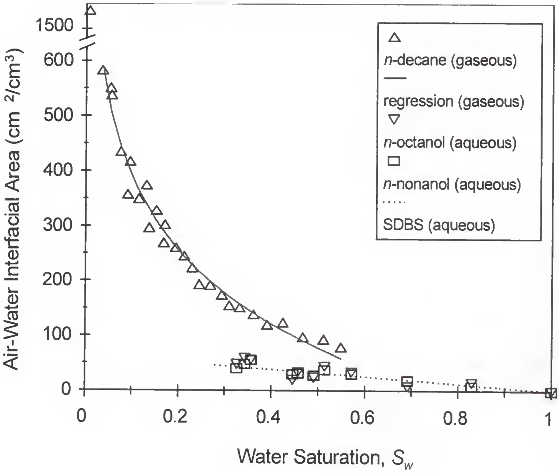

Figure 3-5. Measured specific air-water interfacial areas (a_i) using gaseous and aqueous interfacial tracers; SDBS (Kim, et al., 1997): alcohols (from Chap. 2): regression curve (*n*-decane): $a_i = -196.0 \ln S_w - 58.9$ ($r^2 = 0.978$).

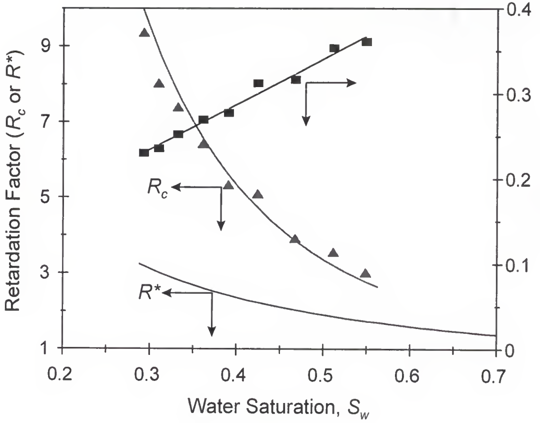

Figure 3-6. The ratio of interfacial velocity to the bulk pore-water velocity (α) with the observed sodiumdodecylbenzene sulfonate (SDBS) retardation factors (Kim et al., 1997) and the hypothetical retardation factors of SDBS estimated based on the specific air-water interfacial areas (a_i) measured by gaseous interfacial tracer (*n*-decane) experiments.

CHAPTER 4

EFFECTS OF WATER-PARTITIONING AND AIR-WATER INTERFACIAL ADSORPTION ON THE GASEOUS TRANSPORT OF ORGANIC CONTAMINANTS IN UNSATURATED POROUS MEDIA

Introduction

Understanding the sorption mechanisms of organic contaminants in all physical domain in unsaturated soils is of great importance for the estimation and prediction of their transport and fate in the subsurface environment. Since, at many contaminated sites, hazardous organic compounds are trapped in the vadose zone providing a source for the gaseous plume, volatile organic chemical (VOC) transport in the gaseous phase is of interest not only for the assessment of the time-dependent spatial distribution of those contaminants, but also for the optimal design of vapor-phase remediation techniques (e.g., soil vapor extraction, bioventing). Three mechanisms have been identified as causing retardation of VOCs during gaseous phase transport in unsaturated porous media (Okamura and Sawyer, 1973; Conklin et al., 1995; Popovicova and Brusseau, 1998). Sorption by the soil mineral and organic components is often responsible for significant retardation of VOCs during gaseous transport. The magnitude depends on the solubility (or Henry's law constant) of the chemical, the degree of water saturation (S_w), and the fraction of soil organic matter (f_{oc}). Soil water is the second physical domain capable of retaining VOCs during gaseous transport. VOCs with relatively high aqueous solubility are retained longer in the soil water, thus increasing the total retardation. Finally, the air-water interface also can be a significant source of chemical retention; the specific air-water interfacial area (a_i) and the interfacial adsorption coefficient (K_{ia}) of a chemical determine such retardation of the VOC.

Although it has been known that a substantial mass of VOCs can accumulate at the air-water interface in unsaturated soils (Posner et al., 1952; Karger et al., 1971; Dorris and Gray, 1981; Hauxwell et al., 1992; Pennell et al., 1992; Valsaraj, 1994), a systematic investigation of this effect on the vapor-phase transport of VOCs has not been performed quantitatively, primarily because of the difficulties encountered in measuring a_i in water-unsaturated porous media. A gaseous interfacial tracer technique has been reported by Brusseau et al.(1997) recently for the experimental measurement of a_i that is exposed to a continuous gaseous phase. Note that an aqueous interfacial tracer technique was also reported by Saripalli et al.(1997) and Kim et al.(1997) to measure air-water [or non-aqueous phase liquid (NAPL)-water] interfacial areas using anionic surfactants as tracers, which detect the air-water interface in contact the continuous aqueous phase. The effect of interfacial adsorption on the aqueous-phase transport of surface-active organic chemicals was described in Chapter 2.

In this chapter, the effect of air-water interfacial adsorption on the retardation of VOCs during gaseous phase miscible displacement in water-unsaturated columns packed with a natural soil and a clean sand was studied. The partial retardation factors due to the interfacial adsorption for the VOCs used in this study were compared to the total retardation factors and the retardation factors from other retention sources. Changes in partial and total retardation factors for VOCs with varying water saturation were also investigated.

Theoretical Background

The total retardation factor (R_t) for a VOC transport via the gaseous phase can be divided to four terms, each representing the physical domain where the chemical retention occurs (Conklin et al., 1995; Popovicova and Brusseau, 1998):

$$R_t = \beta'_g + \beta'_w + \beta'_i + \beta'_d \tag{4-1}$$

$$\beta'_g = 1, \quad \beta'_w = \frac{\theta_w}{K_H \theta_a}, \quad \beta'_i = \frac{a_i K_{ia}}{\theta_a}, \quad \beta'_d = \frac{\rho K_d}{K_H \theta_a} \tag{4-2}$$

The interfacial adsorption coefficients (K_{ia}) of common VOCs from the vapor phase to the air-water interface are available in the literature (Hartkopf and Karger, 1973; Hoff et al., 1993b). The K_{ia} that represents the relationship between the gaseous phase concentration (C_g, mol/cm^3) and the surface excess of a chemical at the air-water interface (Γ, mol/cm^2) can be estimated from the surface tension- C_g relationship. Since the sorption capacity of soils for a VOC varies depending the chemical composition and the organic carbon content (f_{oc}) of the soils, it is necessary to measure the K_d values for each soil-VOC pair. However, approximate values of K_d can be estimated (Schwarzenbach et al., 1993) based on the f_{oc} of the soil and the carbon-normalized sorption coefficient (K_{oc}).

In order to investigate the relative magnitudes of β'_g, β'_w, β'_i, and β'_d as water saturation varies, or for different porous media, it is useful to normalize these terms with respect to the total retardation factor, R_t.

$$f_g = \frac{\beta'_g}{R_t}, \quad f_w = \frac{\beta'_w}{R_t}, \quad f_i = \frac{\beta'_i}{R_t}, \quad f_d = \frac{\beta'_d}{R_t} \quad ; \sum_j f_j = 1 \tag{4-3}$$

Note that β'_g is always 1 (Eq. 4-2), while the normalized term f_g varies depending on the magnitude of total retardation factor (R_t).

The total retardation factor (R_t) for a breakthrough curve (BTC) with a pulse input of a chemical is estimated based on the normalized first temporal moments of non-reactive tracer and the chemical of interest (Eq. 2-11):

$$\mu' = \frac{\int_0^{\infty} C(t)t \; dt}{\int_0^{\infty} C(t) \; dt} - \frac{1}{2}t_p \qquad 4\text{-}4$$

where μ' (min) is the normalized first temporal moments of a chemical, $C(t)$ is the gaseous concentration of the chemical in the effluent (mol/cm^3), t is time (min), and t_p is the input pulse duration (min). When the input duration is sufficiently instantaneous, such as GC injection, compared to the normalized temporal first moment, t_p may be assumed to be zero as in this study.

Materials and Methods

Materials

Compressed methane gas with 99 % purity was purchased from Aldrich Chemical Co. Perchloroethylene (PCE), 1,1,1-trichloroethane (TCA), and straight-chain hydrocarbons (hexane, heptane, octane, nonane, decane) were supplied by Aldrich Chemical Co. Aromatic compounds (chlorobenzene, ethylbenzene, and *p*-xylene) were purchased from Fisher Scienctific Co. All of the chemicals used in this study were reagent grade, and were used as recieved without further treatments. High-purity nitrogen was used as the carrier gas for the gaseous transport experiments. Chemical properties relavant to this study are listed in Table 4-1.

Two types of soils were used: (1) a soil collected at Dover Air Force Base (Delaware) that consists of mostly silt with small fractions of sand and clay, and (2) the same clean sand used in the previous studies (Saripalli et al., 1997; Kim et al., 1997). The soil from Dover Air Force Base (AFB) was washed with HPLC-grade water several times, and dried in an oven at 105 °C for 24 hours before packing. The sand sample used in this study was washed with HPLC-grade water, and baked in an muffle furnace at 500 °C for 24 hours before packing.

Miscible Displacement Experiments

The experimental procedure used in this study are identical to that of the previous chapter, and is only slightly different from those found in other literature (Brusseau et al., 1997; Conklin et al., 1995) where gaseous-phase transport experiments were conducted using GC systems. A stainless steel column [30.0 cm (length) × 1.0 cm (inner diameter)] was packed with the soil and installed in a GC (Shimadzu, GC-14A). A bubble humidification flask was installed between the carrier gas supply and the GC injection port to prevent water loss from the column during the experiment. The column temperature was maintained at room temperature (22 ± 0.5 °C) for the all experiments. The temperature at the GC injection port was set at 120 °C. A flame ionization detector (FID)was used for monitoring the VOC concentrations in the gas-effluent from the column. The FID temperature was set at 240 °C. The carrier gas flow rate was controlled using a needle valve to generate a constant pore-gas velocity of about 10 cm/min throughout the experiment.

The soil columns were packed, initially, with dry soils. To achieve an intended water saturation for each experiment, an equal amount of water (100 -200 μl) was injected into each end of the column through using a syringe. The column was then put in an oven and heated at 105 °C for about 24 hours to allow the water to distribute uniformly along the column. The column was then cooled down to the room temperature and installed in the GC. Homogeneous water saturation along the column was verified by measuring the water contents in segments of soil samples from the column after the experiments with the highest water saturation. After each experiment, another small increment of water was injected and the same treatment followed. Water saturation change was carefully monitored before and after a set of experiments. Water saturation changes during an experiment was found to be negligible (< 0.5 %).

About 10 ml of each VOC except methane were put into 40 ml vials, and vapor samples from the headspace were taken using a gas-tight syringe for GC injection. The injection volume varied between 0.5 and 10 μl depending on the vapor pressure of the VOCs at room temperature. Compressed methane gas was depressurized to the ambient atmospheric pressure prior to the injection on the soil column. The retardation factor measurements were based on injected pulses of individual VOCs. The retention time and BTC of each chemical were monitored using a GC integrator (Shimadzu, CR601) and a chart recorder (Fisher Scientific Co., Recodall® Series 5000) simultaneously. The temporal, first moment for each experiment was calculated by numerical integration of Eq. 4-4.

All 12 VOCs were used for the experiments with the Dover soil column, but only methane, *p*-xylene and *n*-decane were used for the clean sand column.

Results and Discussion

The first, temporal moments (representing mean retention times) of the n-alkanes from the experiments with Dover AFB soil, decreased with increasing water saturation. The retardation of the rest of the VOCs decreased initially as the water saturation increased, reaching a minimum point, and then increased with further increase in water saturation (Fig. 4-1). Although BTCs of only *n*-nonane are presented in Fig. 4-1, those of other three *n*-alkanes were found to have the same trend as shown in Fig. 4-1. Likewise, the gaseous transport of other VOCs used for Dover soil experiments except *n*-alkanes, was found to have the same characteristics as chlorobenzene. This combined effect of water-partitioning and interfacial adsorption at the air-water interface was similar to that observed by Okamura and Sawyer.(1973). The total retardation factors of *n*-decane with clean sand column were smaller than those from the experiments with Dover AFB soil, but the trend of retardation factors with changing water saturation followed the same pattern as those with Dover AFB soil. All of the BTCs of the *n*-alkanes were reasonably symmetric, implying and interfacial adsorption processe is not significantly rate-limited under the conditions employed for the gaseous-phase transport with the soils used in this study. That is because the mean residence time was apparently long enough to ensure equilibrium phase distribution.

Based on the R_t values for the *n*-alkanes, the specific air-water interfacial areas (a_i) were estimated for both soils. Since the *n*-alkanes have extremely low aqueous solubilities (Table 4-1), the R_t measured is primarily due to VOC adsorption at the air-water interface. Note that low aqueous solubilities of several VOCs minimize their sorption by soil, provided that the soil surface is completely water-wet. Thus, neglecting the β_w and β_d terms in Eqs 4-1 and 4-2, the specific air-water interfacial area can be estimated with known K_{ia} and gas content, θ_a.

The estimated a_i values for both soils decreased with increasing water saturation (Fig. 4-2). Though the two soils have very different mean particle sizes and size distributions, the estimated a_i showed roughly the same functional dependency upon the water saturation. However, the a_i values of Dover AFB soil are about 1-2 order of magnitude larger than those of the clean sand. The largest a_i values of Dover soil, which were measured at the lowest water saturation achieved in this study, is comparable with the a_i values reported by Conklin et al.(1995) and Brusseau et al.(1997). Air-water interfacial adsorption coefficients (K_{ia}) from Hoff et al.(1993b) were used for *n*-hexane, *n*-heptane, and *n*-octane for the a_i calculation. The average a_i values estimated at water saturation of 0.08, 0.10, and 0.12, based on the total retardation factors of *n*-hexane, *n*-heptane, and *n*-octane, were used to determine the K_{ia} values of *n*-nonane and *n*-decane. Although the total retardation factors of these *n*-alkanes vary considerably depending on their carbon-chain lengths, the estimated a_i values were very consistent; cases where $R_t \leq 1.1$ were not used due to concerns of reliability when retardation is too small.

Prediction of the R_t values as well as the individual terms (β', in Eq 4-1 and 4-2) for the VOCs used in this study was attempted using the estimated a_i values based on the first moments of the *n*-alkanes, the Henry's law constants, and the water/gas contents measured gravimetrically (Fig. 4-3). In general, the predicted R_t values for all of the VOCs were in good agreement with those measured. As expected, the R_t values for *n*-alkanes decreased consistently with increasing water saturation. However, the retardation behavior of other VOCs varies as the water saturation changes, depending on the relative magnitude of K_{ia} and K_H. In experiments with Dover AFB soil, R_t for methylene chloride, which has relatively small K_{ia} and K_H values, increased over most of the water saturation region except at a very low water saturations. This implies that the water-partitioning effect is dominant over most water saturations unless the air-water interfacial area is large enough to contribute significantly to R_t. When the rate of decreasing partial retardation from interfacial adsorption with respect to the change of water saturation ($=d\beta'_i/dS_w$) is smaller than the rate of increasing partial retardation due to the combined effect of water partitioning and soil sorption [$=d(\beta'_w+\beta'_d)/dS_w$], R_t increases regardless of the absolute magnitudes of β'_i, β'_w, and β'_d. The total retardation of PCE,TCA, ethylbenzene, and *p*-xylene decreased rather rapidly at low S_w range, reached the minimal point, and then increased slowly from that point compared to R_t for methylene chloride. This trend is due to the larger K_{ia}, and K_H values for the four VOCs compared to those of methylene chloride.

The contribution of different processes to observed R_t for chlorobenzene is illustrated in Fig. 4-3. It is obvious that at low S_w, the major contributor to the total retardation is that from the air-water interfacial adsorption (β'_i), while the water-partitioning effect becomes more significant as the water saturation increases in the absence of soil sorption.

The normalized, fractional retardation factors (*f*) for *p*-xylene in Dover soil and clean sand columns are shown in Fig. 4-4. Note that the advantage of normalized fractional retardation factors is that the relative composition of each partial retardation factor with respect to the total retardation factor is easily identified and assessed regardless of the magnitude of the total retardation factor. It is clear that there is a distinct difference in the relative composition of R_t depending on the porous media. This difference is mainly due to the absolute amount of air-water interfacial area generated in the media. For the clean sand, within the water saturation range achieved in this study, R_t for *p*-xylene increased consistently. Although the effect of (air-water) interfacial adsorption is responsible for about 20 % of the total retardation at 5 % of water saturation, the rate of β'_w increase with increasing S_w is enough to mask the decreasing effect of β'_i as described earlier. It is also apparent that the fractional retardation factor due to the retention of *p*-xylene in the gaseous phase (f_g) during transport increased in the low water saturation range for Dover AFB soil, even though the partial retardation factor, β'_i remained constant. This is because of decreasing total retardation factor, again, due to decreasing air-water interfacial area with increasing water saturation.

The magnitude of the fractional retardation factor due to air-water interfacial adsorption, and its rate of change with respect to water saturation, are dependent not only on the specific air-water interfacial areas in the media but also on the chemical properties of the VOCs. With relatively large K_{ia}, and K_H values, the f_i of *p*-xylene is larger than that for other VOCs used in this study (Fig. 4-5). The rate of change in f_i values with respect to the water saturation change differs depending on the magnitude of K_{ia}, and K_H values.

The data discussed so far were acquired from gaseous transport experiments involving the injection of a small pulse of a single VOC. In order to investigate whether there is interaction between reactive and non-reactive chemicals during gaseous transport, three VOC mixtures (methane and *n*-heptane; methane and methylene chloride; methane and chlorobenzene) were tested using the same experimental procedure used for the single-VOC experiments. The GC retention times of methane (used as non-reactive tracer) and other VOCs, when injected together, were close to those of single injection within ±3 % (Fig. 4-6). The shape of BTCs of VOCs with single and mixture injections was also identical. However, it is recommended to apply single chemical because of the difficulty associated with the data analysis (i.e., numerical integration for moment analysis, Eq. 4-4) and the possible interaction between different species of chemicals at the air-water interface when multiple reactive tracers are to be used together.

No difference in the temporal first moment for the breakthrough curves of *n*-heptane was found with different input concentrations (Fig. 4-7). This result indicates that the adsorption isotherm of *n*-heptane at the air-water interface is linear within the concentration range used in this study. The response of dectector (FID) was found to be linear (in BTC areas and heights) with respect to the volume (thus the mass of tracer) of the tracer injected.

Summary

A series of laboratory experiments were conducted using gas chromatographic techniques to evaluate the effect of interfacial (air-water) adsorption and air-water partitioning on the gaseous transport of volatile organic chemicals (VOCs) in water-unsaturated soil columns. VOCs used in this study were representative of : (1) chemicals with small interfacial adsorption coefficient (K_{ia}) and small Henry's law constant (K_H) (methylene chloride); (2) chemicals with medium K_{ia} and large K_H (1,1,1-trichloroethane; perchloroethylene); (3) chemicals with large K_{ia} and medium K_H (chlorobenzene; *p*-xylene; ethylbenzene), and (4) straight chain-hydrocarbons with a wide range of K_{ia} values and very large K_H (*n*-alkanes). Up to 50 % of water saturation (S_w) was achieved for the experiments with two columns, one packed with a clean sand, and the other with soil from Dover Air Force Base, DE. Air-water interfacial areas (a_i) were estimated from the meaured retardation of *n*-alkanes. At low S_w, interfacial adsorption contributed most of the retardation for all VOCs during vapor-phase transport in the Dover soil which does not have significant sorption capacity for the chemicals used in this study. As water saturation increases, the fraction of retardation factor attributed to interfacial adsorption decreases, while that due to water partitioning increases. As S_w approaches 50 %, the water-partitioning effect was dominant responsible for the observed retardation of the VOCs. The fraction of retardation factors attributed to interfacial adsorption, water partitioning, and retention during gaseous phase transport was quantified. The observed total retardation factors for the VOCs agreed well with those predicted based on the sorption coefficients (K_{ia}, K_H) and the quantity of retention domains (S_w, a_i).

Table 4-1. The chemical properties of the VOCs used in this study (25 °C)

chemical	molecular weight (amu)	K_H [a] (kPa m^3/mol)	K_{ia} [b] (μm)	vapor pressure[a] (kPa)	solubility in water[a] (g/m^3)
methane	16.04	67.4 ± 2.0	-	27,260	24.1
n-hexane	86.17	170 ± 25	0.109	20.2	9.5
n-heptane	100.21	230 ± 50	0.233	6.11	2.93
n-octane	114.23	300 ± 50	0.541	1.88	0.66
n-nonane	128.26	500 ± 200	1.23[c]	0.571	0.122
n-decane	142.28	700 ± 200	2.84[c]	0.175	0.052
methylene chloride	84.9	0.26 ± 0.02	0.186	58.4	19,400
PCE	165.83	2.3 ± 0.4	0.327	2.48	140
TCA	133.4	2.8 ± 0.04	0.292	16.53	720
chlorobenzene	112.56	0.35 ± 0.05	1.23	1.581	472
ethylbenzene	106.2	0.80 ± 0.07	2.35	1.27	152
p-xylene	106.2	0.71 ± 0.08	2.41[d]	1.17	185

[a] data from Mackay and Shiu (1981).

[b] data from Hoff et al. (1993b).

[c] estimated based on the K_{ia} values of *n*-hexane, *n*-heptane, and *n*-octane, and the measured air-water interfacial areas.

[d] data from Pennell et al.(1992).

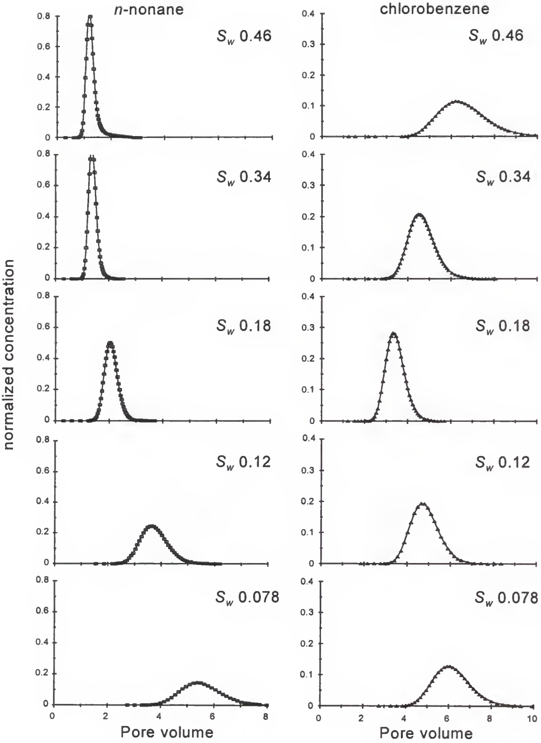

Figure 4-1. The breakthrough curves of *n*-nonane and chlorobenzene at different water saturations (medium : Dover AFB soil).

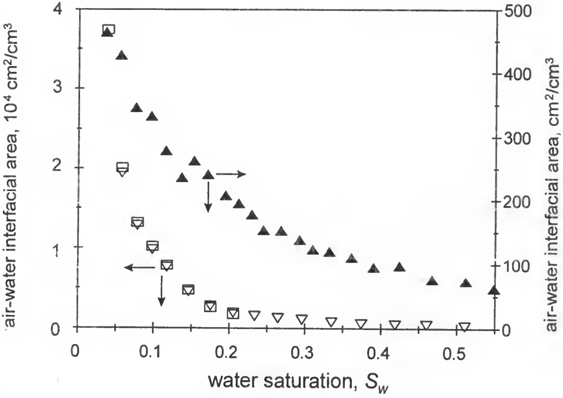

Figure 4-2. Estimated specific air-water interfacial areas of the columns packed with Dover AFB soil and a clean sand in water saturation range of 5 - 55 %.

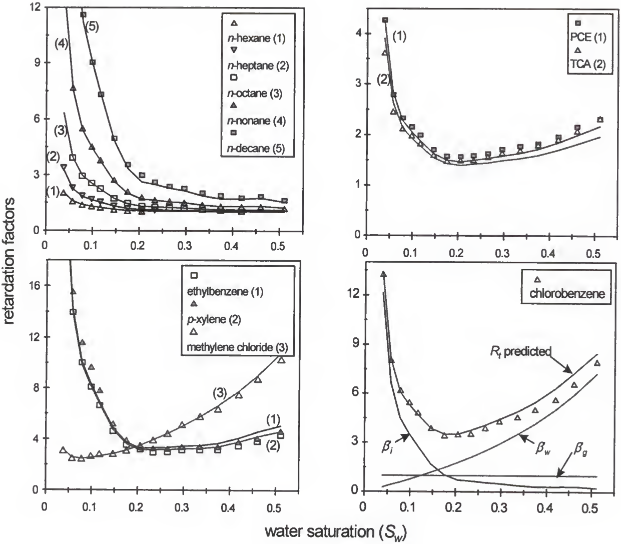

Figure 4-3. Observed and predicted total retardation factors of VOCs for Dover AFB soil. The components (β') of predicted total retardation factor of chlorobenzene were shown with the observed total retardation factor.

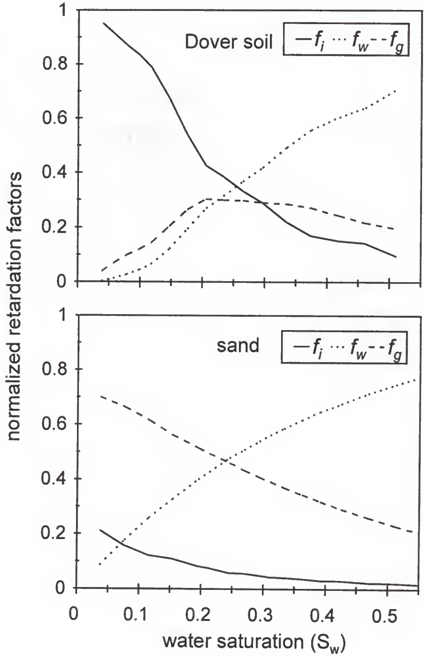

Figure 4-4. The fractions of predicted total retardation factors of *p*-xylene for the Dover AFB soil and clean sand. The fractional retardation factors (*f*) were normalized with respect to the predicted total retardation factors, which were reduced to unity.

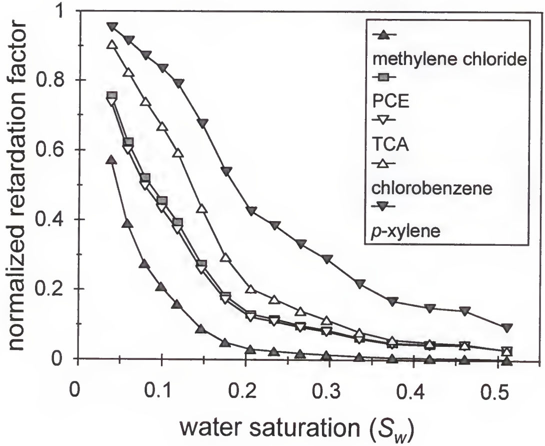

Figure 4-5. The fraction (f_i) of predicted total retardation factors of interfacial (air-water) adsorption for VOCs used in this study.

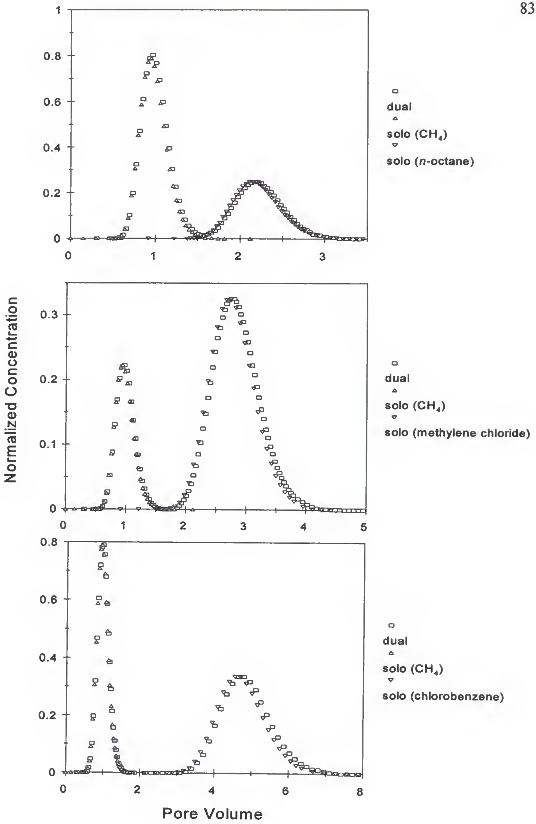

Figure 4-6. Comparison of VOC breakthrough curves at water saturation of 0.117: dual - mixture injection; solo - single component injection.

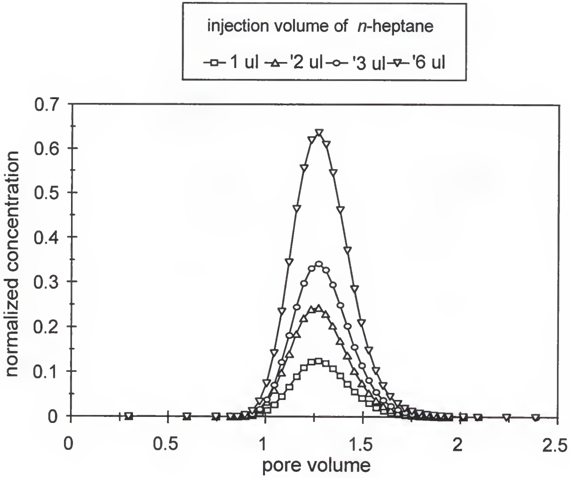

Figure 4-7. Breakthrough curves of *n*-heptane at water saturation of 0.146 with different injection volumes; the volume *n*-heptane and air mixture taken from the head space in the sample preparation vial, used as the input pulse.

CHAPTER 5
EXPERIMENTAL EVALUATION OF THE QUANTITATIVE VALIDITY OF INTERFACIAL TRACERS

Introduction

The quantity and geometry of the fluid-fluid interface at NAPL (non-aqueous phase liquid) contaminated sites are of great interest, along with the degree of NAPL saturation (S_N) and spatial distribution. Understanding the fundamental nature of NAPL-contaminated porous media is the starting point for designing a feasible, cost-effective remediation strategy. Physical, chemical, and biological processes which affect the fate of toxic chemicals are often considered to be associated with the spatial distribution and magnitude of the NAPL-water interfacial area (a_{nw}). Quantitative evaluation of S_N and a_{nw} distributions in a contaminated site is important because mass transfer processes across the NAPL-water phase boundaries determine the efficiency and effectiveness of a remediation technique proposed. Recent progress in *in situ* characterization technologies include a method for quantifying S_N and its spatial distribution using partitioning tracers. Field applications as well as lab-scale experimental results have been reported for various cases (Jin et al., 1995; Nelson and Brusseau, 1996; Annable et al., 1995, 1998b).

In spite of the importance of specific interfacial areas between immiscible liquids in porous media, lab-scale or field-scale techniques to measure this quantity were not available until a tracer displacement technique was developed recently (Saripalli et al., 1997, 1998; Kim et al., 1997, 1998; Annable et al., 1998a). Lack of appropriate experimental methods has prompted the development of a number of theoretical approaches, resulting in a variety of models for calculating a_{nw} in porous media (Gvirtzman and Roberts, 1991; Hassanizadeh and Gray, 1993; Cary, 1994; Reeves and Celia, 1996; Bradford and Leij, 1997). Each of these models, however, was developed based on a number of critical assumptions. Geometric simplification of porous media, including the solid matrix and the immiscible fluid phases, is common for most of the theoretical models, while some models depend on the thermodynamic interpretation of the system of interest (e.g., Leverett, 1941; Hassanizadeh and Gray, 1993; Bradford and Leij, 1997). Regardless of the theoretical soundness, the reliability of these models remains untested due to the lack of experimental proof. Experimental quantification of fluid-fluid interfaces (e.g., between NAPL-water or air- water) in porous media has required very sophisticated imaging techniques (Ronen et al., 1986; Gvirtzman et al., 1987).

The new method we developed (Saripalli et al., 1997, 1998; Kim et al., 1997) utilizes water-soluble surfactant as an interfacial tracer which is adsorbed at the NAPL-water or air-water interface, but does not partition into bulk NAPL or air phase from the flowing aqueous phase as do partitioning tracers used for estimating NAPL saturation. In this method, tracer retardation resulting from interfacial adsorption is measured, and used to determine the interfacial area. The interfacial tracer method was validated using the following approaches: (1) Using a porous medium with a known fluid-fluid interfacial area to examine that the a_{nw} value estimated from interfacial tracer experiments agrees with the known values, (2) Confirmation of the interfacial adsorption isotherm used to interpret the tracer miscible displacement data, (3) Concurrence among different experiments with different interfacial tracers and NAPLs. It should be emphasized that an independent evaluation of NAPL-water interfacial area in porous media estimated by the tracer method is currently not available.

A porous medium (glass beads packing) with a known NAPL-water interfacial area was used for this study. The same tracer test procedure proposed in previous papers (Saripalli et al., 1997) was employed. The experimental estimates of the interfacial areas were then compared with the known a_{nw} value. In order to build the isotherm for tracer adsorption onto the NAPL-water interface, a series of miscible displacement column experiments were conducted using a wide range of tracer input concentrations. The adsorption isotherm from the column experiments was compared with an isotherm based on the Gibbs adsorption equation using interfacial tension data.

Theoretical Background

Surfactant Adsorption at the NAPL-Water Interface

Interfacial tracers are surface active agents that have the unique chemical property to adsorb at the interface between two immiscible fluids (e.g., oil-water, air-water), but not partition into the immiscible phase. The degree of adsorption, or surface excess, of surfactant depends mostly on its hydrophilic-lipophilic balance (HLB), as well as on the nature of fluids in the system at a given set of thermodynamic conditions (Rosen, 1989). The desired general properties of selected interfacial tracer are that it should not significantly adsorb to the solid matrix or any other phases except the fluid-fluid interface of interest.

Anionic surfactants are a reasonable choice for most natural soils unless anion exchange is significant due to metal oxides, and the pH of the aqueous solution is below the isoelectric point (IEP) of the oxides. In order not to alter the NAPL saturation and NAPL-water interface, the concentration of an interfacial tracer should be lower than critical micelle concentration (CMC) where the NAPL solubility in bulk aqueous solution starts to increase dramatically. The adsorption coefficient (K_{in}) for tracer accumulation at the interface must be such that a reasonable retardation factor ($1.2 \leq R_t \leq 4.0$) at a given surfactant concentration is obtained for the displacement experiments. It is preferred that the selected tracer is conserved during the displacement experiments, but an approximation can be made if degradation occurs (Annable et al., 1998b). For both lab- and field-scale applications, the interfacial tracer should be easily detectable by standard laboratory analytical methods. Based on the success of earlier experiments (Saripalli et al., 1997, 1998; Kim et al., 1997), we selected sodium dodecylbenzene sulfonate (SDBS) as the primary tracer in this study because it met the requirements described above. A cationic surfactant, cetylpyridinium chloride (CPC), was used for confirmation of the a_{nw} measured in SDBS experiments.

Adsorption of 1:1 ionic surfactant at the fluid-fluid interface is expressed by the Gibbs adsorption equation with a dissociation factor 2:

$$\Gamma = -\frac{1}{2RT}\left(\frac{\partial \gamma}{\partial C}\right)_T C \qquad 5\text{-}1$$

where all the parameters are the same as defined in Eq. 2-8. The assumption associated with Eq. 5-1 is that the aqueous solution contains only a 1:1 ionic surfactant species (Rosen, 1989) which dissociates completely in the aqueous phase.

The interfacial adsorption isotherm for surfactant is a strong non-linear function of the bulk concentration for most fluid-fluid interfaces. Therefore, it is necessary to utilize an interfacial adsorption coefficient (K_{in}) value that optimally represents the distribution characteristics of the tracer between bulk phase and interface for the calculation of interfacial areas based on the results of column displacement experiments. One of the simplest approaches is to use the secant of isotherm at the maximum surfactant concentration, C_o;

$$\Gamma_o = K_{in} C_o \qquad 5\text{-}2$$

where

$$K_{in} = -\frac{1}{2RT}\left(\frac{\partial \gamma}{\partial C}\right)_{C_o,T} \qquad 5\text{-}3$$

where Γ_o and K_{in} are the surface excess (mol/cm^2) and adsorption coefficient (cm) at a tracer concentration of C_o (mol/cm^3), respectively. Note that even though the K_{in} is valid only at the C_o, exact zero-th and first moments of the tracer can be calculated for the breakthrough curve (BTC) obtained using a continuous step input with C_o (Nkedi-Kizza et al., 1987; Annable et al., 1998a) ; however, higher moments are not reproduced.

Interfacial Tracer Displacement Experiment - Interfacial Area Calculation

Estimation of the retardation factors from BTCs with a continuous, step-input of interfacial tracers was described in previous papers (Saripalli et al., 1997; Kim et al., 1997, 1998). The retardation factor (R_t) can be split into component terms representing all of the significant sorption sources in the system. For example, if the solid matrix as well as fluid-fluid interface contribute to the adsorption of the tracer, the total retardation factor (R_t) will be expressed as:

$$R_t = 1 + \frac{\rho K_d}{\theta_w} + \frac{a_{nw} K_{in}}{\theta_w} \qquad 5\text{-}4$$

where a_{nw} is the specific interfacial area (cm^2/cm^3), and K_{in} is the interfacial adsorption coefficient (cm). Although the adsorption of interfacial tracer by the solid matrix, including soil organic matter, is restricted to a minimum by an appropriate choice of tracer, incorporation of K_d in the retardation factor is essential. With constant K_d and other parameters, a_{nw} can be estimated at the corresponding K_{in} value obtained from the interfacial tension measurement data or subsequently, the isotherm.

Note that the specific NAPL-water interfacial areas (a_{nw}) estimated using interfacial tracer displacement experiments may not represent the total NAPL-water interfacial area. Since the interfacial tracer travels along the column in the bulk water, only the NAPL-water interfaces that are hydrodynamically connected to the mobile water are detected.

Comparison of Isotherms

An isotherm for surfactant adsorption at a NAPL-water interface can be built from the retardation factors (R_t) measured at different surfactant input concentrations (C_o). In order to do that, it is necessary to fix the interfacial area (a_{nw}) (Eq. 5-4). If the true a_i value of the system is known and used to estimate K_{in} values based on Eq. 5-4, the isotherm calculated based on Gibbs adsorption equation (Eq. 5-1) can be compared directly with that independently obtained from the measured retardation factors. However, when the a_{nw} value is not available or is uncertain, an a_{nw} estimated using a retardation factor determined from a column experiment can be used. The interfacial adsorption isotherm [Γ(C)] obtained using the estimated a_{nw} is not completely independent on the interfacial tension data [γ(C)] because the K_{in} value used to estimated a_{nw} was calculated using the Gibbs adsorption equation. Nonetheless, the functional dependency of adsorbed concentration (Γ) of the tracer at the interface on the bulk concentration (C) can be compared with that estimated from interfacial tension data and Gibbs adsorption equation. It is recommended to use an a_i value that is representative of the system. One option is to use the a_{nw} estimated at the surface excess saturated region (i.e., where the molecular cross-sectional area of a surfactant molecule is known, and surface excess is at a maximum, and not a function of surfactant concentration in the bulk aqueous phase). This approach, however, requires that the retardation factor at the tracer input concentration within the saturation region should be large enough (e.g., R_i>1.2) to provide a reliable estimate.

If the tracer adsorption isotherm based on column displacement experiments, conducted under dynamic flow conditions, is in acceptable agreement with that predicted by Gibbs equation, interfacial tension measurements would be acceptable for determining the adsorption isotherm, and for estimating adsorption coefficients. The comparison of the isotherms will also verify the validity of Gibbs equation as the primary basis for interfacial area calculations through tracer displacement experiments.

Materials and Methods

Materials

Purified sodium dodecylbenzene sulfonate (SDBS) was provided by Dr. D. O. Shah, Chemical Engineering Department, University of Florida. Purity of the SDBS was assured to be 99% by elemental analysis (Shah, 1979). Cetylpyridinium chloride (CPC), with 99%

purity, was purchased from Sigma Chemical Co., and used as received. Bromide as potassium bromide, with 98% purity, was purchased from Fisher Co., and used without further treatment. High purity *n*-decane (Fisher Co., purity >99.8%), and perchloroethylene (Aldrich, purity >99%) were used as NAPLs for column experiments. Dimethyldichlorosilane (DMDCS)-treated glass beads (Alltech, stock #5430) were used as the packing medium for the column experiments. The DMDCS-treated beads were used to produce an oil-wet solid surface for experiments with a constant NAPL-water interfacial area that is not altered by changing the interfacial tension between two phases. The average diameter of the glass beads was 110 μm determined by visual inspection under an optical microscope. About 18 g of glass beads were coated with 0.09 g of *n*-decane or 0.20 g of perchloroethylene (PCE) by a vibration mixer (Thermolyne, type 16700). About 7 g of *n*-decane coated glass beads (DMDCS-treated) were packed in a stainless steel column [Alltech, 6.0 cm(l)×1.0 cm(id)], which resulted in a pore volume of 2.0 ml and a *n*-decane saturation (S_N) of approximately 2 %. About 7 g of PCE-loaded glass beads were packed in a stainless steel column of the same dimensions as the *n*-decane column. Perchloroethylene saturation (S_N) in the packed column was estimated to be about 2.4 %, and the pore volume was about 2 ml. For all aqueous solutions used in this study, HPLC grade water (Fisher Co., W5-4) was used.

Column Displacement Experiments

In order to measure the pore volume of the packed columns, a non-reactive tracer displacement experiment was conducted. After flow through the column was stabilized by flushing with several pore volumes of degassed HPLC grade water, the influent solution was switched to 30 mg/L bromide solution and the bromide concentration in the column effluent was monitored continuously with an ultraviolet detector (ISCO model V^4) at 205 nm until the bromide concentration in the column effluent was equal to that in the influent. Displacement experiments with SDBS and CPC were conducted, separately, employing similar protocols except that the detection wavelength was set at 260 nm. The flow rate in all experiments was fixed at 0.2 ml/min, achieved using a syringe infusion pump (Harvard Apparatus, model 22). This flow rate is equivalent to an average pore water velocity of 0.6 cm/min, or a mean residence time of about 10 minutes for a non-reactive tracer. Thirteen different SDBS concentrations (0.01 ~ 2.2 mM), and six CPC concentrations (0.03 ~ 0.9 mM) were used for the column experiments with *n*-decane coated glass beads. Two different SDBS concentrations (0.2, 0.4 mM) were used for PCE loaded column. The schematic experimental set up is shown in Figure 5-1.

Interfacial Tension Measurement

The interfacial tensions (γ) between aqueous surfactant solutions and *n*-decane, and PCE were measured by the drop weight method (Harkins and Brown, 1919). A glass tube and two Teflon tubes were used for the interfacial tension measurements for *n*-decane-surfactant solutions (SDBS and CPC), and PCE-SDBS solution, respectively. Stock solutions of SDBS (8 mM) and CPC (5 mM) were prepared and subsequently diluted to achieve the desired concentrations. Polished tubes were immersed into the less-dense liquid (e.g., water drops were formed in *n*-decane phase at the tip of tube), and 3 ~ 50 drops were collected and weighed using a chemical balance.

Results and Discussion

NAPL-Water Interfacial Area

Interfacial tensions (γ) for all the NAPL-surfactant aqueous solution systems show a typical exponential decay (Fig. 5-2), and the estimated CMCs for the purified SDBS (2.2 mM) and CPC (0.9 mM) were in agreement with reported values (Shah, 1979; Rosen, 1989). The minimum molecular cross-sectional areas of SDBS and CPC at a *n*-decane-water interface were calculated as 69 and 66Å^2, respectively, which also agree with numbers reported in the literature (Shah, 1979; Rosen, 1989). The surface excess of SDBS and CPC at a NAPL-water interface was calculated by fitting the γ - C curves and using the local slopes of the fitted curves (Eq. 5-1). Interfacial adsorption coefficients (K_{in}) were calculated using Eq.5-3 (Table 5-1) and the surface excess concentrations of surfactant.

From the BTCs measured in miscible displacement experiments with SDBS and CPC (Fig. 5-3), it is evident that there is a significant retardation of SDBS due to the existence of a NAPL-water interface. A uniform thin coating of NAPL on the glass beads eliminates the likelihood of interaction of tracers with the solid surface. A mass balance calculation also verified that the volume of air entrapped in the system is negligible, precluding tracer adsorption at the air-water interface. According to equation 5-4, the retardation factor, R_t, is expected to decrease as the bulk tracer concentration increases due to a rapid decrease in adsorption coefficient, K_{in}. The measured retardation factors are shown in Figure 5-4, as a function of tracer concentration, which clearly reflect the nonlinear dependency of retardation factors on the tracer concentration.

Calculated NAPL-water interfacial areas are presented in Table 5-1. Over the influent concentration ranges of SDBS and CPC used in this study, the calculated *n*-decane-water and PCE-water interfacial areas were fairly consistent. No significant difference was observed between the NAPL-water interfacial areas measured using SDBS (480 ± 60 cm^2/cm^3) and CPC (420 ± 60 cm^2/cm^3). The estimated specific PCE-water interfacial areas were also consistent with *n*-decane-water interfacial areas. Since the measured NAPL-water interfacial areas were consistent regardless of the types of interfacial tracers (SDBS-anionic, CPC-cationic) and NAPLs (*n*-decane and PCE), the use of ionic surfactants as interfacial tracers is proven to be applicable for the estimation of NAPL-water interfacial areas in porous media with sound theoretical and practical bases. The same technique has also been successfully used for the estimation of air-water interfacial areas in an unsaturated porous medium (Saripalli et al, 1997; Kim et al, 1997).

Using a simple geometric analysis based on assumptions that the surface is completely smooth and that all the solid particles are identical in size, the specific surface area of the glass beads used in this study was calculated to be about 310 cm^2/cm^3. The mean diameter of the glass beads was determined by visual inspection using a microscope. A number of depressions and irregularity on the surface were observed for the glass bead. The calculated thickness of *n*-decane and PCE coating on the beads was 0.3 μm. This NAPL coating thickness is not enough to make the coated surface completely smooth. Therefore, the absolute specific surface area of glass bead packing will be larger than the values calculated assuming smooth surface. However, the calculated areas are expected to be a slight underestimation because the NAPL coating effectively eliminates the contact of tracer molecules with micropores of the solid support. Therefore, the estimated NAPL-water interfacial areas (400 ~ 500 cm^2/cm^3) using interfacial tracers are considered to be close to the true value, which also confirms the quantitative validity of interfacial tracer technique.

The morphology index (H_N, cm^2/cm^3) is used as an indicator of the efficiency of a unit volume of NAPL to produce a NAPL-water interface (Kim et al., 1997; Saripalli et al., 1997; Annable et al., 1998a):

$$H_N = \frac{a_{nw}}{\epsilon \, S_N} \tag{5-5}$$

where ϵ is the porosity (cm^3/cm^3). The morphology indexes of glass bead columns were presented in Table 5-1. Morphology index maybe useful to test if the matrix of a porous medium is oil-wet or water-wet (Saripalli et al., 1997, 1998b). Conceptually, a relatively large H_N means that the solid surface is oil-wet forming film on the surface, while small H_N suggests a water-wet solid surface (Annable et al., 1998a).

Estimated a_{nw} values of natural porous media, unlike a homogeneous glass bead column, may not represent all of the NAPL-water interface present due to the heterogeneity of the system (Annable et al., 1998a). The water in immobile regions is not as readily accessible to the interfacial tracers as is the water in the mobile region. Moreover, dead zones where the NAPL-water interfaces are completely isolated by a solid or liquid barrier will not allow the tracers to contact the interfaces. Unlike partitioning tracers which can travel across NAPL-water boundaries and eventually reach an equilibrium state, an interfacial tracer will behave as if there are no such interfaces when hydrodynamic access is blocked by other interfaces. Therefore, the NAPL-water interfacial area using an aqueous interfacial tracer is an "effective quantity" rather than an "absolute quantity", which should be interpreted with caution (Reeves and Celia., 1996). For homogeneous glass beads with NAPL films on the surface, all of the NAPL-water interfaces is regarded as accessible to the tracer without substantial error at water-saturated condition.

Interfacial Adsorption Isotherm

The retardation factor (R_t) is a function of adsorption coefficient (K_{in}) of the tracer being used, as well as the quantity of interface (a_{nw}) and water content (θ_w) in a water saturated condition (Eq.5-4) when the effects of other sorption processes (e.g., soil sorption) on the retardation factor are negligible. Suppose a porous medium has a fixed NAPL-water interfacial area (a_{nw}) and is saturated with water. The retardation factor, R_t, is then solely the function of the interfacial adsorption coefficient, K_{in}. Therefore, retardation factors from a series of column experiments with varying influent tracer concentrations (C_o) will result in the corresponding adsorption coefficients, which, in turn, can be utilized to estimate the surface excess (Γ) at the bulk aqueous concentrations of the tracer. The interfacial adsorption isotherm [$\Gamma(C)$] estimated through such a process can be compared with that calculated from the interfacial tension data to confirm that the interfacial tracer behaves in a similar manner during column displacement experiments (retardation factor measurement) as in the batch experiments (interfacial tension measurements).

The solid adsorption coefficient (K_d) in Eq. 5-4 was assumed to be zero since the glass bead surface was coated with a thin film of NAPL, eliminating access to the tracers from the aqueous phase. Unlike the a_{nw} calculation performed in the previous section (where K_{in} values from interfacial tension data were used), it is necessary to fix the a_{nw} value for K_{in}

estimation. The a_{nw} value estimated using the retardation factor obtained from a column experiment with an influent concentration of CMC and a K_{in} value from the saturated surface excess of the tracer was used. Instead of using the estimated value, it is also useful to use the absolute solid surface area, if available, which will lead to independent estimation of K_{in} values without any information from interfacial tension data. Since we used the K_{in} at the CMC, all other K_{in} values at different concentrations estimated from retardation factors are, consequently, normalized to the K_{in} at the CMC. This approach, however, still provides very important information on whether the isotherm predicted by the Gibbs equation is compatible with those estimated from the retardation factors.

As concentrations (C) of SDBS and CPC in the bulk aqueous phase decrease, the surface excess (Γ) decreases in a non-linear fashion and the magnitude of the interfacial adsorption coefficient (K_{in}) increases. The Γ - C relationship is a typical Langmuir-type isotherm where the saturation of surfactant at the NAPL-water interface is reached below the CMC (Fig. 5-5). Confirmation of the Gibbs equation by direct detection of surface adsorbed surfactant using radioactive-labeled surfactant, can be found in the literature (e.g., Tajima et al., 1970) , which is consistent with the results represented in this study. Figure 5-5 also shows that the surface excess concentrations of both interfacial tracers (SDBS, CPC) in a *n*-decane-water system, calculated from column-measured retardation factors, are in good agreement with the interfacial adsorption isotherms predicted by Gibbs equation using interfacial tension data. These results suggest that the interfacial tracer retardation is sensitive to their bulk concentrations, and that the tracer technique correctly reflects fluid-fluid interfacial areas.

Summary

Miscible displacement experiments were employed using sodium dodecylbenzene sulfonate (SDBS) and cetylpyridinium chloride (CPC) as interfacial tracers to measure non-aqueous phase liquid (NAPL)-water interfacial areas (a_{nw}) in columns packed with silanized glass beads coated with either n-decane or perchloroethylene (PCE). The quantitative validity of the experimental technique was tested by comparing (1) the measured a_{nw} values with the particle surface area of the glass beads of known size and shape, and (2) the adsorption isotherm estimated from the surfactant retardation factors with that predicted from the interfacial tension data and Gibbs adsorption equation. Using the miscible displacement technique with SDBS and CPC, interfacial areas for *n*-decane-water and PCE-water in glass bead columns were determined to be in reasonable agreement with the solid surface area estimated by a geometric analysis. No significant difference was observed in NAPL-water interfacial areas measured for both NAPLs using the two interfacial tracers. The surface adsorption isotherm obtained from a series of column experiments using different tracer concentrations was also in good agreement with that predicted by Gibbs adsorption equation using measured data for NAPL-water interfacial tension.

Table 5-1. Summary of expeirmental parameters and results.

column[a]	S_N (%)	R_t	C_o (mM)	K_{in} (10^{-3}cm)	a_{nw} (cm^2/cm^3)	H_N (10^4cm^2/cm^3)
GB–I	2.2	8.03	0.012	7.10	430	4.7
		6.37	0.024	4.53	520	5.6
		4.58	0.048	2.77	560	6.2
		3.70	0.071	2.06	570	6.2
		2.94	0.095	1.66	510	5.6
		1.92	0.18	1.02	390	4.3
		1.56	0.36	0.59	420	4.6
		1.40	0.59	0.39	450	5.0
		1.34	0.78	0.31	490	5.3
		1.27	0.95	0.25	470	5.2
		1.22	1.19	0.20	480	5.3
		1.17	1.60	0.15	500	5.5
		1.10	2.20	0.11	410	4.4
				average[b]	480 ±60	5.2±0.6
GB–II	1.9	3.85	0.027	3.02	420	4.7
		3.21	0.056	1.96	530	5.9
		1.98	0.11	1.25	370	4.2
		1.67	0.22	0.80	390	4.4
		1.43	0.45	0.51	400	4.5
		1.25	0.89	0.28	410	4.6
				average[b]	420±60	4.7±0.6
GB–III	2.4	2.00	0.20	0.79	480	5.3
		1.68	0.40	0.39	650	7.1
				average	560	6.2
				total average	470	5.2

[a] GB–I: SDBS, glass bead column with *n*-decane coating, GB–II: CPC, glass bead column with *n*-decane coating, GB–III: SDBS, glass bead column with PCE coating

[b] includes ± 1 standard deviation

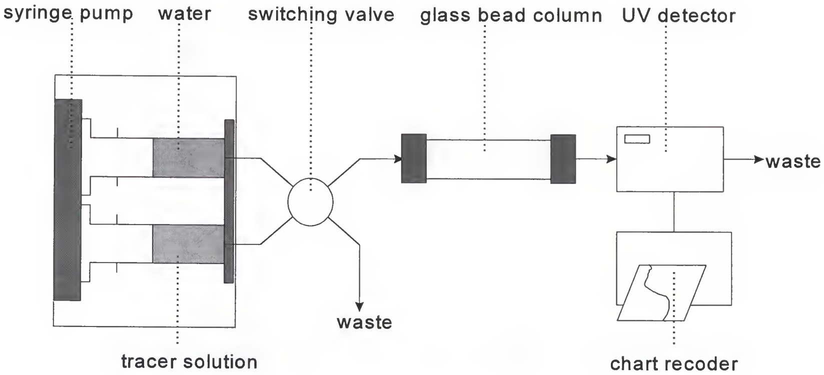

Figure 5-1. Schematic diagram of the experimental set-up.

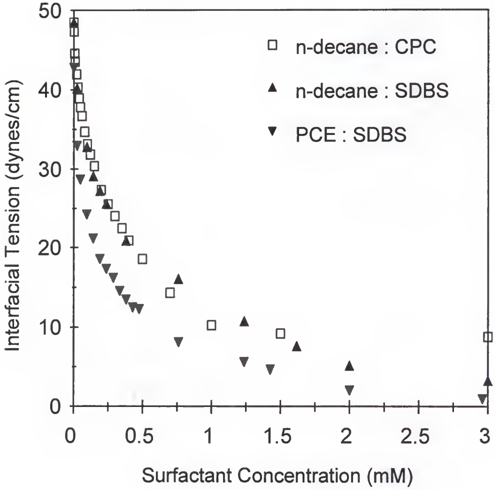

Figure 5-2. Interfacial tensions between NAPL-surfactant aqueous solutions.

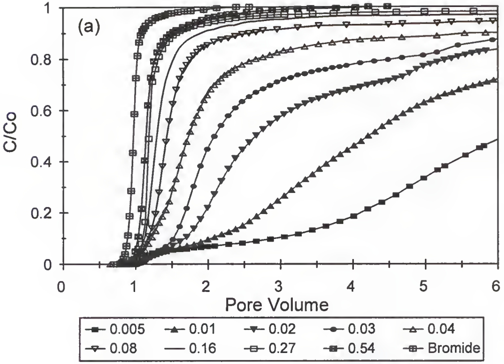

SDBS normalized concentration (CMC=1.00)

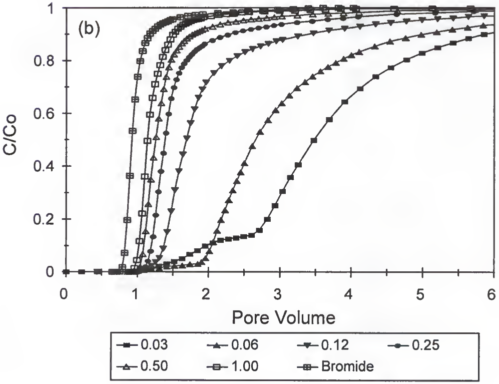

CPC normalized concentration (CMC=1.00)

Figure 5-3. Breakthrough curves of interfacial tracers : (a) SDBS (CMC=2.2 mM), *n*-decane column; (b) CPC (CMC = 0.9 mM), *n*-decane column; (c) SDBS, PCE column.

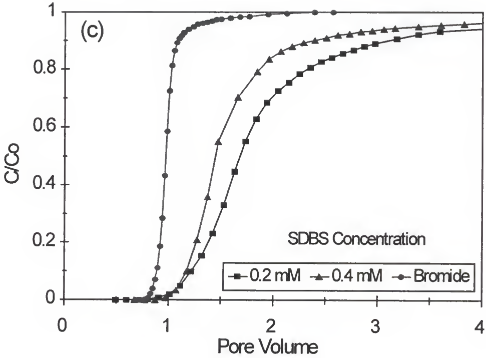

Figure 5-3 (continued). Breakthrough curves of interfacial tracers : (c) SDBS, PCE column.

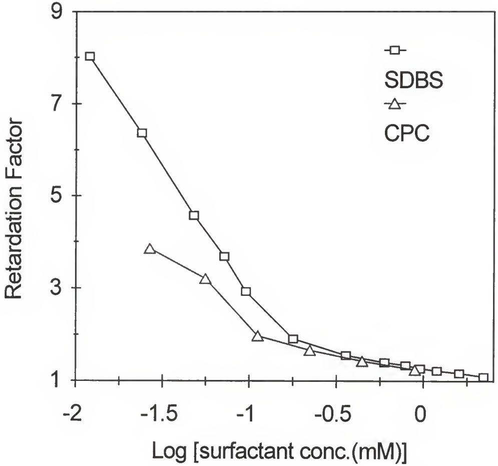

Figure 5-4. Retardation factors of SDBS and CPC as a function of tracer influent concentrations from *n*-decane glass bead column experiments.

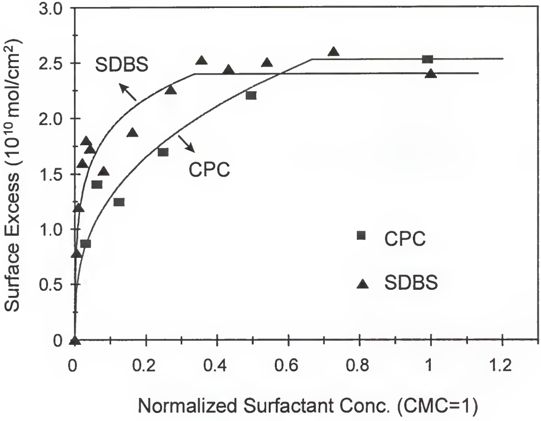

Figure 5-5. Interfacial adsorption isotherms of SDBS and CPC calculated from interfacial tension data and the Gibbs equation (solid line), and column (*n*-decane) experiment data.

CHAPTER 6
TRANSPORT OF INTERFACIAL AND WATER-PARTITIONING TRACERS: IMPACT OF NON-EQUILIBRIUM SORPTION AND NONLINEAR ADSORPTION ISOTHERM

Introduction

Although several examples of lab or field experiments of interfacial tracers demonstrating the applicability of this technique are to be found (Saripalli et al., 1997, 1998a,b; Annable et al., 1998a; Kim et al., 1997), a detailed study of the combined effects of non-equilibrium sorption and a nonlinear adsorption isotherm on the transport behavior of these tracers has not been performed. The adsorption isotherms of surfactant used as the aqueous-phase interfacial tracers, for both air-water and NAPL-water systems, were found to have typical Langmuirian shape as shown in Fig. 4-5 (Adamson, 1989; Rosen, 1989; Kim et al., 1997). The isotherms for adsorption of volatile organic chemicals (VOCs) at the air-water interface are different from those of surfactant. At a low concentration range (or Henry's region), the VOC adsorption isotherms are fairly linear, such that a constant value of the adsorption coefficient (K_{iw} or K_{ia}) for each chemical can be used. These K_{iw} or K_{ia} values can be found in the literature (Table 1-1). However, it should be recognized that the threshold bulk concentration, in either aqueous or gaseous phase, beyond which this linear relationship does not hold differs from chemical to chemical. Based on the surface (interfacial) tension versus bulk concentration relationship, the linear adsorption range of a VOC at the fluid-fluid interface can be identified.

Whenever a sorption process does not occur instantaneously during transport in porous media, or time scales required for sorption are much longer compared to the mean residence time in the flow domain of interest, the transport pattern of the chemical deviates from an ideal one based on instantaneous sorption equilibria. In general, there are three different categories of possible mechanisms that may cause non-equilibrium transport: (1) flow domain related non-equilibrium, which is caused by the heterogeneity of the media, (2) time-dependent chemical interaction between sorbate and sorbent (in this case, the interface), and (3) diffusion-dependent sorption processes that occur when at least part of the active "sites" of sorption reside where the mobile fluid can not directly access. The first cause of non-equilibrium is not likely a factor for experiments in homogeneously packed lab-scale column, unless the column is packed in such way that heterogeneity should be tested.

Among the rate-limited chemical sorption and diffusion-dependent processes, a thorough investigation of the physical configuration of the system as well as an understanding of the kinetics of the sorption are required to determine which is the dominantly responsible cause of the non-equilibrium. For example, flow in an aggregated porous medium may exhibit a strong non-equilibrium sorption during transport because most of the sorptive surface is located inside of the aggregates, and the only means for the sorbate molecules to reach these surface are via diffusion. Non-equilibrium transport due to intrasorbent diffusion has been the basis of two-region models (Coats and Smith, 1964; van Genuchten and Wierenga, 1976; Cameron and Klute, 1977; Brusseau and Rao, 1989), where the flowing domain (e.g., water in most cases) is divided into two parts; mobile and immobile regions.

The non-equilibrium caused by slow sorption kinetics during solute transport was modeled by Selim et al. (1976) and by Cameron and Klute (1977) for the first time. This two-site model was used later by Rao et al. (1979), De Camargo et al. (1979), and Hoffman and Rolston (1980) for evaluating various cases of chemical sorption. Although the two models (two-site and two-region) are based on different conceptualization of the observed non-equilibrium situations, it is shown that the two models are mathematically equivalent (Nkedi-Kizza, et al., 1984). More detailed discussion of various conceptual models and their mathematical formulations for non-equilibrium solute transports can be found in the literature (e.g., Brusseau and Rao, 1990).

Theoretical Background

Two-Region Model

In this model, the fluid (water) in the soils is partitioned into the mobile and immobile regions. The sorption and desorption of chemicals by soil are assumed to take place instantaneously. Transport, by either convection or dispersion, of chemicals occurs only in the mobile region, while the solute transfer between mobile and immobile regions is controlled by diffusion, which is the main cause of the non-equilibrium. The governing equation of one-dimensional, convective-dispersive, two-region model for a homogeneous medium and steady flow condition is:

$$\theta_m \frac{\partial c_m}{\partial t} + f\rho \frac{\partial s_m}{\partial t} + \theta_{im} \frac{\partial c_{im}}{\partial t} + (1-f)\rho \frac{\partial s_{im}}{\partial c_m} = \theta_m D_m \frac{\partial^2 c_m}{\partial z^2} - \theta_m v_m \frac{\partial c_m}{\partial z} \qquad 6\text{-}1$$

$$\theta_{im}\frac{\partial c_{im}}{\partial t} + (1-f)\rho\frac{\partial s_{im}}{\partial t} = \alpha_1(c_m - c_{im}) \qquad 6\text{-}2$$

where c (g/cm^3) and s (g/g) represent the concentrations of a solute associated with the liquid phase and the solid phase, respectively, the subscripts, m and im refer to the mobile and immobile regions, ρ (g/cm^3) is the bulk density of the soil, f represents the mass fraction of soil that is in direct contact with the mobile (dynamic) liquid, D (cm^2/min) is the hydrodynamic dispersion coefficient, v (cm/min) is the pore water velocity, t (min) is time, z (cm) is distance, and α_1 (1/min) is the first-order mass transfer coefficient for the diffusion between mobile and immobile region. Assuming the sorption of a chemical at the soil has a linear isotherm, and the sorption coefficient K_d (cm^3/g) is identical for both mobile and immobile regions:

$$s_m = K_d\, c_m, \qquad s_{im} = K_d\, c_{im} \qquad 6\text{-}3$$

and the total sorption s is:

$$s = f s_m + (1-f)s_{im} \qquad 6\text{-}4$$

Combining Eq. 6-1 ~ 6-4:

$$(\theta_m + \rho f K_d)\frac{\partial c_m}{\partial t} + [\theta_{im} + (1-f)\rho K_d]\frac{\partial c_{im}}{\partial t} = \theta_m D_m\frac{\partial^2 c_m}{\partial z^2} - \theta_m v_m\frac{\partial c_m}{\partial z} \qquad 6\text{-}5$$

$$[\theta_{im} + (1-f)\rho K_d]\,\frac{\partial c_{im}}{\partial t} = \alpha_1(c_m - c_{im}) \qquad 6\text{-}6$$

The Eqs 6-5 and 6-6 can be converted to dimensionless forms using the following dimensionless variables:

$$\beta R_t \frac{\partial c_1}{\partial T} + (1-\beta) R_t \frac{\partial c_2}{\partial T} = \frac{1}{P} \frac{\partial^2 c_1}{\partial x^2} - \frac{\partial c_1}{\partial x} \qquad \text{6-7}$$

$$(1-\beta) R_t \frac{\partial c_2}{\partial T} = \omega \, (c_1 - c_2) \qquad \text{6-8}$$

where

$$c_1 = \frac{c_m}{C_o} \; ; \quad c_2 = \frac{c_{im}}{C_o} \qquad \text{6-9}$$

$$T = \frac{vt}{L} = \frac{v_m \phi_m t}{L} \; ; \quad \phi_m = \frac{\theta_m}{\theta_w} \; ; \quad v = v_m \phi_m \qquad \text{6-10}$$

$$x = \frac{z}{L} \qquad \text{6-11}$$

$$P = \frac{v_m L}{D_m} \qquad \text{6-12}$$

$$R_t = 1 + \frac{\rho K_d}{\theta_w} \qquad \text{6-13}$$

$$\beta = \frac{\theta_m + f \rho K_d}{\theta_w + \rho K_d} = \frac{\phi_m R_m}{R_t} \; ; \quad R_m = 1 + \frac{f \rho K_d}{\theta_m} \qquad \text{6-14}$$

$$\omega = \frac{\alpha_1 L}{q} \; ; \quad q = \theta_m v_m \qquad \text{6-15}$$

In Eqs 6-7 to 6-15, C_o (g/cm^3) is the influent concentration of a solute, L (cm) is the length of the system, and θ_w is the total volumetric water content. Among the dimensionless variables, P and R_t, are referred as the Peclet number and retardation factor, respectively, while ω and β represent the factors contributing to non-equilibrium. Note that the derivation of Eqs 6-7 and 6-8 is based on a linear sorption isotherm, instantaneous sorption kinetics at the soil surface, and reversible (non-hysteretic) sorption-desorption.

Two-Site Model

In this model, the non-equilibrium during chemical transport is interpreted as the result of slow chemical sorption kinetics rather than diffusion-controlled mass transfer between mobile and immobile regions. All of the water in the system is considered to be mobile and participates in advective-dispersive transport. First type of the sorptive sites in this model is that a fast equilibrium is achieved, and second type sites are where the time-dependent kinetic sorption takes place. At equilibrium, assuming that a linear isotherm applies and that the sorption coefficient in both fast and slow sites are the same, the relationship between sorbed and bulk solute concentrations is:

$$s_1 = K_1 c = FK_d c \qquad 6\text{-}16$$

$$s_2 = K_2 c = (1-F)K_d c \qquad 6\text{-}17$$

where the subscripts *1* and *2* now refer to the fast and slow sorption sites, K (cm^3/g) is the apparent sorption coefficient, F is the fraction of all fast sorptive sites, and K_d is the same as in the two-region model. The total sorption s is the sum of both fast and slow sites:

$$s = s_1 + s_2 \qquad 6\text{-}18$$

The rate of sorbed concentration change over time for the fast site is:

$$\frac{\partial s_1}{\partial t} = FK_d \frac{\partial c}{\partial t} \qquad 6\text{-}19$$

and that for the slow kinetic sites is:

$$\frac{\partial s_2}{\partial t} = \alpha_2[(1- F)K_d c - s_2] \qquad 6\text{-}20$$

where α_2 represents the first order kinetic rate constant (1/min). Using Eqs 6-19 and 6-20, the governing equation for the two-site model is:

$$\left[1 + \frac{F\rho K_d}{\theta_w}\right]\frac{\partial c}{\partial t} + \frac{\rho}{\theta_w}\frac{\partial s_2}{\partial t} = D\frac{\partial^2 c}{\partial z^2} - v\frac{\partial c}{\partial z} \qquad 6\text{-}21$$

Introducing following dimensionless variables for Eqs 6-20 and 6-21:

$$c_1 = \frac{c}{C_o} \; ; \quad c_2 = \frac{s_2}{(1-F)K_d C_o} \qquad 6\text{-}22$$

$$T = \frac{vt}{L} \; ; \quad x = \frac{z}{L} \qquad 6\text{-}23$$

$$R_t = 1 + \frac{\rho K_d}{\theta_w} \; ; \quad R_m = 1 + \frac{F\rho K_d}{\theta_w} \qquad 6\text{-}24$$

$$\beta = \frac{\theta_w + F\rho K_d}{\theta_w + \rho K_d} = \frac{R_m}{R_t} \qquad 6\text{-}25$$

$$\omega = \frac{\alpha_2(1 - \beta)\, R\, L}{v} \qquad 6\text{-}26$$

the dimensionless transport equation becomes the same as that of two region model (Eq. 6-7). Since the dimensionless governing equations are the same for both two-site, and two-region models, the dimensionless analytical solutions for both models are identical.

Nonlinear Isotherm

In many situations, the sorbed and bulk concentration of a chemical does not follow a simple linear relationship as described in the previous sections. The non-linear nature of sorption isotherms is often expressed as two well-known equations; Freundlich and Langmuir isotherms. For Freundlich type isotherms, the sorbed solute concentration is expressed as the power function of the bulk concentration:

$$S = K_f \, C^N \tag{6-27}$$

where S (g/g), and C (g/cm^3) represent the sorbed and bulk solute concentrations, respectively, K_f [g^{N-1}(cm^3)^N/g] is the Freundlich sorption coefficient, and N is a constant. The general shape of a isotherm varies depending on N value. Note that there is no upper limit of sorbed concentration S with the Freundlich equation. This type of isotherms are found to be appropriate in many solute-soil interactions (e.g., Rao and Davidson, 1979).

The general equation of Langmuir type isotherm is (Langmuir, 1918):

$$S = \frac{S_m C}{C + a} \tag{6-28}$$

where S_m (g/g) is the maximum sorbed concentration, and a (g/cm^3) is a constant that is related to the Gibbs free energy change during the sorption process.

Temporal Moment Analysis

Temporal moment analysis, one of the standard chemical engineering procedures, is a useful technique for the quantitative description of chemical concentration breakthrough curves for packed bed type reactors (Turner, 1972; Suzuki and Smith, 1971; Fahim and Wakao, 1982). For a BTC generated by injecting a pulse input into a soil column, the concentration distribution monitored at the exit boundary of the column is described by its absolute, temporal moments:

$$m_n = \int_0^\infty T^n c(x,T) \, dT \tag{6-29}$$

where, m_n (g min^n/cm^3) is the nth absolute moment, c (g/cm^3) is the concentration and the notations for other parameters are the same as in Eq. 6-7. Absolute zero-th moment m_0, for example, represents the total mass that is monitored at the point of observation. The *n*th normalized moment μ'_n is defined as:

$$\mu'_n = \frac{m_n}{m_0} \qquad 6\text{-}30$$

The normalized first moments of reactive and non-reactive chemicals were used to estimated the retardation factor of the reactive chemicals (Eq. 4-6). The *n*th central moment is given as:

$$\mu_n = \frac{\int_0^\infty (T-\mu'_1)^n \; c(x,T) \; dT}{m_0} \qquad 6\text{-}31$$

The second and third central moments represent the spread and skewness of the BTC, respectively.

Valocchi (1985) investigated the relationship between the moments (absolute zero-th, second and third central) and the parameters used in Eqs. 6-7 and 6-8;

$$\mu'_1 = xR_t \qquad 6\text{-}32$$

$$\mu_2 = \frac{2xR_t^2}{P} + \frac{2x(1-\beta)^2R_t^2}{\omega} \qquad 6\text{-}33$$

$$\mu_3 = \frac{12xR_t^3}{P^2} + \frac{12x(1-\beta)^2R_t^3}{P\omega} + \frac{6x(1-\beta)^3R_t^3}{\omega^2} \qquad 6\text{-}34$$

where all the parameters are dimensionless and the same as Eq. 6-7. Equations 6-32~34 are useful because the parameters related to the non-equilibrium sorption (e.g., ω) can be estimated based on temporal moment analysis.

Experimental

The experimental procedure, and the chemicals used in this chapter are the same as in the previous chapters (Chap. 3~5). In addition, a series of aqueous interfacial tracer experiments were conducted to investigate the effect of the change in concentration of input tracer pulse on the retardation factor. In these experiments, approximately 0.5 pore volumes of a pulse input of CPC was injected into a column packed with *n*-decane coated glass beads (see Chap. 5). After a pulse input column experiment, a corresponding step input of CPC with C_o concentration that is the same as the maximum peak concentration of the pulse input BTC was applied.

Results and Discussion

Gaseous Transport

The temporal, central second and third moments of methane, used here as a gaseous non-reactive tracer, did not change with water saturation change at the same pore-air velocity. No significant functional relationship was found between water saturation (S_w) and the central moments. This result indicates that either the gas-phase of the porous media (sand and Dover AFB soil) is fairly homogeneous, or the mass transfer (or diffusion) rate of methane between mobile and immobile regions during transport is fast enough not to cause diffusion rate-limited non-equilibrium. Since water fills the smallest pores first, the geometry of gas-filled space becomes less complicated as the water saturation increases. Thus, the concept of immobile gaseous region is not likely applicable for the cause of non-equilibrium during gaseous transport. At the same time, the diffusion rate of gaseous molecules is approximately four orders of magnitude larger than that in the aqueous phase at the same temperature (Schwarzenbach et al., 1993). Therefore, the diffusion rate of the gaseous molecules may not be a constraining factor that causes an apparent non-equilibrium. A combination of these two effects, rather than one or the other, is very likely the reason for symmetric methane BTCs. Lack of physical non-equilibrium due to diffusion-dependent mass transfer between different spatial domains *within the gaseous phase* eliminates the source of non-equilibrium associated with the geometry of flowing domain (two-region model).

Figure 6-1 shows the BTCs of a series of aliphatic hydrocarbons (used as gaseous interfacial tracers) and methane, where no apparent non-equilibrium appears. The change of longitudinal dispersion of methane at different pore-gas velocities is illustrated in Fig. 6-2. The dispersion of methane BTC is larger at the lower gas flow rate than that at the higher flow rate maintaining the BTC symmetry, which supports the point that gaseous diffusion is the major factor for peak spreading. This result is contradictory to those reported by Popovicova and Brusseau (1998) who did not observe any change of BTC shape with different pore-gas velocities in displacement through homogeneous media. This may be because of the difference in the range of pore-gas velocities. In their study, the pore-gas velocity ranged from 60 to 270 cm/min, while much slower velocities (7 - 66 cm/min) were used for methane transport experiment in this study. Therefore, it may be concluded that gaseous diffusion is a factor responsible for the BTC spread at low pore-gas velocity, while the hydrodynamic mixing may be the dominant control factor at sufficiently high pore-gas velocity resulting in no significant change in the shape of BTC with further increase in the gas velocity.

Figure 6-3 shows the normalized central second moments of VOCs used in this study. As expected, the BTCs spread more with increasing retardation factor regardless of the cause of the retardation (e.g., partitioning into aqueous phase, adsorption at the air-water interface).

The shape of BTCs of water-partitioning tracers changed with changing water saturation. As water saturation increases, the BTCs of methylene chloride are skewed to the right side of the center of mass (Fig. 6-4). Since non-equilibrium was not a factor for methane transport (for the same medium, sand), this non-equilibrium effect should be induced by some processes other than diffusion-limited gaseous phase non-equilibrium. The only possible cause of this non-ideal behavior of methylene chloride during gaseous transport is the slow mass transfer rate from the gaseous phase into the bulk aqueous phase. Note that solid phase sorption for methylene chloride was negligible. As water saturation increases, the overall thickness of water film on the surface of the sand increases. Thus, methylene chloride molecules have to diffuse longer distance with increasing water saturation. The other factor that might induce this non-equilibrium is that the air-water interfacial area decreases with an exponential fashion as the water saturation increases. The temporal, central second and third moments of methylene chloride, estimated from the BTCs, are shown in Fig. 6-5. Note that the second and third central moments increase exponentially with increasing water saturation.

The two-site model can be used to estimate the non-equilibrium-related parameters for the transport of methylene chloride. But the equations for this model (Eqs 6-16~6-26) need to be recast to account for the difference in the mobile phase (gas) and the sorption domain (water). Following is the necessary changes in these equations:

$$K_d \rightarrow \frac{1}{K_H}\ ; \quad \theta_w \rightarrow \theta_a\ ; \quad \rho \rightarrow \theta_w \qquad 6\text{-}35$$

where θ_a and θ_w are the volumetric gas and water contents, respectively, and K_H is the Henry's law constant defined in Eq. 2-7. The two-site model was chosen because it represents the system better than two-region model, even though the aqueous phase diffusion rate of methylene chloride, rather than slow sorption kinetics as in the original model, is responsible for the non-equilibrium processes.

Based on the shape of BTCs of non-reactive tracer (methane) at different water saturation and pore-gas velocities, there is no distinguishable immobile gas-phase identified. Since the non-equilibrium effect for methylene chloride BTCs is not caused by the heterogeneous characteristics of gaseous phase, the mass transfer related dimensionless term (Damkohler numer) ω should be also defined as in Eq. 6-26. The α_2 term in Eq. 6-26 now represents the diffusion-related (lumped) mass transfer coefficient instead of the adsorption rate constant:

$$\alpha_2 = k_f a_i = \frac{D_f a_i}{\delta} \qquad 6\text{-}36$$

where k_f is the mass transfer coefficient (cm/min), D_f is the effective diffusion coefficient in the aqueous phase (cm^2/min), and δ is the thickness of the stagnant water film layer at the air-water interface (cm). Using Eq. 6-36 and the ω values (Eq. 6-26), it is now possible to evaluate the thickness of water film layer δ.

The BTCs for methylene chloride (Fig. 6-4) were fit with 2-site model with a constant sorption coefficient (K_H). The Peclet number P, was fixed to be 116 estimated from the BTC for methylene chloride measured at a water content of 0.07. For these experiments, fixing P value is a reasonable assumption because the BTCs of the non-reactive tracer (methane) are almost identical regardless of water content change. The estimated P of the methane BTC at a water content of 0.07 was about 83, which is smaller than that of methylene chloride. This is due to the difference in the gaseous diffusion coefficient. Note that molecular diffusion is the responsible mechanism for the dispersion of tracers during gaseous transport under the experimental conditions used in this study.

The results of fitting the methylene chloride BTCs to the 2-site model are shown in Table 6-1. The total retardation factors estimated from the temporal first moments of observed BTCs were used for the fitting. As expected, the overall mass transfer coefficient, α_2, and the fraction of fast sorption sites, F, decreased as the water content increased, implying that it takes longer for methylene chloride to reach the equilibrium state at higher water contents. The normalized, temporal, second central moments from direct calculation for the observed BTCs were in good agreement with the predicted moments using Eq. 6-33. Thus, the degree of spread for the fitted BTCs are close to that of observed BTCs (Fig. 6-6). However, the normalized, temporal, third central moments which were estimated using Eq. 6-34 are much smaller than those calculated directly from the observed BTCs. This is because Peclet number was fixed for the fitting process although the observed BTCs seemingly become broader as the water content increases. A small change in the beginning and tailing part of BTCs resulted in substantial errors in the estimated third moments due to the third-powered time (or pore volume) dependency of the temporal, third central moments (Eq. 6-31).

Based on α_2 values and Eq. 6-36, the estimated thickness of stagnant water film layer (δ) that controls the mass transfer (water-partitioning) rate was found to be at least 2 orders of magnitude larger than the mean water film thickness estimated from the volumetric water content (θ_w) and the measured specific air-water interfacial area (a) using gaseous phase interfacial tracer (*n*-decane) (see Table 6-1). First, the mean thickness of water film calculated from θ_w and a_i may not properly represent the effective thickness of the water film that results in slow water partitioning of methylene chloride during a gaseous transport. The water in the medium is expected to be distributed on the surface of sand grains, pore spaces, and particularly at the contact points between particles. The fraction of water with thick film or trapped in small pores, which has much longer diffusion path lengths may dominantly control the non-equilibrium process of water partitioning.

Second possible cause of this discrepancy is that Eq. 6-36 may not be adequate for describing the non-equilibrium transport behavior of methylene chloride. Equation 6-36 is based on an assumption that the aqueous phase stagnant film (in fact, all the aqueous phase is considered to be stagnant because there is no flow or turbulence in the aqueous phase) dominantly controls the diffusion rate. This may not be the case if a gaseous phase stagnant film does exist and poses a significant mass-transfer barrier for the gas to water diffusion process. However, the evidence from this study that the effective thickness value δ, is constant with respect to the water content change, is not conclusive to support this possibility, because the non-equilibrium effect for the BTC at the lowest water content (θ_w = 0.07) is not evident (i.e., $\beta = 0.965$).

It is interesting that the overall mass transfer coefficient, α_2, reflects the skewness of the BTCs maintaining relatively consistent δ values except the fitting result at $\theta_w = 0.07$. This result suggests that the specific air-water interfacial area rather than the thickness of the water film is apparently the controlling factor responsible for the non-equilibrium sorption during the gaseous transport of methylene chloride in the water content range of 0.12~0.18.

Aqueous Transport

The bromide BTCs observed from displacement experiments with a column packed with *n*-decane coated column (described in Chapter 5) were fairly symmetric (Fig. 6-7a). At the same time, no difference was found between the frontal and distal portions of the bromide BTCs. This result was expected because of the homogeneous nature of the column that was packed with glass beads with nearly identical size. However, an indisputable difference in the shape of the CPC BTCs between the frontal and distal portions was found (Fig. 6-7 b,c). The CPC BTCs also show early breakthrough and much longer tailing compared to the bromide BTCs (Fig. 6-8). There are at least two different causes combined that distort the BTCs of CPC during aqueous phase transport: one is the rate-limited adsorption/desorption kinetics, and the other is the nonlinear adsorption isotherm of CPC at the *n*-decane-water interface (Fig. 4-5). Freundlich (with N<1, Eq. 6-27), or Langmuir type sorption isotherms (Eq. 6-28) often cause late breakthrough and early completion of the frontal part of the BTCs, while the opposite happens for the distal part of the BTCs. On the other hand, non-equilibrium sorption usually decreases the breakthrough time and causes excessive tailing. Since the BTCs of CPC in Figure 6-8 shows earlier breakthrough than the expected time, the non-equilibrium effect is obvious considering the adsorption isotherm of CPC at the air-water interface is a Langmuir type. The adsorption isotherm of CPC at the *n*-decane-water interface was shown in Figure 6-9 with a regression result.

The simulated and observed CPC BTCs (front side only) are shown in Figure 6-10. It is demonstrated that the Langmuir-type non-linearity of CPC isotherm causes a "self-sharpening" on the front side of the BTC when an instantaneous equilibrium is achieved during the CPC displacement (line b in Fig. 6-10). The fitting using 2-site model for the frontal side CPC BTC was successful to describe the non-equilibrium sorption process of CPC between the aqueous phase and *n*-decane-water interface (line d in Fig. 6-10). The fitting result for the BTCs of CPC using 2-site model are shown in Table 6-2. Except the fitting result of one experiment (C_o=0.03 mM), the fraction of fast sorption site (F) was consistent with respect to the change of input concentration of CPC. This result is expected because the experiments were performed under the same flow conditions.

The sorption mass transfer coefficient, represented as a demensionless term $\alpha_2 L/v$, varied responding to the input CPC concentrations. It appears that the sorption rate of CPC at the *n*-decane-water interface is slower at lower C_o concentration. Lin et al.(1995) demonstrated the relationship between the surface adsorption rate (represented as Diffusion coefficient in their work) of *n*-decanol at the air-water interface and the its bulk aqueous concentration. And based on the dynamic surface tension change over time, it took more time to reach the equilibrium adsorption concentration at lower bulk *n*-decanol concentration. Although the result of this study (Lin et al., 1995) is consistent with the fitting results for the

CPC BTCs, it is still not clear that the adsorption of ionic surfactant at the NAPL-water interface follows the same sorption kinetics of *n*-decanol at the air-water interface. Further investigation for the adsorption kinetics of ionic surfactant at the NAPL-water interface is required for more conclusive interpretation of the transport behavior of surfactant interfacial tracers in NAPL-water systems.

The non-equilibrium parameters from the fitting of frontal part of the CPC BTCs using 2-site model was applied to the distal part of the BTCs (Fig. 6-11). The predicted BTCs using the β and ω showed similar general non-equilibrium trend (e.g., early breakthrough and extended tailing). However, compared to the observed BTCs, the desorption rate of CPC from the *n*-decane-water is apparently slower than the adsorption process. There are at least two possible mechanisms that may be responsible for this discrepancy. First, the desorption rate of CPC molecules from the adsorbed state at the interface to the bulk aqueous phase may slower than the adsorption rate. If this is the case, it must be related to the energetics of molecular interaction between sorbed surfactant molecules. In order to desorb from the interface, the molecules have to break the lateral attractive force (hydrophobic interaction) between molecules, which requires more activation energy than adsorption process, where the lateral interaction is rather favorable for the adsorption. Second possible cause is that the desorption isotherm may not be the same as adsorption isotherm (hysteretic isotherm). In general, the sorbed concentration during desorption process is higher than the adsorption process. If this applies to the CPC/water/*n*-decane system, an effect similar to what is caused by the slow desorption rate will take place on the back side BTC as shown in Fig. 6-11. More detailed study is necessary to elucidate the true cause of the difference between the front (adsorption) and back side (desorption) BTCs under the same experimental conditions.

Effect of Pulse Size on the Retardation Factor

For most contaminated sites, using a step input for interfacial tracer experiments is not a practical option due to the excessive quantity of tracer solution required (Annable et al., 1998a). Calculating the specific NAPL-water interfacial areas based on the BTCs of interfacial tracers requires two essential pieces of information; the retardation factor (or temporal first moment) and the adsorption coefficient (K_{in}) of the tracer at the NAPL-water interface. Retardation factors of tracers can be obtained with appropriate numerical analysis of the BTCs. However, determination of the K_{in} for pulse-input BTCs is somewhat problematic because of the non-linear nature of the adsorption isotherms of aqueous interfacial tracers (surfactant). For step input BTCs, this is not a critical issue because the maximum tracer concentration is fixed. Therefore, regardless of the non-linearity of the isotherm and the non-equilibrium of sorption processes, the final sorbed concentration of interfacial tracer at the NAPL-water interface must agree with that predicted from the K_{in} value at the influent concentration for continuous step input. A simple mass-balance analysis proves that the non-linearity of isotherm and non-equilibrium do not affect the retardation calculation. The adsorbed mass of the interfacial tracer, applied as a continuous step input after the tracer concentrations in effluent becomes the same as that in influent, is:

$$M_{ad} = (R_t - 1)V_p C_o \qquad 6\text{-}37$$

where M_{ad} is the total mass of the interfacial tracer adsorbed at the NAPL-water interface (mol), R_t is the retardation factor, V_p is the pore volume (cm^3), and C_o is the influent concentration (mol/cm^3). Since the system is a complete equilibrium state when the influent and effluent tracer concentrations are the same, the adsorbed total mass M_{ad} can be expressed in terms of the interfacial adsorption isotherm K_{in} and the total NAPL-water interfacial area A_{nw} :

$$M_{ad} = K_{nw} C_o \, A_{nw} \tag{6-38}$$

where A_{nw} is the total NAPL-water interfacial area in the medium (cm^2). Combining Eqs 6-37 and 6-38 gives:

$$R_t = 1 + \frac{K_{in} A_{nw}}{V_p} = 1 + \frac{K_{in} a_{nw}}{\theta_w} \tag{6-39}$$

where a_{nw} is the specific NAPL-water interfacial area (cm^2/cm^3). This mass balance analysis also applies to the air-water system (see Eqs 2-2~2-4). As seen in Eqs 4-1, 4-2, the same form of equation as Eq. 6-39 can be used for a pulse input BTC to estimate the fluid-fluid interfacial area as long as the sorption coefficient is a constant. Unfortunately, this is not exactly the case for the aqueous interfacial tracers with nonlinear interfacial adsorption isotherms. The concentration profile of the tracer changes as the plume progresses during the transport mainly due to dispersion (even without non-equilibrium), which makes it difficult to determine the correct K_{in} value that returns an exact a_{nw} which corresponds with the retardation factor. Determining an appropriate K_{in} value becomes more difficult when non-equilibrium adsorption occurs simultaneously. One approximation is using a K_{in} value of the peak concentration of a BTC (Annable et al., 1998a), when no obvious non-equilibrium is observed.

The BTCs of CPC with both step and pulse input are shown in Fig. 6-12. It was found that CPC, applied as a pulse input, breakthroughs the decane-coated glass bead column earlier than that of step input, although the retardation factors of each pair of BTCs are fairly consistent. The CPC plume breakthroughs the column earlier than that of continuous step input because the initial concentration (or the pulse concentration) is larger than the C_o of the step input. Since the K_m value at a high concentration is smaller than that at a lower concentration for chemicals with Langmuir type isotherms, the tracer plume with pulse input travels faster initially than the plume of step input. However, this trend is reversed at the tail side of the BTCs, which, in overall, compensates the early breakthrough effect of pulse input BTCs. The concentrations and estimated retardation factors of CPC were compared for the step and pulse input experiments (Table 6-3).

Summary

The effect of non-equilibrium sorption processes on the transport of VOCs were investigated. Gaseous non-reactive tracers did not show a significant non-equilibrium during gas-phase transport over a wide range of water saturation, leading a conclusion that no diffusion rate-limited non-equilibrium occurs in the gas phase for pore-gas velocity up to 66 cm/min. No substantial non-equilibrium was observed for the gaseous interfacial tracers (straight-chain aliphatic hydrocarbons) under the same experimental conditions as the gaseous non-reactive tracer. This result indicates that the sorption of VOCs at the air-water interface from the gaseous phase takes place relatively quickly with respect to the pore-gas flow velocity.

The water-partitioning gaseous tracer (methylene chloride) was found to behave differently compared to the gaseous non-reactive and gaseous interfacial tracers. The central third temporal moment of methylene chloride increases progressively with the water content increase. Considering there was no significant non-equilibrium effect for non-reactive tracer, the non-equilibrium of methylene chloride during gaseous transport is attributed to the slow diffusion rate of the chemical in the aqueous phase and to the increasing water volume to air-water interfacial area ratio with increasing water saturation.

Non-equilibrium transport was found for the aqueous interfacial tracer (CPC). The non-equilibrium adsorption of CPC at the NAPL-water interface is manifested in an early breakthrough and a longer tailing of the tracer BTCs. This non-equilibrium effect was combined with the nonlinear isotherm effect, which resulted in a clear difference between the frontal and distal sides of BTCs for the aqueous interfacial tracer.

With a homogeneous medium (glass beads with spherical shape and identical size), the pulse input of the interfacial tracer (CPC) resulted in similar retardation with those of continuous step input displacement experiments with the same influent tracer concentrations as the peak tracer concentration of the pulse input BTC. This indicates that the approximation method of using the peak concentration of a pulse input BTC for the calculation of the specific NAPL-water interfacial areas gives comparable results as the continuous step input experiments.

Table 6-1. Parameters and fitting results for BTCs of methylene chloride: advective-dispersive, linear isotherm, nonequlilibrium model (2-site model); parameters were defined in Eqs 6-16~26, 6-36; R_t– total retardation factor, used as estimated from the first temporal moments of the observed BTCs, and fixed for the fitting; Peclet number was fixed at 116.3 (fitting result of exp #10); effective aqueous diffusion coefficient, D_f of 6.9×10^{-4} cm^2/min used for δ calculation was estimated from a generalized equation, D_f (cm^2/min) $=2.7\times10^{-4}/(\mathrm{Mw})^{0.65}$ (Schwarzenbach et al., 1993).

exp. #	θ_w	R	L/v (min)	a_i (cm^{-1})	β	ω	F	α_2 (min^{-1})	moments (Valocchi, Eq.6-33, 34)		moments (from BTC, Eq. 6-31)		δ (mm)	θ_w/a_i (mm)
									μ_2	μ_3	μ_2	μ_3		
10	0.070	3.13	2.15	261	0.965	0.095	0.95	0.40	0.42	9.26	0.23	0.12	4.47	0.0027
17	0.120	5.43	1.90	151	0.906	0.760	0.89	0.79	1.19	2.15	1.11	1.37	1.33	0.0079
18	0.130	5.91	2.01	139	0.876	1.184	0.85	0.80	1.50	1.88	1.48	1.93	1.19	0.0094
19	0.140	6.55	1.95	120	0.830	1.545	0.80	0.71	2.34	3.03	2.15	2.86	1.16	0.0117
20	0.153	7.34	1.78	124	0.791	1.654	0.76	0.60	3.77	6.21	4.38	14.96	1.42	0.0123
21	0.168	7.32	1.85	97	0.730	2.103	0.70	0.58	4.63	6.73	4.77	13.51	1.16	0.0162
22	0.184	9.67	1.95	93	0.711	2.246	0.68	0.41	8.56	15.83	10.61	49.72	1.55	0.0198

Table 6-2. Parameters and fitting results for BTCs of CPC; advective-dispersive, non-linear isotherm, non-equlilibrium, 2-site model; parameters were defined in Eqs 6-16~26; R_t– total retardation factor, used as estimated from the temporal first moments of the observed BTCs, and fixed for the fitting; Peclet number was fixed at 150 (fitting result of bromide BTC); $N = 0.353$ from regression (Eq. 6-27, Fig. 6-9).

exp #	C_o (mM)	K_{in} (10^{-3})	a_i (cm^2/cm^3)	R_t	β	ω	F	$\alpha_2 L/v$
1	0.89	0.28	410	1.25	0.871	0.43	0.353	2.68
2	0.45	0.51	400	1.43	0.803	0.48	0.348	1.70
3	0.22	0.80	390	1.67	0.753	0.48	0.382	1.16
4	0.11	1.25	370	1.98	0.653	1.00	0.299	1.45
5	0.06	1.96	530	3.21	0.520	1.33	0.300	0.86
6	0.03	3.02	420	3.85	0.260	3.02	<0.01	0.09

Table 6-3. The concentrations and retardation factors of CPC displacement experiment; column packed with *n*-decane coated silanized glass beads.

exp. #	concentrations (mM)			retardation factors		
	pulse		step	pulse	step	
	influent	peak	influent		front	back
1	0.892	0.559	0.562	1.39	1.43	1.44
2	0.562	0.414	0.415	1.58	1.53	1.47
3	0.415	0.264	0.263	1.91	1.67	1.55
4	0.263	0.156	0.157	2.03	1.88	1.74
5	0.157	0.064	0.064	2.68	2.78	2.43
replication						
3	0.263	0.145	-	2.09	-	-
4	0.415	0.256	-	1.87	-	-

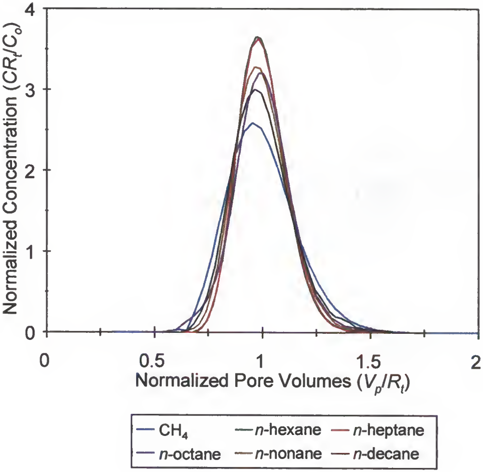

Figure 6-1. Breakthrough curves of the interfacial tracers; Dover AFB soil, water saturation 0.15.

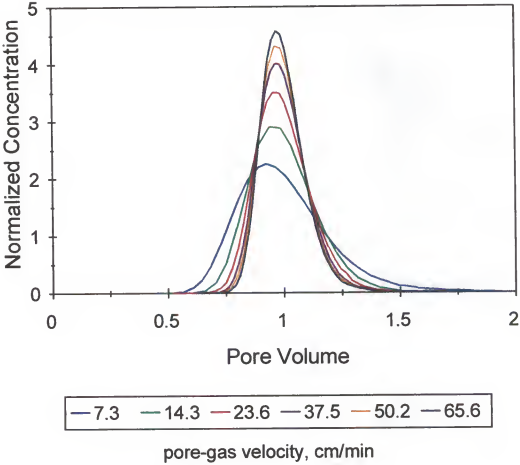

Figure 6-2. Breakthrough curves of methane at different pore-gas velocities, sand column, water saturation 0.31.

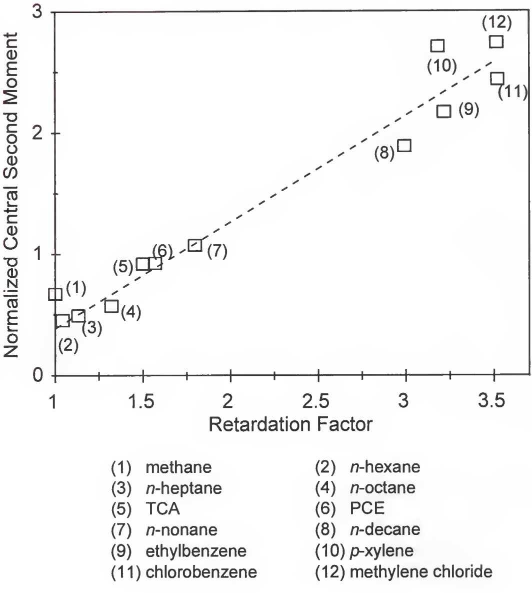

Figure 6-3. The normalized, temporal, central moments of volatile organic chemicals with respect to the retardation factor.

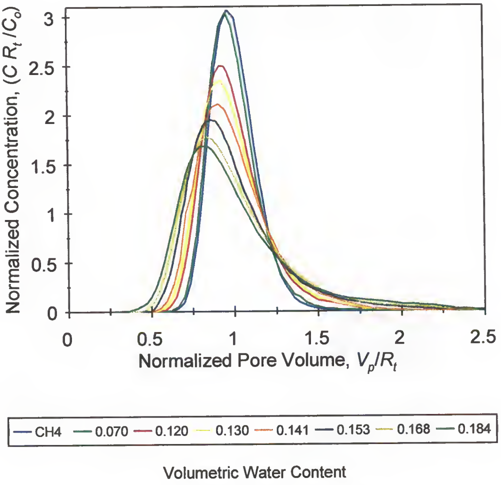

Figure 6-4. Normalized breakthrough curves of methylene chloride (gaseous water-partitioning tracer) at different water contents, sand column.

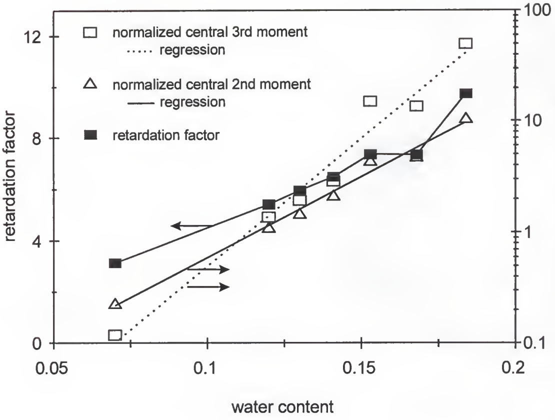

Figure 6-5. The change of the normalized, temporal, central moments of methylene chloride (water-partitioning tracer) with volumetric water content change.

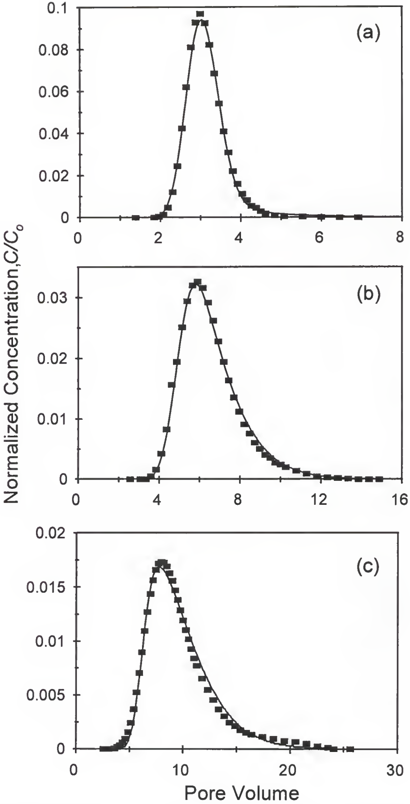

Fugre 6-6. Fitted BTCs of methylene chloride using 2-site model; squares-observed data, solid line-fitting; (a) water content 0.070, (b) water content 0.141, (c) water content 0.184.

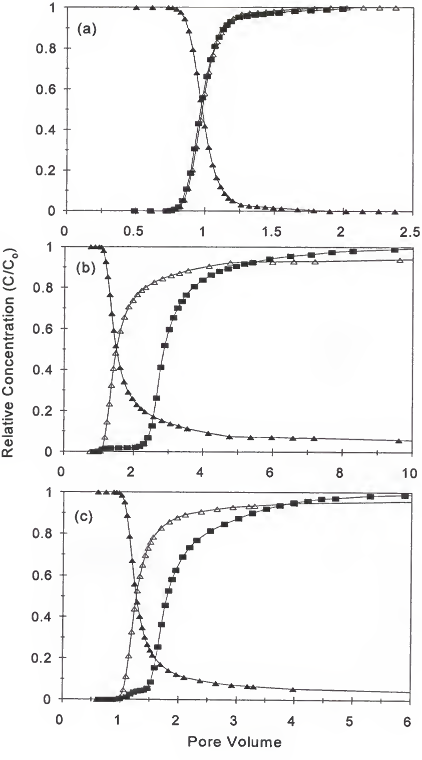

Figure 6-7. The breakthrough curves of tracers: (a) bromide, (b) CPC 0.0596 mM, (c) CPC 0.199 mM; pore water velocity 0.9 cm/min.; rectangle - front side of BTC, closed triangle - back side of BTC, open triangle - inverted back side of BTC.

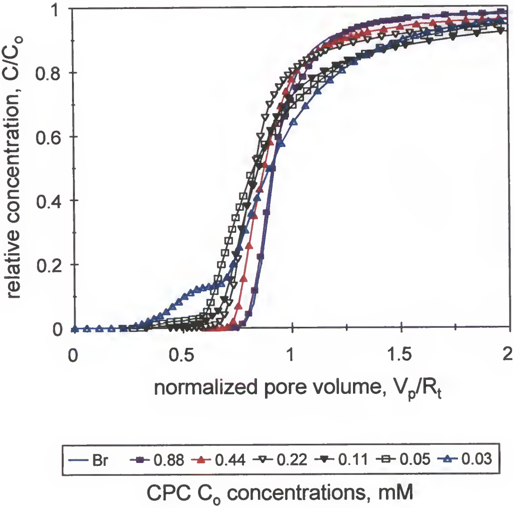

Figure 6-8. Normalized breakthrough curves of CPC with different input concentrations, glass bead column coated with *n*-decane; data from Chap. 5.

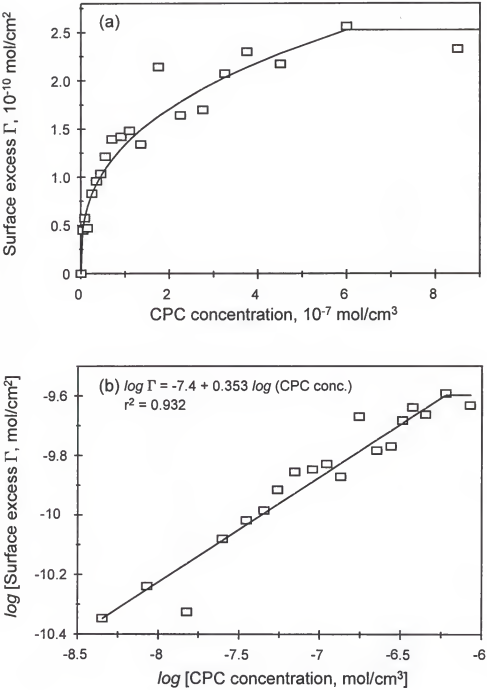

Figure 6-9. The adsorption isotherm of CPC at the *n*-decane-water interface at 22°C (a); and regression result using Freundlich isotherm model (Eq. 6-27) for the CPC concentration up to the saturation point (CPC conc = 5×10^{-7} mol/cm^3) (b): squares - observed data; solid line - regression.

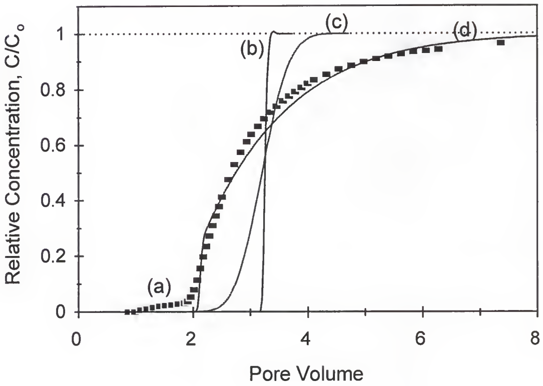

Figure 6-10. Breakthrough curves of CPC: (a) observed, C_o=0.056 mM, (b) simulated BTC using equilibrium, non-linear isotherm, 2-site model, N=0.353 (Freundlich isotherm model), (c) simulated BTC using equilibrium, linear isotherm model, (d) fitted BTC using non-equilibrium, non-linear isotherm (N=0.353), 2-site model, β= 0.52, ω= 1.33: all BTCs have the same retardation factor of 3.21.

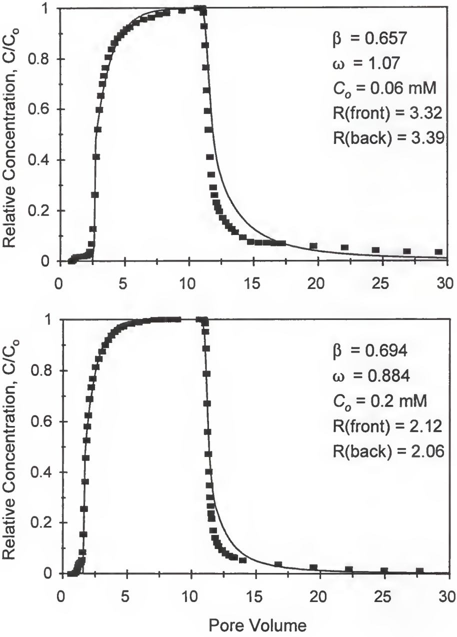

Figure 6-11. Breakthrough curves of CPC; the fitting parameters (β and ω) for the frontal side of the BTC were used to predict the back side of BTC; N = 0.353 (Eq. 6-27, Fig 6-9).

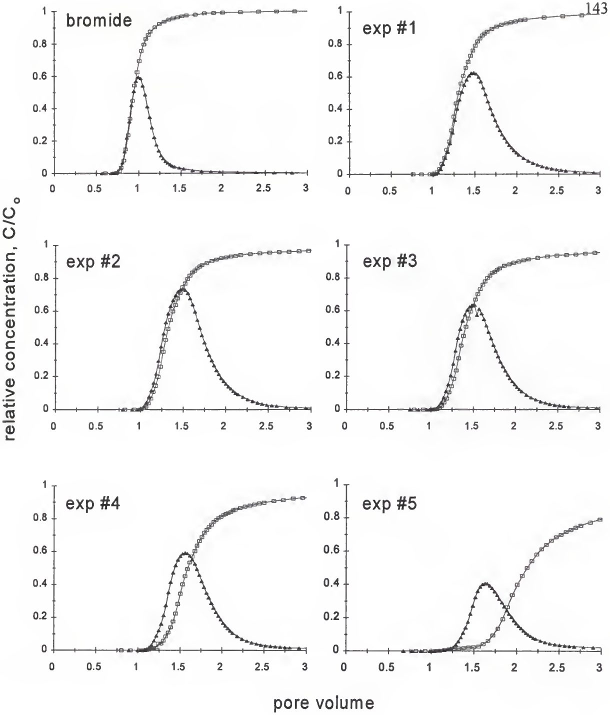

Figure 6-12. Breakthrough curves of CPC; the size of input pulse is not corrected; influent concentrations (C_o) are shown in Table 6-3.

CHAPTER 7
CONCLUSIONS AND RECOMMENDATIONS

Conclusions

The objectives of this study were three fold: (1) examination of the effect of interfacial adsorption on the transport velocities of volatile organic contaminants in both aqueous and gaseous phases, (2) further evaluation of the interfacial tracer technique developed at University of Florida in 1995, (3) investigation of the effects of non-equilibrium/non-linear isotherm on the transport of volatile organic contaminant in light of the sorption processes involving the interfacial phenomena. The following is the outline of the overall research conclusions:

(1) The air-water interfacial areas measured using different tracers (i.e., alcohols, and an anionic surfactant) were consistent, implying that the aqueous tracer technique for air-water systems produces consistent data regardless of the chemical types of interfacial tracers chosen.

(2) Effect of air-water interfacial adsorption on the transport of organic chemicals dissolved in aqueous phase depends on two major variables: the chemical property of the solutes (interfacial sorption coefficient, K_{iw}) and the physical property of the media (specific air-water interfacial area, a_I). Chemicals with relatively large K_{iw} values (aliphatic alcohols, ionic surfactants) are found to be retarded during aqueous transport mainly due to interfacial

(surface) adsorption. Aqueous transport of chemicals with relatively small K_{iw} values (aromatic compounds, e.g., BTEX) was not affected significantly by the interfacial adsorption at the air-water interface in a sandy soil. However, using all of the sorption related parameters (K_{iw}, Henry's law constants, and soil sorption coefficient, K_d), it was found that the total predicted retardation factors (R_t) of organic chemicals during aqueous phase transport were in good agreement with the measured R_t.

(3) Vapor-phase straight chain hydrocarbons were successfully applied as the gaseous interfacial tracers for the estimation of a_i in water-unsaturated soil columns. Regardless of the chain length of the tracers, as long as the tracers have large enough retardation factors, the measured interfacial areas were consistent.

(4) Specific air-water interfacial areas measured by gaseous interfacial tracers (e.g., *n*-decane) were at least two times larger than those measured by aqueous tracers (surfactant, alcohols) for the same medium and at the same water saturations. Based on this information, the linear velocities at the air-water interface at different water saturations were estimated. The linear velocity at the air-water interface was about 23-36 % of the pore water velocity, and increased as the water saturation increased.

(5) The volumetric water contents (θ_w) were measured using chlorinated methanes (methylene chloride and chloroform) as the gaseous water-partitioning tracers. The measured θ_w values were in excellent agreement with those estimated gravimetrically.

(6) During gaseous transport in soil packed columns, the effect of air-water interfacial adsorption on the total retardation of volatile organic chemicals (VOCs) was measured. The fraction of total retardation factor, resulting from the adsorption at the surface of water varied

depending on the chemical and soil types. In a column packed with silty sand, up to 95 % of the total retardation was due to the interfacial adsorption (*p*-xylene) at 3-5 % of water saturation. This interfacial adsorption effect was significant for most of the chemicals used in this study at low water saturation, and decreased as the water saturation increases, while other sorption mechanisms (e.g., water-partitioning) becomes more dominant.

(7) The NAPL-water interfacial areas (a_{nw}) measured by different tracer types (SDBS-anionic, CPC-cationic) were consistent. The measured a_{nw} were comparable to the estimated surface area of the medium (glass bead coated with thin film of NAPL), and were not sensitive to the NAPL types (*n*-decane and PCE). Using different influent concentrations of interfacial tracers (both SDBS and CPC) did not affect the a_{nw} measurement. These results lead to the conclusion that the aqueous phase interfacial tracer technique for a_{nw} measurement is robust with respect to the types of NAPL, tracer, and the applied concentrations of tracers.

(8) The non-linearity of NAPL-water interfacial adsorption isotherms of aqueous phase interfacial tracers was correctly reflected to their total retardation factors.

(9) For gaseous interfacial tracers (aliphatic hydrocarbons), there were no significant rate-limited sorption effects found during the transport under the experimental conditions used in this study. However, distinctive changes of the shapes of BTCs for the gaseous, water-partitioning tracers were observed, and discussed in light of the slow partitioning kinetics between gaseous and aqueous phases.

(10) It was also found that the observed BTCs of aqueous interfacial tracers (NAPL-water system) deviate from the predicted ones based on equilibrium models. The observed non-equilibrium effect on the aqueous transport of interfacial tracers were discussed.

(11) Overall, both of the aqueous and gaseous interfacial tracer techniques were found to produce reliable estimates of fluid-fluid (air-water, and NAPL-water) interfacial areas in porous media. Thus the effect of interfacial adsorption along with other sorption mechanisms such as soil sorption, and gas- (or water-) partitioning were accurately predicted.

Recommendations

Although the validity of the interfacial tracer technique has been proven in several different ways in this study, there are still many aspects that need to be improved for an unambiguous measurement of fluid-fluid interfacial areas in porous media. Recommendations for future research can be divided to two parts : the refinement of the technique and its applications.

Throughout this study, all aqueous interfacial tracers were introduced as step input. This is because of the non-linearity of the adsorption isotherms, which would cause complications for correct interpretation of the observed BTCs if used as pulse input. Since for most field- or semi-field-scale experiments, usage of pulse input is much more realistic, a rigorous data analysis protocol for pulse input interfacial tracer application should be established. Since an ideal aqueous interfacial tracer is one that is pure, minimally interacts with the background solid matrix, is non-volatile, should be resistant against biotic/abiotic degradation, and should be easily detectable with good sensitivity, effort in searching for such candidates should be continued. Compared to aqueous interfacial tracers, gaseous tracers posed few problems. Upscaling the gaseous interfacial tracer technique for the field scale experiments may require reconfiguration of the experimental set up used in this study.

The research areas where the interfacial tracer technique can be used may go all over the science and engineering disciplines. Followings are some of the potential applications of interfacial tracer technique:

(1) Mass transfer study for NAPL dissolution kinetics in both lab and field scales.

(2) Mass transfer study for gas exchange in unsaturated porous systems.

(3) Relationship between microbial activity and gas transfer rate in unsaturated porous systems.

(4) Optimization and performance assessment of VOC removal technologies from contaminated vadose zone or aquifer (e.g., soil vapor extraction, bioventing, air sparging).

(5) Characterization of wetting property of solid matrix influenced by chemical flooding or chemical property change in water (or aquifer).

(6) Characterization of multi-fluid systems with more than two immiscible fluids.

(7) Characterization of NAPL morphology in contamination source zone in both vadose and aquifer.

(8) The effect of interfacial morphology on the energy/heat exchange processes in porous systems.

(9) Assessment of surface (interface) area as a quantity that influence chemical reactions where the reaction rates are facilitated by the fluid surface (or interface) (e.g., synthesis of triglyceride from mono- or di-glyceride).

(10) Feasibility study of aquifer remediation technologies.

APPENDIX

SURFACE (INTERFACIAL) TENSION MEASUREMENT DATA

Surface Tension: Aqueous Solutions of Alcohols

n-octanol		*n*-nonanol	
concentration $\times 10^{-7}$mol/cm^3	surface tension dynes/cm	concentration $\times 10^{-7}$mol/cm^3	surface tension dynes/cm
0.000	72.67	0.000	72.80
0.178	72.29	0.591	72.16
0.356	71.97	1.201	71.48
0.505	71.54	1.762	70.74
0.694	71.07	2.595	69.10
0.911	70.71	3.244	67.75
1.135	69.59	4.135	66.07
1.381	67.76	5.551	62.45
1.742	65.50	7.434	58.20
2.200	62.50		
2.728	60.15		
3.546	54.80		

Interfacial Tension: Aqueous Solutions of Surfactant - *n*-decane

SDBS		CPC	
concentration $\times 10^{-7}$mol/cm^3	interfacial tension dynes/cm	concentration $\times 10^{-7}$mol/cm^3	interfacial tension dynes/cm
0.000	48.50	0.000	48.49
0.238	40.17	0.002	47.34
0.475	34.16	0.007	44.57
0.950	32.81	0.10	43.56
1.425	29.12	0.20	41.95
1.900	27.25	0.30	40.30
2.375	25.59	0.40	38.94
2.850	24.62	0.50	37.80
3.325	24.08	0.60	36.72
3.800	20.91	0.80	34.74
7.600	16.11	1.00	33.18
12.36	10.79	1.20	31.85
16.16	7.62	1.50	30.38
20.00	5.17	2.00	27.35
30.00	3.29	2.50	25.55
40.00	4.16	3.00	24.03
56.00	4.45	3.50	22.46
80.00	4.39	4.00	20.95
		5.00	18.57
		7.00	14.33
		10.0	10.23
		15.0	9.21
		30.0	8.79
		50.0	8.31

Interfacial Tension: Aqueous Solutions of Surfactant - PCE

SDBS	
concentration $\times 10^{-7}$mol/cm^3	interfacial tension dynes/cm
0.000	42.80
0.238	32.95
0.475	28.67
0.950	24.23
1.425	21.19
1.900	18.60
2.375	17.37
2.850	16.23
3.325	14.56
3.800	13.49
4.275	12.50
4.750	12.27
7.607	8.14
12.36	5.65
14.26	4.68
20.00	2.07
29.62	0.97
40.00	1.30
56.00	1.46
80.00	1.60

REFERENCES

Adamson, A. W. 1989. Physical Chemistry of Surfaces, 4th edition, Wiley-Interscience, New York, pp 84-88.

Annable, M. D., J. W. Jawitz, P. S. C. Rao, D. P. Dai, H. Kim, and A. L. Wood. 1998a. Field evaluation of interfacial and partitioning tracers for characterization of effective NAPL-water contact areas. Ground Water, 36: 495-502.

Annable, M.D., Rao, P.S.C., Hatfield, K. and Graham, W.D., 1995. Use of partitioning tracers for measuring NAPL distribution in a contaminated aquifer: Preliminary results from a field-scale test. In Proceedings of Second Annual Tracer Workshop, University of Texas, Austin, TX., pp. 77-85.

Annable, M.D., Rao, P.S.C., Hatfield, K., Graham, W.D., Wood, A.L., and Enfield, C.G., 1998b. Partitioning tracers for measuring residual NAPL: field-scale test Results. J. Env. Eng., 124: 498-503.

Annable, M. D., Wallace, R. B., Hayden, N. J., Voice, T. C., 1993. Reduction of gasoline component leaching potential by soil venting, J. Contam. Hydrol., 12: 151-170.

Bear, J., 1972. Dynamics of Fluids in Porous Media. Dover, Mineola, NY.

Blank, M., and Ottewill, R. H., 1964. The adsorption of aromatic vapors on water surfaces. J. Phys. Chem., 68: 2206-2211.

Bradford, S. A., and Leij, F. J., 1997. Estimating interfacial areas for multi-fluid soil systems. J. Contam. Hydrol., 27: 83-106.

Brusseau, M. L., Popovicova J., and Silva J. A. K., 1997. Characterizing gas-water interfacial and gas-phase transport of organic contaminants in unsaturated porous media. Environ. Sci. Technol., 31: 1645-1649.

Brusseau, M. L., and Rao, P. S. C., 1989. Sorption nonideality during organic contaminant transport in porous media. CRC Crit. Rev. Environ. Control, 19: 33-99.

Brusseau, M. L., and Rao, P. S. C., 1990. Modeling solute transport in structured soils : A review. Geoderma, 46: 169-192.

Cameron, D. R., and Klute, A., 1977. Convective-dispersive solute transport with a combined equilibrium and kinetic adsorption model. Water Resour. Res., 13: 183-188.

Campbell, G. S., 1974. A simple method for determining unsaturated conductivity from moisture retention data. Soil Sci., 117: 311-314.

Carman, P. C., 1941. Capillary rise and capillary movement of moisture in fine sands. Soil Sci., 52: 1-14.

Cary, J.W., 1994. Estimating the surface area of fluid phase interface in porous media. J. Contam. Hydrol., 15: 243-248.

Clint, J. H., Corkill, J. M., Goodman J. F., and Tate, J. R., 1968. Adsorption of n-alkanols at the air/aqueous solution interface. J. Colloid Interface Sci., 28: 522-530.

Coats, K. H., and Smith, B. D., 1964. Dead-end pore volume and dispersion in porous media. Soc. Pet. Eng. J., 4: 73-84.

Conklin, M. H., Corley, T. L., Roberts, P. A., Davis, J. H., van de Water, J. G., 1995. Nonequilibrium processes affecting forced ventilation of benzene and xylene in a desert soil. Water Resour. Res., 31: 1355-1365.

Corey, A. T., 1994. Mechanics of Immiscible Fluids in Porous Media. Water Resources Publications, Highlands Ranch, Colorado, pp 47-49.

De Camargo, O. A., Biggar, J. W., and Nielsen, D. R., 1979. Transport of inorganic phosphorus in an Alfisol. Soil Sci. Soc. Am. J., 43: 884-890.

Dorris, G. M., and Gray, D. G., 1981. Adsorption of hydrocarbons on silica supported water surfaces. J. Phys. Chem., 85: 3628-3635.

Fahim, M. A., and Wakao, N., 1982. Parameter estimation from tracer response measurements. Chem. Eng. J., 25: 1-8.

Freeze, R. A., and Cherry, J. A., 1979. Groundwater, Prentice-Hall, Englewood Cliffs, NJ.

Fried, J. J., Muntzer, P., and L. Zilliox, 1979. Ground-water pollution by transfer of oil hydrocarbons. Ground Water, 17: 586-594.

Gardner, W. H. 1986. Water Content. In A. Klute (Ed.) Method of soil analysis. Part 1. 2nd edition. Anron. Monogr., 9, ASA and SSSA, Madison, WI., pp. 493-544.

Gray, W. G., and Hassanizadeh, S. M., 1991. Paradoxes and realities in unsaturated flow theory. Water Resour. Res., 27: 1855-1863.

Gvirtzman, H., Magaritz, M., Klein, E., and Nadler, A., 1987. A scanning electron microscopy study of water in soil. Transp. Porous Media, 2: 83-93.

Gvirtzman, H., and Roberts, P.V., 1991. Pore scale spatial analysis of two immiscible fluids in porous media. Water Resour. Res., 27: 1165-1176.

Harkins, W.D., and Brown, F.E., 1919. The determination of surface tension (free surface energy), and the weight of falling drops: The surface tension of water and benzene by the capillary height method. J. Am. Chem. Soc., 6: 499-524.

Hartkopf, A.; Karger, B. L., 1973. Study of the interfacial properties of water by gas chromatography. Acc. Chem. Res., 6: 209-216.

Hassanizadeh, S.M., and Gray, W.G., 1993. Thermodynamic basis of capillary pressure in porous media. Water Resour. Res., 29: 3389-3405.

Hauxwell, F., and Ottewill, R.H., 1968. The adsorption of Toluene vapor on water surface. J. Colloid Interface Sci., 28: 514-521.

Hauxwell, F., and Ottewill, R.H.,1970. A study of the surface of water by hydrocarbon adsorption. J. Colloid Interface Sci., 34: 473-479.

Hauxwell, R., Pallas, N. R., and Pethica, B. A., 1992. Adsorption of n-alkane vapors on water. Langmuir, 8: 602-603.

Herman, B., Lemasters, J. J., 1993. Optical microscopy: Emerging Methods and Applications. Academic Press, NY.

Hillel, D. 1982. Introduction to Soil Physics. Academic, San Diego, CA.

Hoff, J. T., Gillham, R., Mackay, D., and Shiu, W. Y., 1993a. Sorption of organic vapors at the air-water interface in a sandy aquifer material. Environ. Sci. Technol., 27: 2789-2794.

Hoff, J. T., Mackay, D., Gillham, R., and Shiu, W. Y., 1993b. Partitioning of organic chemicals at the air-water interface in environmental systems. Environ. Sci. Technol., 27: 2174-2180.

Hoffman, B., 1971. Dispersion of soluble hydrocarbons in groundwater stream, In Advances in Water Pollution Research, Jenkins, S. H. (Ed.), Pergamon, NY., pp. HA-7(b)/1-HA-7(b)/8.

Hoffman, D. L., and Rolston, D. E., 1980. Transport of organic phosphate in soil as affected by soil type. Soil Sci. Soc. Am. J., 44: 46-52.

Iwata, S., T. Tabuchi, and B. P. Warkentin, 1988. Soil-Water Interactions. Marcel Dekker, NY.

Jin, M., Delshad, M., Dwarakanath, V., McKinney, D.C., Pope, G.A., Sepehnoori, K., and Tilburg, C., 1995. Partitioning tracer test for detection, estimation, and remediation performance assessment of subsurface nonaqueous phase liquids. Water Resour. Res., 31: 1201-1211.

Karger, B. L., Castells, R. C., Sewell, P. A., Hartkopf, A., 1971a. Study of the adsorption of insoluble and sparingly soluble vapors at the gas-liquid interface of water by gas chromatography. J. Phys. Chem., 75: 3870-3879.

Karger, B. L., Sewell, P. A., Castells, R. C., Hartkopf, A., 1971b. Gas chromatographic study of the adsorption of insoluble vapors on water. J. Colloid Interface Sci., 35: 328-339.

Karkare, M. V., and Fort, T., 1996. Determination of the air-water interfacial area in wet "unsaturated" porous media. Langmuir, 12: 2041-2044.

Kim, H., 1996. Determination of air-water interfacial area in partially-saturated porous media. M. S. Thesis, University of Florida.

Kim, H., Rao, P.S.C., and Annable, M.D., 1997. Determination of effective air-water interfacial area in partially saturated porous media using surfactant adsorption. Water Resour. Res., 33: 2705-2711.

Langmuir, I., 1918. The adsorption of gases on plane surfaces of glass, mica and platinum. J. Am. Chem. Soc., 40: 1361-1403.

Leverett, M.C., 1941. Capillary behavior in porous solids. Trans. Am. Inst. Min. Metall. Pet. Eng., 142: 152-169.

Lide, D. R. Ed., 1993. Section 16, Health and Safety Information. In Handbook of Chemistry and Physics, 74th edition. CRC Press Inc., Boca Raton, FL.

Lin, S. -Y., Lu, T. -L., and Hwang, W. -B., 1995. Adsorption kinetics of decanol at the air-water interface. Langmuir, 11: 555-562.

Mackay, D., and Shiu, W. Y., 1981. A critical review of Henry's law constants for chemicals of environmental interest. J. Phys. Chem. Ref. Data, 10:1175-1199.

Miller, C. T., Poirier-McNeill, M. M., and Mayer, A. S., 1990. Dissolution of trapped nonaqueous phase liquids: Mass transfer characteristics. Water Resour. Res., 26: 2783-2796.

Montemagno, C. D., and Gray, W. G., 1995. Photoluminescent volumetric imaging: a technique for the exploration of multiphase flow and transport in porous media. Geophys. Res. Lett., 22: 425-428.

Morrow, N. R., 1970. Flow through porous media, In Physics and Thermodynamics of Capillary Action in Porous Media. de Wiest, R. J. M. (Ed.), Academic Press, New York.

Nelson, N. T., and Brusseau, M. L., 1996. Field study of the partitioning tracer method for detection of dense nonaqueous phase liquid in a trichloroethene-contaminated aquifer. Environ. Sci. Technol., 30: 2859-2863.

Nkedi-Kizza, P., Biggar, J. W., Selim, H. M., van Genuchten, M. Th., Wierenga, P. J., Davidson, J. M., and Nielsen, D. R., 1984. On the equivalence of two conceptual models for describing ion exchange during transport through an aggregated oxisol. Water Resour. Res., 20: 1123-1130.

Nkedi-Kizza, P., Rao, P. S. C., and Hornsby, A. G., 1987. Influence of organic cosolvent on leaching of hydrophobic organic compounds through soils. Environ. Sci. Technol., 21: 1107-1111.

Okamura, J.P.; Sawyer, D.T., 1973. Gas chromatographic studies of sorptive interactions of normal and halogenated hydrocarbons with water-modified soil, silica, and Chromosorb W. Anal. Chem., 45: 80-84.

Pennell, K. D., Rhue, R. D., Rao, P. S. C., and Johnston, C. T., 1992. Vapor phase sorption of p-xylene and water on soils and clay minerals. Environ. Sci. Technol., 26: 756-763.

Popovičová, J., and Brusseau, M. L., 1998. Contaminant mass transfer during gas-phase transport in unsaturated porous media. Water Resour. Res., 34: 83-92.

Posner, A. M., Anderson, J. R., and Alexander, A. E., 1952. The surface tension and surface potential of aqueous solutions of normal aliphatic alcohols. J. Colloid Sci., 7: 623-644.

Powers, S. E., Abriola, L. M., Weber, Jr., W. J., 1992. An experimental investigation of nonaqueous phase liquid dissolution in saturated subsurface systems: Steady state mass transfer rates. Water Resour. Res., 28: 2691-2705.

Rao, P. S. C., Davidson, J. M., 1979. Adsorption and movement of selected pesticides at high concentrations in soils. Water Res., 13: 375-380.

Rao, P. S. C., Davidson, J. M., Jessop, R. E., and Selim, H. M., 1979. Evaluation of conceptual models for describing nonequilibrium adsorption-desorption of pesticides during steady-state flow in soils. Soil Sci. Soc. Am. J., 43: 22-28.

Reeves, P.C., and Celia, M.A., 1996. A functional relationship between capillary pressure, saturation, and interfacial area as revealed by a pore-scale network model. Water Resour. Res., 32: 2345-2358.

Ronen, D., Magaritz, M., Paldor, N., and Bachmat, Y., 1986. The behavior of groundwater in the vicinity of the water table evidence by specific discharge profiles. Water Resour. Res., 22: 1217-1224.

Rose, W., 1958. Volumes and surface areas of pendular rings. J. Appl. Physics, 29: 687-691.

Rose, W., and Bruce, W. A., 1949. Evaluation of capillary character in petroleum reservoir rock. Trans. Am. Inst. Min. Metall. Pet. Eng., 186: 127-142.

Rosen, M.J., 1989. Surfactant and Interfacial Phenomena, 2nd Ed., John Wiley and Sons, New York, NY.

Saripalli, K.P., Kim, H., Rao, P.S.C., and Annable, M.D., 1997. Measurement of specific fluid-fluid interfacial areas in porous media. Environ. Sci. Technol., 31: 932-936.

Saripalli, K. P., Rao, P. S. C., and Annable, M. D., and Hatfield, K., 1998a. Measurement of Specific Interfacial Areas of Immiscible Fluids in Flow Systems. U.S. Patent No. 5,744,709. U.S. Patent Office, Washington, D.C. (April 28, 1998).

Saripalli, K. P., Rao, P. S. C., and Annable, M. D., 1998b. Determination of specific NAPL-water interfacial areas of residual NAPLs in porous media using the interfacial tracers technique. J. Contam. Hydrol., 30: 375-391.

Schwarzenbach, R. P.; Gschwend, P. M.; Imboden, D. M., 1993. Environmental Organic Chemistry. Wiley-Intersicence, New York.

Selim, H. M., Davidson, J. M., and Mansell, R. S., 1976. Evaluation of a two-site adsorption-desorption model for describing solute transport in soils. Proceedings of the Computer Simulation Conference, Am. Inst. of Chem. Eng., Washington D. C., pp. 444-448.

Shah, D.O., Chan, K.S., and Giordano, R.M., 1979. The Effect of Dissolved Oils and Alcohols on the CMC of Synthetic and Petroleum Sulfonates. In Solution Chemistry of Surfactants, Vol. 1. K.L. Mittal (Ed.), Plenum Press, NY.

Skopp, J., 1985. Oxygen uptake and transport in soils: Analysis of the air-water interfacial area. Soil Sci. Soc. Am. J., 49: 1327-1331.

Suzuki, M., and Smith, J. M., 1971. Kinetic studies by chromatography. Chem. Eng. Sci., 26: 221-235.

Tajima, K., Muramatsu, M., and Sasaki, T., 1970. Radiotracer studies on adsorption of surface active substance at aqueous surface. I. Accurate measurement of adsorption of tritiated sodium dodecylsulfate. Bull. Japan. Chem. Soc., 43: 1991-1998.

Turner, G. A., 1972. Heat and Concentration Waves. Academic, New York.

Valocchi, A. J., 1985. Validity of the local equilibrium assumption for modeling sorbing solute transport through homogeneous soils. Water Resour. Res., 21: 808-820.

Valsaraj, K. T., 1994. Hydrophobic compounds in the environment: Adsorption equilibrium at the air-water interface. Water Res., 28: 819-830.

van Genuchten, M. Th., Wierenga, P. J., 1976. Mass transfer studies in sorbing porous media : I. Analytical solutions. Soil Sci. Soc. Am. J., 53: 1303-1310.

van Genuchten, M. Th., Wierenga, P. J., 1986. *Physical and Mineralogical Methods.* In Method of Soil Analysis, Part 1, Klute, A., (Ed.), Agron. Monogr. Ser., Vol. 9, 2nd ed., Chap. 44, Am. Soc. of Agron., Madison, WI., pp 1025-1039.

Wiesendanger, R., 1994. Scanning Probe Microscopy and Spectroscopy: Methods and Applications. Cambridge University Press, NY.

Yaws, C., H.-C. Yang, and X. Pan. 1991. Henry's law constants for 362 organic compounds in water. Chem. Eng., 98: 179-185.

Zilliox, L., and Muntzer, P., 1975. Effects of hydrodynamic processes on the development of ground-water pollution: Study on physical models in a saturated porous medium. Prog. Water Technol., 7: 561-568.

BIOGRAPHICAL SKETCH

Heonki Kim was born in Kang-Reung city, Korea, on October 13, 1963. After his graduation from Kang-Reung High School in 1982, he was accepted in the Department of Chemistry of Yonsei University, Seoul, Korea. During his study in the University, he joined the Korean Army for two and half years and came back to school to continue his study. He received a Bachelor of Science degree in 1989.

After his graduation, he started to work in the Research Center of Han-Wha Group in Taejon city, Korea, as a research chemist. During the next five and half years, he was involved in a number of research activities and exposed to a variety of technologies in the field of analytical chemistry.

In August, 1994, he came to University of Florida, Gainesville, to continue his study in the Soil and Water Science Department. In August, 1996, he earned the degree of Master of Science, and was accepted as a Ph. D. student in the department of Environmental Engineering Sciences.

Heonki Kim had the good fortune to marry Hea-Young Ryu in 1992. They are blessed with a beautiful and gifted daughter, Jeong-Yon, born in 1993.

I certify that I have read this study and that in my opinion it conforms to acceptable standards of scholarly presentation and is fully adequate, in scope and quality, as a dissertation for the degree of Doctor of Philosophy.

Michael D. Annable
Associate Professor of
Environmental Engineering Sciences

I certify that I have read this study and that in my opinion it conforms to acceptable standards of scholarly presentation and is fully adequate, in scope and quality, as a dissertation for the degree of Doctor of Philosophy.

PSC Rao

P. Suresh C. Rao
Graduate Research Professor of
Soil and Water Science

I certify that I have read this study and that in my opinion it conforms to acceptable standards of scholarly presentation and is fully adequate, in scope and quality, as a dissertation for the degree of Doctor of Philosophy.

Kirk Hatfield
Associate Professor of
Civil Engineering

I certify that I have read this study and that in my opinion it conforms to acceptable standards of scholarly presentation and is fully adequate, in scope and quality, as a dissertation for the degree of Doctor of Philosophy.

William R. Wise
Associate Professor of
Environmental Engineering Sciences

I certify that I have read this study and that in my opinion it conforms to acceptable standards of scholarly presentation and is fully adequate, in scope and quality, as a dissertation for the degree of Doctor of Philosophy.

Paul A. Chadik
Assistant Professor of
Environmental Engineering Sciences

I certify that I have read this study and that in my opinion it conforms to acceptable standards of scholarly presentation and is fully adequate, in scope and quality, as a dissertation for the degree of Doctor of Philosophy.

Kurt D. Pennell
Assistant Professor of
School of Civil and Environmental
Engineering, Georgia Institute of Technology

This dissertation was submitted to the Graduate Faculty of the College of Engineering and to the Graduate School and was accepted as partial fulfillment of the requirements for the degree of Doctor of Philosophy.

December, 1998

Dean, College of Engineering

Dean, Graduate School